ADDIS ABABA UNIVERSITY
SCHOOL OF GRADUATE STUDIES
DEPARTMENT OF MECHANICAL ENGINEERING

POSTGRADUATE PROGRAM IN *MECHANICAL DESIGN*

MASTERS DEGREE THESIS

ON

OPTIMIZED DESIGN OF A DYNAMICALLY-BASED MOTION GENERATING SPATIAL FOUR-BAR MECHANISM ON RIGID MULTIBODY SYSTEMS

A Thesis Submitted to the School of Graduate Studies of Addis Ababa University, Faculty of Technology *in Partial Fulfillment of the requirements for* the Award of the *Degree of Masters of Science in Mechanical Engineering (Mechanical Design Stream)*

By**: Yirga Kelem**

Advisor: **Dr.Alem Bazezew**

October, 2009

ADDIS ABABA UNIVERSITY
SCHOOL OF GRADUATE STUDIES
POSTGRADUATE PROGRAM IN MECHANICAL DESIGN

Optimized Design of a Dynamically-Based Motion Generating Spatial Four-Bar Mechanism on Rigid Multibody Systems

By: Yirga Kelem

Approved by Board of Examiners:

Chairman of Department Graduate Committee (DGC)	Signature	Date
Advisor	Signature	Date
External examiner	Signature	Date
Internal examiner	Signature	Date

DECLARATION

I here by declare that the work which is being presented in this thesis entitled "Optimized Design of a Dynamically-Based Motion Generating Spatial Four-Bar Mechanism on Rigid Multibody Systems" is original work of my own, has not been presented for a degree of any other university and all the resources of materials used for the thesis have been duly acknowledged.

_____ _____

Yirga Kelem Date
(Candidate)

This is to certify that the above declaration made by the candidate is correct to the best of my knowledge.

_____ _____

Dr.Alem Bazezew Date
(Thesis Advisor)

ACKNOWLEDGEMENT

In the first place, I am grateful to my thesis advisor ***Dr.Alem Bazezew*** for his insightful brilliant guidance, fruitful discussions, and support in making this thesis work happen. His vast knowledge in the field of mechanics, his systematic approach in solving problems has been so inspiring during my stay in undergraduate and post graduate studies. Specially, the course "kinematic and dynamic simulation of multibody systems" taught by him in the post graduate program has been a very inspiring course to do my thesis work in this area. Those all his qualities have motivated me to do my thesis work in the dynamics of multi-body systems as a problem solving work with him. Besides, the interaction he made with his students in lecture times and his fatherly advices in every wakes of life are some of his best qualities to take him as a role model doctor in my career.

In the second place, I want to express my deepest gratitude to my friend Solomon Negash for his simulating suggestions and support. I would like to express my appreciation also to my colleagues from Mechanical Engineering Department, all my postgraduate instructors, and all computer lab administrators of Mechanical Engineering Department from AAU, and to all my friends for their constant moral support and my stuff members at the college where I am working currently as a lecturer.

Thirdly, I would like to show appreciation to my sincere friend Teklay T/brhan and my sister Tirhas Kelem for their help in all my endeavors that keep me to accomplish my thesis work visible and consequent.

Finally, I would like to extend my gratitude to my father, my mother, my brothers, and my sisters for their never-ending love and encouragement.

Yirga Kelem

October, 2009

ABSTRACT

The four-bar spatial mechanism is the most basic chain that can be composed of four links and can include joints with any combination of rotational and translational freedom used in thousands of applications. This thesis will present some of the techniques and introduce solution tools that were not needed for planar motion. One of the new techniques known as the Euler parameters will be considered in this work.

The thesis includes modeling, optimizing computer-aided dynamic analysis and simulation of four-bar spatial mechanism composed of rigid bodies that are used for different applications of spatially moving motion generating mechanisms. The Motions of the rigid bodies are predicted by numerically integrating Differential-Algebraic Equations (DAEs) developed from principles of mechanics by the Newton-Euler's approach.

The computer program, MSC.ADAMS2005 will be used to model, solve, simulate, and optimize the dynamics of the appraised spatial four-bar mechanism as a lens-polishing mechanism by integrating the differential equations.

Unlike analytical synthesis, optimization allows direct incorporation of a greater number of design constraints, thus resulting in solutions that are more practical. In this thesis, an efficient algorithm known as the Generalized Reduced Gradient (GRG) is used to synthesize all kinematic linkages of the spatial mechanism. This approach will allow monitoring and controlling objectives and constraints, which will yield practical solutions to realistic mechanism design problems with lower kinematic pairs.

In addition to the above mentioned points, a mobility analysis has been done for the RSSR mechanism, which is a one degree of freedom, single loop, and spatial mechanism.

Thus, this thesis specifically discusses a practical example of a lens polishing four-bar spatial mechanism that simply substitutes the extremely expensive existing polishing robots. This mechanism is applicable in polishing lenses of military fire control instruments found in the Ethiopian Defence Forces. Thus, the design presented in this thesis provides a relatively low-cost solution for the existing problem as compared to the robots. This can be created with ease of manufacture in a machine shop quickly and simply. Numerical results obtained in this thesis are compared with existing literatures.

TABLE OF CONTENTS

ACKNOWLEDGEMENT iv
ABSTRACT v
LIST OF FIGURES ix
LIST OF TABLES xi
NOMENCLATURE xii
Latin symbols xii
Greek symbols xiv
Abbreviations xv
Operators xvi
CHAPTER 1-INTRODUCTION 1
1.1 Background 1
1.1.1 Definitions 2
1.2 Applications of Spatial Mechanisms 3
1.3 Advantages of Spatial Mechanisms 4
1.4 Disadvantages of Spatial Mechanisms 5
1.5. Problem Definition and Scope of Research 5
1.6. Objectives and Assumptions 5
1.7. Organization of the Thesis 6
CHAPTER 2-LITERATURE SURVEY 8
CHAPTER 3-DYNAMICS OF SPATIAL MULTI-BODY SYSTEMS 12
3.1 Introduction 12
3.2 Euler Parameters 14
3.2.1 Coordinates of a Body 14
3.2.2 Euler's Theorem 18
3.2.3 Euler parameters 18
3.2.4 Determination of Euler parameters 21
3.2.5 Identities with Euler Parameters 24
3.2.6 The Concept of Angular Velocity 29
3.2.7 Time Derivative of Euler Parameters 31
3.3 Kinematic Constraints 33
3.3.1 Spherical Joint 33

3.3.2 Revolute Joint 34
3.3.3 Translational (Prismatic) Joint 36
3.4 Formulation of Equations of Motion for spatial Multibody Systems 37
3.4.1 Introduction 37
3.4.2 Vector of Coordinates 38
3.4.3 Vector of Forces 40
3.4.4 Equations of Motion for a Constrained Body 42
3.4.5 Formulation of Spatial Constrained Multi-body Systems 45
CHAPTER 4-OPTIMAL DYNAMIC SIMULATION OF SPATIAL FOUR-BAR MECHANISMS 53
4.1 Introduction 53
4.2 Method of Lagrange Multipliers 55
4.3 Stiff Differential Equation Method 57
4.4 Body of Matrix Equations 60
4.4.1 Mass Matrix 62
4.4.2 External Vectors of Forces and Torques 62
4.4.3 Jacobian Matrix 63
4.5 Introduction to Optimization 64
4.5.1 Formal Definition of the Optimization Problem 65
4.5.2 Objective Function 65
4.5.3 Non-linear Programming Methods 66
4.5.4 Generalized Reduced Gradient (GRG) Mathematical Formulation 66
CHAPTER 5-THE DESIGN OF LENS-POLISHING SPATIAL FOUR-BAR MECHANISM USING ADAMS SOFTWARE PACKAGE 70
5.1 Some Points about the MSC. ADAMS† Software Package 70
5.2 Problem Descriptions of the Lens-polishing Spatial Mechanism 73
CHAPTER 6–DISCUSSION OF RESULTS AND OPTIMIZATION 83
6.1 Discussion of Results 83
6.2 Improving the Model (Optimization) 100
6.2.1 Parameterizing the Design Variables 100
6.2.2 Creating a Design Variable for the Driving Crank 100
6.2.3 Optimizing the Position of Slider-block using GRG Algorithm 101
6.2.4 Optimizing the CM_Velocity of Slider-block System using GRG Algorithm 106

6.2.5 Optimizing the Angular Velocity of the Coupler using GRG Algorithm..... 110
CHAPTER 7-CONCLUSION AND RECOMMENDATION FOR FUTURE WORK.....115
7.1 Conclusion of the Thesis Work.....115
7.2 Recommendation for Future Works.....116
REFERENCES.....118
APPENDICES 121
Appendix–A 121
Appendix–B 126
Appendix–C 130

LIST OF FIGURES

Figure 1.1.1 Four-bar spatial linkage notations 3
Figure 3.2.1 Configuration of Cartesian coordinate systems: (a) translation and rotation; (b) rotation only 15
Figure 3.2.2 Unit vectors along the axes of the local and global coordinate systems 15
Figure 3.2.3 Translation and rotation of body in three-dimensional space 18
Figure 3.2.4 Vector diagram for derivation of rotation formula 19
Figure 3.2.5 projection of vector $\vec{e}$ on ξ, η, ζ, x, y and z axes 22
Figure 3.2.6 (a) rotating $\xi\eta\zeta$ coordinate system, (b) rotating and translating $\xi\eta\zeta$ coordinate system 29
Figure 3.3.1 A spherical joint 34
Figure 3.3.2 A revolute joint: (a) general case, (b) special case when the ζ_i axis, the ζ_j axis, and the joint axis are parallel. 36
Figure 3.3.3 A translational joint 37
Figure 3.4.1 Definition of the Cartesian coordinates for a rigid body 39
Figure 3.4.2 Applied force 41
Figure 4.4.1 Assembly drawing of a spatial four-bar lens polishing mechanism 61
Figure 4.5.1 GRG nonlinear constraint satisfaction 69
Figure 5.2.1 Linkage parameters of spatial four-bar lenses polishing mechanism 75
Figure 5.2.2 Different joints and input torque at equilibrium position (t=0) under gravitational force: (a) all joint descriptions, (b) upper section zoomed-in, and (c) lower section zoomed-in 82
Figure 6.1.1 Positions and angular orientations of the (a) crank; (b) coupler; (c) slider-block versus time 85
Figure 6.1.2 Output results of CM-velocities for (a) crank; (b) coupler; (c) slider-block; versus Time 87
Figure 6.1.3 Output results of CM-accelerations for (a) crank; (b) coupler; (c) slider-system versus Time 89
Figure 6.1.4 Output results of CM-angular-velocities for (a) crank; and (b) coupler links versus Time 91

Figure 6.1.5 Output results of CM-angular-accelerations for (a) crank; and (b) coupler links versus Time....92
Figure 6.1.6 Output results of translational momentums of the (a) crank; (b) coupler; and (c) slider-block links about CM versus Time....93
Figure 6.1.7 Output results of angular momentums of the (a) crank; and (b) coupler links about CM versus Time....94
Figure 6.1.8 Output results of Lagrange multipliers for the (a) Revolute joint near the crank; (b) Spherical joint-1; (c) Spherical joint-2; and (d) Translational joint with their zoomed-in joint force elements Vs Time....99
Figure 6.2.1 Design study results a) running design study; b) driving crank's mass effect on slider-block position Vs Time; c) report; d) slider-block position trials for 2.5s....103
Figure 6.2.2 Optimization (a) running an optimization b) report; c) slider-block position iterations Vs Time....105
Figure 6.2.3 Design study results a) running design study; b) driving crank's mass effect on slider-block velocity Vs Time; c) report; d) slider-block velocity trials for 2.5s....108
Figure 6.2.4 Optimization (a) running an optimization b) report; c) slider-block velocity iterations Vs Time....109
Figure 6.2.5 Design study results a) running design study; b) driving crank's mass effect on coupler angular velocity (magnitude) Vs Time; c) report; d) coupler angular velocity trials for 2.5s....112
Figure 6.2.6 Optimization (a) running an optimization b) report; c) coupler angular velocity iterations Vs Time....114

LIST OF TABLES

Table 3.1.1 Classification of kinematic pairs 12
Table 3.4.1 Components in expansion of the most common constraints 52
Table 5.1.1 Design process steps in MSC.ADAMS software package 73
Table 5.2.1 Geometric parameters of each linkage for the spatial four-bar mechanism 76
Table 5.2.2 Geometric parameters of each linkage for the spatial four-bar mechanism 77
Table 5.2.3 Location coordinates for the extruded slider-block with length of 0.04m along z-axis . 77
Table 5.2.4 Location coordinates for the extruded connecting-bar with length of 0.012m along x-axis 77
Table 5.2.5 Material properties used in the dynamic simulation of the four-bar spatial lens-polishing mechanism 78
Table 5.2.6 Mass and inertia properties of the spatial four-bar lens polishing mechanism 78
Table 5.2.7 Key points for modeling of the spatial four-bar lens polishing mechanism 79
Table 5.2.8 Joints and linkages definitions used in the spatial four-bar lens polishing mechanism.. 79

NOMENCLATURE

Latin symbols

Symbols	Description
$\mathbf{A}$	Rotational transformation matrix
a_{ij} , $\mathbf{i},\mathbf{j}=1,2,3$	Direction cosines
$\widetilde{a}$	Skew-symmetric matrix of vector $\boldsymbol{a}$
$\vec{\mathbf{d}}$	Displacement vector in prismatic joint
D	Degree of freedom of the mechanism
$e_0, \mathbf{e}_1, \mathbf{e}_2,\ \mathbf{e}_3$	Euler parameters
$\mathbf{f}$	Force vector
$\vec{f}_i$,	Resultant force acting on body i
$\vec{n}_i$	Resultant moment acting on body i
$\mathbf{G}$	Auxiliary matrices orthogonal to $\mathbf{p}$
$\mathbf{L}$	Auxiliary matrices orthogonal to $\mathbf{p}$
$\mathbf{g}$	Generalized force vector
$\mathbf{g}^{(c)}$	Vector of constraint reaction equation
$\mathbf{f}^{(c)}$	Vector of constraint reaction forces
h	Time increment in Gear algorithm
$\vec{\mathbf{h}}_i, \vec{\mathbf{h}}_j$	Cylindrical vectors on bodies i and j , respectively
b_{-1}	Iteration Corrector coefficient in Gear algorithm
$\mathbf{I}$	Identity matrix
$\mathbf{I}_{gi}$	Inertia tensor
i	Relative to body i
$\mathbf{J}_i^{'}$	Inertia tensor (inertia matrix)
$\mathbf{J}_i^{*}$	Inertia tensor (inertia matrix)
j	Relative to body j
j_k	Number of joints having k degrees of freedom
l_n	Newton-Raphson iterations number
$\mathbf{M}$	System mass matrix
m	Number of Independent constraint equations
m_2	Driving crank mass
m_3	Coupler mass
m_4	Sliding-block system mass
$\mathbf{N}$	Local mass of each link nb
n	The number of links in the mechanism
nb	Number of bodies

nc	Number of Cartesian coordinates
nh	Number of holonomic constraints
$\mathbf{p}$	Euler parameter (rotational coordinate) vector
$\dot{\mathbf{p}}$	Rotational angular velocity vector
$\ddot{\mathbf{p}}$	Rotational angular acceleration vector
Q_i, Q_j	Points on bodies i and j, respectively
$\mathbf{q}$	Vector of generalized coordinates
q	Generalized coordinate
$\dot{\mathbf{q}}$	Vector that contains the state of velocities
$\ddot{\mathbf{q}}$	Vector that contains the state of accelerations
R_i, R_j	Points on bodies i and j, respectively
$\mathbf{r}$	Global position vector
$\mathbf{r}^{\mathbf{P}}$	Vector from the origin to point **p** of the xyz system
r_2, r_3, r_4	Length of three moving ridged bodies
$\mathbf{r}_i, \mathbf{r}_j$	Global position vector wrt to bodies i and j
$\ddot{\mathbf{r}}_i$	Vector of translational accelerations
$\mathbf{r_e}$	Residual error vector
r_{gi}	Basic links position of center of mass
$\mathbf{s}^{\mathbf{p}}$	Global location of a point P
$\vec{s}_i, \vec{s}_j$	Local position vector wrt to bodies i and j
$\mathbf{s}'$	Local position vector
t	Time
Δt	Time step
$\Delta \mathbf{y}^{(l_n)}$	Newton difference
$T_{k,j}$	Torque vectors, k for each link, j=application direction
$\vec{u}_{(\xi)}, \vec{u}_{(\eta)}, \vec{u}_{(\zeta)}$	Unit vectors along the $\xi\eta\zeta$ axes
$\vec{u}_{(x)}, \vec{u}_{(y)}, \vec{u}_{(z)}$	Unit vectors along the XYZ axes
XY	2D global coordinate system
XYZ	3D global coordinate system
$\mathbf{x}, \mathbf{y}, \mathbf{z}$	Local coordinate systems
$\mathbf{X}$	Optimization design vector
X_D	Dependent variables
X_I	Independent variables
$\mathbf{y}$	System position and velocity
$\dot{\mathbf{y}}$	System velocity and acceleration
$\Delta \mathbf{y}$	Newton difference

Greek symbols

Symbols	Description
$\alpha(\mathbf{X}, \theta_i)$	Actual output position results
$\beta(\theta_i)$	Desired output position results
$\Gamma(X, \theta)$	Objective function
Φ	Algebraic constraint equations
$\dot{\Phi}$	Constraint velocity equation
$\ddot{\Phi}$	Constraint acceleration equation
$\Phi_{\mathbf{q}}$	Jacobian matrix of the kinematic constraint equations
Φ_{qt}	Derivative of Jacobian matrix with respect to time
Φ_t	Partial derivative of constraint equations wrt time
Φ_{tt}	Double partial derivative of constraint equations wrt time
Φ^K	Kinematic constraint equation
Φ^D	Driving constraint equation
Φ^P	Euler parameter constraint equation
ϕ	Orientational axis of rotation
Ω	3×3 Skew matrix coefficient
$\vec{\omega}$	Angular velocity
$\dot{\vec{\omega}}$	Angular acceleration of the $\xi\eta\zeta$ coordinate system
λ	Vector of Lagrange multipliers associated with constraints
γ	Right hand side vector of acceleration equations
$\gamma^{\neq}$	Modified right hand side vector of acceleration equations
θ	Independent parameters comprised of time or position values
$\xi\eta$	2D Body-fixed coordinate system
$\xi\eta\zeta$	3D Body-fixed coordinate system

Abbreviations

Symbols	Description
2D	Two-dimensional
3D	Three-dimensional
ADAMS	Automatic Dynamic Analysis of Mechanical Systems
CAD	Computer Aided Design
CADSI	Computer Aided Design Systems, Inc
CADSPAM	Computer Aided Design of Spatial mechanism
CAE	Computer Aided Engineering
CM	Center of mass for each main linkage
DADS	Dynamic Analysis and Design System
DAE	Differential Algebraic Equation
DIM	Direct Integration Method
DOF	Degrees Of Freedom
DV	Design variable
GRG	Generalized Reduced Gradient
IMP	Integrated Mechanism Program
MBS	Multi-body system
O.F	Objective Function
ODE	Ordinary Differential Equation
RCCC	Revolute-Cylindrical- Cylindrical- Cylindrical
RPSPR	Revolute-Prismatic- Spherical- Prismatic- Revolute
RSRC	Revolute-Spherical- Revolute- Cylindrical
RSSR	Revolute-Spherical- Spherical- Revolute
SQP	Sequential quadratic programming

Operators

Symbols	Description
$(\ )^T$	Matrix or vector transpose
$(')$	Vector Components in a body-fixed coordinate system
$(\cdot)$	Scalar or internal product
$(\times)$	Cross or external product
(∂)	Partial derivative
$(\tilde{})$	Skew-symmetric matrix or vector
$(\dot{})$	First derivative with respect to time
$(\ddot{})$	Second derivative with respect to time
Δ	Increment
∇^2	Gradient

Intentionally left

CHAPTER 1-INTRODUCTION

1.1 Background

Mechanisms are mechanical devices composed of links connected by kinematic pairs, forming open or closed mobile chains. Mechanisms are used in almost every machine to transfer motion or force.

The main problem that is addressed when a mechanical device or linkage is assembled from a set of links and joints is to determine its mobility. We say the linkage is a mechanism if the links are mobile otherwise it is a structure.

The majority of mechanisms synthesized and found in application are planar devices. These mechanisms have motion such that all elements move in one plane or in parallel planes. The study of planar mechanisms is not as practically limiting as it might first appear since many devices in 3-dimension are constructed of multiple sets of two-dimensional devices coupled together like folding chairs, hood of a car etc. While planar mechanisms have been broadly applied, they lack the ability to perform many general motion-control tasks. Spatial kinematics is used to describe the movement of an object in three-dimensional space. They are useful for generating various paths, motions, functions, or for transferring force and torque to accomplish any desired kinematic task.

Unlike basic kinematics, which studies the movement of objects along straight lines, spatial kinematics is more complex. In basic kinematics, you only need two fixed points, the start and the finish, to describe a motion. With these two points we can measure its speed, velocity, duration of travel and the distance of travel. In spatial kinematics, the movement of an object must be measured from a series of points along the entire range of motion. By using more than one fixed point, scientists and engineers can break down three-dimensional movements into a matrix of one-dimensional movement. Those measurements are then plugged into formulas which allow them to scientifically describe how an object moves.

1.1.1 Definitions

Link is an assembled rigid body which possesses at least two nodes which are points for attachment to other links. For example: binary link is one with two nodes, ternary link is one with three nodes, and quaternary is one with four nodes.

Joint (Kinematic pair) is a connection between two or more links (at their nodes), which allows some motion between the connected links. Joint can be classified as by the:

- type of contact between the link elements; Pont contact (higher pair) or surface contact (lower pair).
- number of degree of freedom allowed at the joint
- type of physical closure of the joint; either force closed or form closed
- number of links joined (order of the joint).

Kinematic chain is an assemblage of links and joints, interconnected in a way to provide a controlled output motion in response to a supplied input motion.

Coupler is a link that undergoes complex motion (translation and rotational) and is not connected to ground.

Crank (input link) is a link that makes a complete revolution and is connected to the ground by a pivot.

Follower (output link) is a link that follows the motion of the crank.

Spatial mechanisms include no restriction on the relative motions of the particles. If the coordinate system is chosen with the x and y axes parallel to the plane(s) of motion, the all z values remain constant and the problem can be solved, either graphically or analytically. Although this is the usual case, spatial mechanisms solution is performed in a different way that of the planar mechanisms.

The simplest closed-loop linkage in the three-dimensional field is the four-bar spatial linkage, which has three moving links, one fixed link to the ground and any combination of joints. As shown in Fig.(1.1.1) below, the link that is connected to the power source or prime mover is

called the input link or the crank (O_2A). The output link or the follower connects the moving pivot B to the ground pivot O_4. The coupler or floating link connects the two moving pivots, A and B, thereby coupling the input to the output link. The input and out put crank angles are θ_2 and θ_4, respectively.

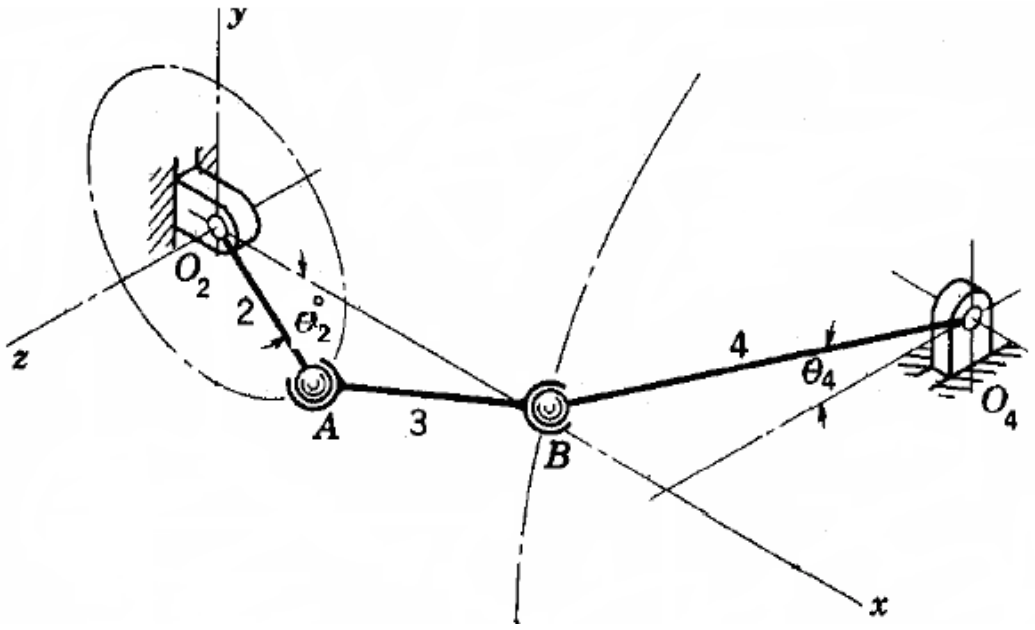

Figure 1.1.1 Four-bar spatial linkage notations

For the above figure, graphical methods may be used because they provide a good understanding of the kinematics but lack accuracy and tend to be time-consuming. These are the reasons why they are not used for three-dimensional analysis. Analytical or closed-form methods can be extremely efficient, although they are application-dependent, and may suffer from an excessive complexity in a multitude of practical problems.

The complexity of solving such problems can be overcome by numerical analysis and the fast processing of computers that emphasize the use of formulations and computational methods for multibody dynamic simulation. Of course, as compared to the planar multibody systems, the three-dimensional mechanical linkages need new techniques; like the Denavit-Hartenberg's convention, Eulerian angles and Euler parameters for their analysis and synthesis.

1.2 Applications of Spatial Mechanisms

Spatial mechanisms have not found wide use and acceptance for several reasons. One of the reasons is that spatial mechanism synthesis and analysis is typically not taught to engineers.

Techniques for analysis and synthesis of these mechanisms usually involve extensive vector mathematics and linear algebra techniques. Even for the experienced mechanical designer, it is labor intensive and difficult to design a spatial mechanism. The visualization of these devices can even be difficult.

Spatial mechanisms applications include the aerospace industry, gymnasium equipment design, robot manipulators, and the rehabilitation medical field etc. Engineers in aerospace are constantly trying to find ways to make things compact, light weight, and able to perform a specific spatial function. For example, spatial mechanisms are especially useful in satellite design and deployment. The exercise industry design could also use spatial mechanisms to design gym equipment that more closely imitate the natural path of the body while performing specific exercises. Human kinetic rehabilitation and aids for people with disabilities likewise would benefit from such a tool to develop sophisticated mechanical devices. Basically, spatial mechanisms could be applied to any task that requires general spatial motion.

1.3 Advantages of Spatial Mechanisms

In many automation situations, a spatial mechanism has a clear advantage over robotic manipulators and combined planar mechanisms. One good example would be a “pick-and-place” task, the universal task for assembly machines, which involves non-coplanar motion. The advantages of spatial, single-degree-of-freedom mechanisms include simplicity, lower cost, higher reliability, and lower energy consumption. Supplying more than one power source to a mechanism needs complex design and higher energy consumption. For these reasons single-degree-of-freedom mechanisms excel over multi-degree-of-freedom manipulators in highly repetitive tasks for mass production by reducing start-up, maintenance, and operating costs, thereby increasing productivity. Spatial mechanisms, being purely mechanical single-input devices, tend to be more reliable and more energy efficient than electronically-controlled multiple-input devices such as robotic manipulators. Also, closed-loop devices, such as spatial mechanisms, are known to be capable of running at higher speeds and carrying greater loads with more precision than open-loop devices, such as the typical serial robotic manipulator.

1.4 Disadvantages of Spatial Mechanisms

The main disadvantage of spatial mechanisms is the lack of flexibility with respect to meeting the changing needs of a desired task. This is a valid point and must be considered before the time and effort is put into designing a spatial mechanism. If the mechanism is going to have a short life span and cannot be reused elsewhere, then it should not be designed and built. On the other hand, if it is going to be an automotive part, a guidance device on a piece of exercise equipment, or part of a manufacturing process that will not be modified for an extended period of time, then flexibility becomes less important.

1.5. Problem Definition and Scope of Research

As it has been stated previously, the focus of this study is on an optimized design of a dynamic based motion generating of a four-bar spatial mechanism on rigid-bodies. The method applied for the formulation of the equations of motion is the Newton-Euler's approach integrated with the Euler parameters.

Therefore, the aim of this research is to develop and demonstrate a computer tool that can help in the dynamic analysis of single-degree of freedom spatial four-bar lens-polishing mechanism. The research includes coded computer for the dynamic analysis of the mechanism using MSC.ADAMS software package. Here in, dynamic analysis refers to the calculation of required joint forces, torques, translational and angular momentums for the linkages in addition to the kinematic analysis.

1.6. Objectives and Assumptions

In this thesis, the optimization, the dynamically-based motion analysis and simulation problems associated with spatial four-bar linkages will be investigated. The principal objective is to create accurate models and practical simulation algorithms that can provide physically sound solutions in describing the gross motion of the rigid-body systems.The specific objective of the study is to design a spatial four-bar lens polishing mechanism which is useful and applicable in the maintenance areas of Ethiopian Defence industries and colleges.

The following are the assumptions and restrictions imposed in this thesis:

Rigidity: A rigid body is defined as being made up of a continuum of particles that are constrained not to move relative to one another. While actual bodies are never perfectly rigid.

But, most attention in the study of the dynamics of machines is devoted to modeling individual bodies in a system as being rigid. This thesis considers the dynamic analysis of rigid bodies in space. That is, macroscopic or global deformations are not allowed when a rigid body is exposed to varying force fields.

Point contact: Point contact is assumed to simplify the modeling process. This is implied by the rigidity assumption in the limiting case.

Mass: Mass of each body is assumed to be concentrated at its center of gravity(center of mass) and connection elements like springs, dampers, actuators and joints are assumed to be mass less.
Force-acceleration approach: Formulation is based on forward dynamics of systems.

Friction: All friction effects are neglected in the dynamic analysis.

Spatial Motion: All links move in space or three-dimensional motion.

Eccentricity: The clearance between the joint surfaces is neglected in the mathematical formulation.

1.7. Organization of the Thesis

The first chapter presented the basic concepts, definitions, mechanism applications, advantages and disadvantages of the mechanisms and the research scope. The second chapter outlined previous research work carried in the field and gave the necessary background to proceed throughout the present thesis. The third chapter deals with the basic concepts in the dynamics of spatial multibody systems. In this chapter, the new techniques for spatial mechanisms analysis, called Euler Parameters will be discussed for this thesis purpose. In addition, Kinematic Constraints, and formulation of equations of motion for spatial multibody Systems will be presented. In the fourth chapter, the dynamic simulation of four-bar spatial mechanisms is discussed by using the Newton-Euler's approach (the method of Lagrange's multipliers).This chapter defines the body of matrix equations analysis and simulation problems, and presents the solution procedures to the problem. A more efficient dynamic solver called the stiff differential equation method is introduced in this chapter since this method is implemented in MSC.ADAMS software. At the end of this chapter an introduction to mechanism optimization is presented. Chapter five presents some points about the software package used, problem descriptions of the four-bar lens polishing spatial mechanism and finally a developed model for lens-polishing

spatial four-bar mechanism will be presented. Chapter six delivers the results, discussions, and optimization of the the mechanism designed in chapter five using MSC.ADAMS 2005. In this chapter, the application of the developed model for lens-polishing spatial four-bar mechanism, analysis methods and optimal simulation techniques will be discussed. Chapter seven gives a conclusion for the thesis, its contribution and possible future research directions. Lastly, references materials and appendix will be included.

CHAPTER 2-LITERATURE SURVEY

Until recently the analysis of spatial mechanisms has not occupied a prominent place in the work of kinematicians. Their reluctance to study these mechanisms was perhaps due to the apparently formidable and tedious tasks of mathematically formulating problems and obtaining solutions. However, recent publications have applied various mathematical tools to the analysis of spatial mechanisms in an effort to simplify the computational process thus make the undertaking of work in this field more attractive.

In the early 1970's, application of numerically based optimization to the design of spherical and spatial mechanisms became a topic of interest. Gupta [1973] demonstrated the synthesis of RSSR and RSRC spatial linkages with minimum structural error, subject to branching, mobility, and transmission constraints. Then Suh and Mechlenburg [1973] synthesized path-generating spatial mechanisms with minimum structural error in the least-squares sense. Kramer [1973] created a more advanced optimization technique called "selective precision synthesis" and later applied it to spatial mechanisms. This method allows the designer to create different size accuracy spheres around each design point in order to make certain points more or less constrained. Later, Premkumar and Kramer [1986] used the method of selective precision synthesis for synthesizing position and later for synthesizing velocity and acceleration of an RRSS mechanism [Premkumar and Kramer, 1989].

Anirvan Das Gupta [**1**] in his paper, "Mobility Analysis of a Class of RPSPR Kinematic chain", Presented the importance of spatial linkages in transmission of motion and complicated motions generation is well understood. Mobility analysis of such mechanisms has been a topic of great interests to kinematicians. Detection of crank in a Kinematic loop, or synthesis of a mechanism with crank(s) calls for mobility analysis to derive the conditions for presence of a crank. This is extremely important from the viewpoint of analysis and design of mechanisms since, in most cases, a mechanism is driven by a unidirectionally rotating prime-mover. The earliest investigation of mobility of planar four-bar linkages is due to Grashof, and the condition is commonly known as Grashof criterion. He derived simple analytical condition in terms of the link lengths which helps one to identify the type of four-bar chain. Later, researchers have analyzed more complicated mechanisms based on spatial mechanisms.

Glen Mullineux [**2**] in his paper,"Modeling Spatial Displacements Using Clifford Algebra" looks at the use of Clifford (or geometric) Algebra for handling both rotations and translations in Euclidean space. The ability to specify and manipulate spatial displacements of three-dimensional objects is required in a number of application areas including computer graphics, mechanism design and robotics. Such displacements are those transformations of Euclidian space which are produced by combinations of rotations and translations. By varying the displacements correctly, smooth spatial motions of objects can be obtained.

J. J. Uicker [**3**] presented a paper, "Dynamic Force Analysis of Spatial Linkages", that used the matrix method of linkage analysis to analyze the bearing forces and torques which result from the inertia of the moving links when a single-loop, single degree of freedom linkage is driven with known input velocity and acceleration. The method is well suited to digital computation and has been tested on several examples of spatial linkages.

J.J. Uicker, G.R. Pennock and J.E. Shigley [**4**] in their work, "Theory of Machines and Mechanisms" discussed the most widely used generalized programs for kinematic and dynamic simulations of three-dimensional rigid-body mechanical systems. ADAMS(Automatic Dynamic Analysis of Mechanical Systems) grew from the research effort of Chace, Orlandea, and others at the university of Michigan, DADS(Dynamic Analysis and Design System) was developed by Haug and others at the university of Iowa and CAD Systems, Inc.(CADSI), and IMP(Integrated Mechanisms Program) developed by Uicker, Sheth and others at the university of Wisconsin-Madison. These and other similar programs are all applicable to single or multiple-degree-of-freedom systems in both open and closed configurations. All are capable of solving position, velocity, acceleration, static force, and dynamic force analyses. All can formulate the dynamic equations of motion and predict the system response to a given set of initial conditions with prescribed motions or forces that may be functions of time. Other commercial softwares in this area include the Pro/MECHANICA Motion simulation Package and MSC Working Model systems.

Freudenstein [**19**] in his paper, "Approximate Synthesis of Four-Bar Linkages," marks the beginning of the shift in emphasis from graphical to analytical methods. The expression, "Approximate Synthesis," was widely used during this era to denote precision-position synthesis to approximate a given function. Freudenstein's later work with Sandor [Freudenstein and

Sandor, 1959] employed complex number theory and a programmed IBM 650 digital computer for the synthesis of path-generating mechanisms. Denavit and Hartenberg [1960] extended the precision-position approach of Freudenstein [1954] to the synthesis of spatial RSSR and RCCC mechanisms and showed the synthesis equations to be linear up to a limited number of precision positions. Wilson [1965] introduced the problem of spatial rigid-body guidance. These precision-position tools were developed and then applied to spatial mechanisms using dyad theory. With this premise in mind, there are many different mathematical techniques that can be employed to synthesize a mechanism.

C.Y.HO [**5**] in his paper, "Tensor Analysis of Spatial Mechanisms" shown that tensor notation provides a convenient and compact means for expressing relationships in spatial mechanisms. Some tensor operations that have no counterparts in vector algebra have been demonstrated as being powerful aids to obtaining problem solutions. Further, the tensor transformations have relieved the burdens of the tedious and confusing references of the coordinate frame. It is evident that the tensor notation lends itself well to programming for computer solution of problems in spatial kinematics and established a basis for future spatial linkage tensor analysis to emphasize the comprehensiveness and brevity of the tensor notation. Denavit and Hartenberg adopted the matrix calculus; Chace, Beyer and Harrisberger used the vector technique; Yang and Freudenstein chose quaternions; and kinematicians in the USSR, for example, Mangeron and Dregan: and Kalitsin,' applied tensor analysis. As a specific example of applying the technique, a mechanism containing two revolute pairs of links and two spherical pairs (R-S-S-R) is analyzed in his paper.

Robel Mitiku [**6**] in his thesis," Computer-Aided Dynamic force analysis and simulation of Four-bar planar linkages" presented the dynamic analysis and simulation of four-bar mechanisms by numerically integrating Differential-Algebraic Equations (DAEs) using the Newton-Euler's approach. The computer program he used for solving the equations developed in the analysis problem and that integrates the differential equations using Matlab.

Hazem A. Attia [**20**] in his paper, "Dynamic Simulation of Constrained Mechanical Systems Using Recursive Projection Algorithm" presented the dynamic simulation of constrained mechanical systems that are interconnected of rigid bodies is studied using projection recursive algorithm. The method is based upon the idea of replacing the rigid body by its dynamically

equivalent constrained system of particles discussed in (De Jalon et al., 1986, Attia, 1993, Nikravesh and Attia, 1994, Attia, 1998 and Attia, 2004) with essential modifications and improvements. The concepts of the linear and angular momentums are used to formulate the rigid body dynamical equations. However, they are expressed in terms of the rectangular Cartesian coordinates of the equivalent constrained system of particles. This groups the advantages of the automatic elimination of the unknown internal forces as in Newton-Euler formulation and results in a reduced system of differential-algebraic equations. Some useful geometrical relationships are used to obtain a reduced dynamically equivalent constrained system of particles.

Matthew E. Doyle [**19**] in his thesis," Foundation of CADSPAM: Computer Aided Design of SPAtial", presents the foundation of a computer program for the unified design of spatial mechanisms. The program he invented is capable of synthesizing any mechanism that can be described using an equivalent chain containing only revolute and prismatic joints.

The supporting analysis routine will be general and will be able to analyze any lower pair mechanism using the iterative approach developed by Sheth and Uicker [1972].

Optimization is employed to synthesize a wide variety of mechanisms. This approach allowed the user to interactively monitor and control objectives and constraints, which will yield practical solutions to realistic mechanism design problems.

For the closed-chain system, the system is transformed to open chain system by cutting suitable kinematical joints and introducing the cut-joint kinematical constraints. For the resulting open-chain system, the equations of motion are generated recursively along the serial chains instead of the matrix formulation derived in (De Jalon et al., 1986, Attia, 1993, Nikravesh and Attia, 1994, and Attia, 1998).

CHAPTER 3-DYNAMICS OF SPATIAL MULTI-BODY SYSTEMS

3.1 Introduction

Unlike to the kinematic analysis, the dynamic analysis of multibody systems integrates the relationship between the motion of the system parts and the causes that produce the motion including external applied forces and moments. The dynamic analysis provides a way to estimate external forces that depend on the relative position between the system's components, such as the forces exerted by springs, dampers and actuators. The internal reaction forces and moments generated at the kinematic joints are also provided by the dynamic analysis. These reaction forces and moments prevent the occurrence of the relative motions in the prescribed directions between the bodies connected through kinematic joints.

A spatial linkage can have all kinds of lower pairs. Since no single projection can reveal the true motion in a three dimensional space, graphical methods are not convenient for kinematic analysis and synthesis of spatial linkages. Analysis and synthesis of spatial mechanisms always require solving nonlinear equations which are usually lengthy and complicated. The usual mathematical methods, matrix and vector algebra can be used for analyzing and synthesizing mechanisms.

An unconstrained rigid body of moving in three dimensions has six degrees of freedom, three of which are translational and the other three rotational. The mobility of a kinematic chain can be obtained from the Kutzbach criterion for three-dimensional as [**4**]:

$$D = 6(n-1) - 5j_1 - 4j_2 - 3j_3 - 2j_4 - 1j_5 \tag{3.1.1}$$

Where, D is the mobility of the mechanism; n is the number of links, and each j_k is the number of joints having *k* degrees of freedom. Some of the kinematic pairs can be grouped according to their joint degrees of freedom as shown in the Table (3.1.1) below.

Table 3.1.1 Classification of kinematic pairs

R. Nº	Joint Types	Joint Degree of Freedom
1	Revolute(R)	1
2	Prismatic(P)	1
3	Helical(H)	1
4	Cylindrical(C)	2
5	Spherical/Globular(S/G)	3
6	Ball in cylinder	4
7	Spatial point contact on plane	5

In three-dimensional analysis, it is observed that the number and complexity of the calculations can make solution by hand a very tedious task. Thus, a general computer program might have a broad range of applications and that the development costs for such a program might be justified through repeated usage and increased accuracy, relief human drudgery, and elimination of human errors. General computer programs for the simulation rigid body kinematic and dynamic systems have been under development. Basic methods for multi-body system simulations are provided by the disciplines of dynamics, linear algebra and computer science.

Spatial kinematic analysis of multibody systems requires much more powerful mathematical techniques than planar kinematics; particularly for describing the angular orientations of a body in a global coordinate system. One of the techniques known as the Euler parameters will be used in this thesis for the synthesis of a particular problem in chapter five as per the mathematical formulation of section (3.2) in this chapter.

The Newton-Euler's methodology involves introducing a set of Lagrange's multipliers representing reaction forces of the joints which require an additional set of algebraic constraint equations. The size of the solution matrix becomes large, thereby occupying a substantial memory space for computation. However, this approach is relatively simple to implement in solving its governing equations of motion. In general, the motion of multibody system (MBS) is described by the so-called Differential Algebraic Equations (DAE).

The transient dynamic response of a constrained multibody system can be obtained by differential equations coupled with algebraic constraints [**7**]. The differential equations are of second order, and the algebraic equations describe the kinematic joints in the system. The solution of this type of equations and their integration in time, introduces several numerical difficulties, namely instability for higher index systems [**8**]. Specific numerical algorithms that enforce the stability of the solution are often required (Shampine and Gordon, 1975; Gear, 1981; Brenan *et al.*, 1989). These algorithms use multi-time stepping procedures and have the ability to deal with stiff systems. An alternative approach for the solution of the equations of motion is to transform the set of DAE in its underlying set of Ordinary Differential Equations (ODE), which are solved by integration in time. It is well known that the substitution of the algebraic equations of the DAE system by their differential counterpart in the ODE system introduces mild instabilities and drift problems in the integration process, which can be attenuated using stabilization techniques.

3.2 Euler Parameters

This section gives attention on a set of orientational coordinates known as Euler parameters, which are free of some of the deficiencies of other commonly used angular coordinates, such as the Euler angles. Furthermore, for large-scale computer programs that treat the angular orientation of bodies, the use of Euler parameters drastically simplify the mathematical formulations.

3.2.1 Coordinates of a Body

The six coordinates in space (Fig.3.2.1) define the location of Cartesian coordinate system that is fixed in the body (body-fixed coordinates) relative to the global (reference or inertial) coordinate axes. Since all points in the body may be located relative to this body-fixed coordinate system, the global locations of all points in the body can thus be determined from the six coordinates. The coordinates of the origin of the body-fixed axes are the translational coordinates. Rotational coordinates are then need to define the orientation of the local axes relative to the global coordinate axes. In the proceeding section, the body-fixed axes will be denoted as $\xi\eta\zeta$ axes and the global axes will be denoted as xyz axes.

Figure (3.2.1) shows how the configuration of the $\xi\eta\zeta$ axes with respect to the xyz axes can be considered a translation (**xyz** to **x'y'z'**) and a rotation (x'y'z' to $\xi\eta\zeta$). A vector $\vec{s}$ from the origin to a point **P**, as shown in Fig.(3.2.2) can be expanded in either of the two coordinate systems. If unit vectors $\vec{u}_{(\xi)}, \vec{u}_{(\eta)}$, and $\vec{u}_{(\zeta)}$ are defined along the $\xi\eta\zeta$ axes and $\vec{u}_{(x)}, \vec{u}_{(y)}$, and $\vec{u}_{(z)}$ are defined along the **xyz** axes, then:

$$\mathbf{s} = s_{(x)}\vec{u}_{(x)} + s_{(y)}\vec{u}_{(y)} + s_{(z)}\vec{u}_{(z)} \tag{3.2.1}$$

or

$$\mathbf{s} = s_{(\xi)}\vec{u}_{(\xi)} + s_{(\eta)}\vec{u}_{(\eta)} + s_{(\zeta)}\vec{u}_{(\zeta)} \tag{3.2.2}$$

Where

$$\mathbf{s}_{(x)} = \vec{s}.\vec{u}_{(x)}, \mathbf{s}_{(y)} = \vec{s}.\vec{u}_{(y)}, \ \mathbf{s}_{(z)} = \vec{s}.\vec{u}_{(z)} \tag{3.2.3}$$

and

$$\mathbf{s}_{(\xi)} = \vec{s}.\vec{u}_{(\xi)}, \mathbf{s}_{(\eta)} = \vec{s}.\vec{u}_{(\eta)}, \ \mathbf{s}_{(\zeta)} = \vec{s}.\vec{u}_{(\zeta)} \tag{3.2.4}$$

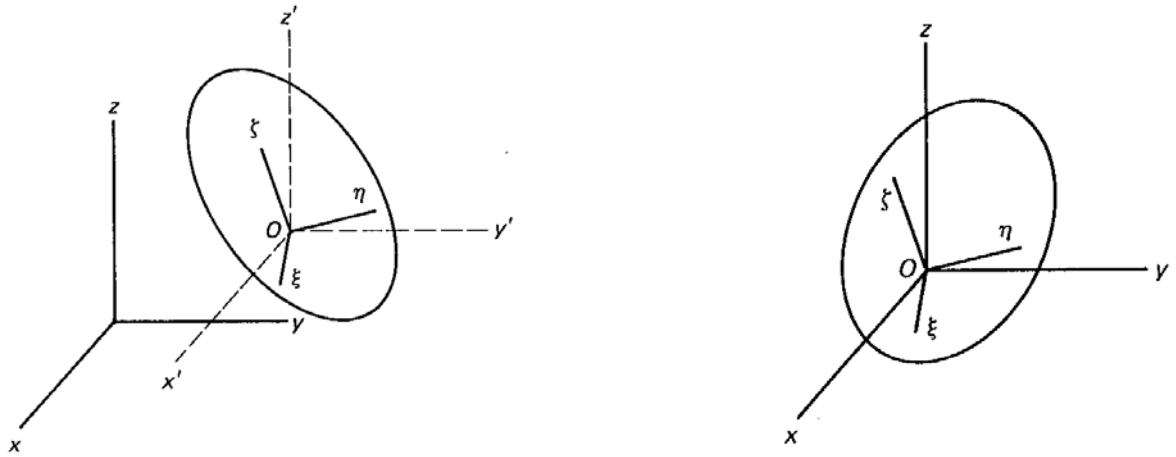

(a) (b)

Figure 3.2.1 Configuration of Cartesian coordinate systems: (a) translation and rotation; (b) rotation only

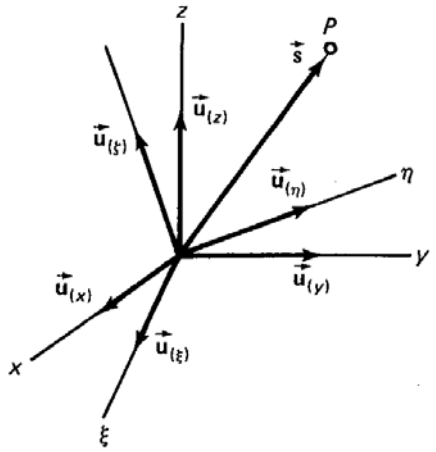

Figure 3.2.2 Unit vectors along the axes of the local and global coordinate systems

The component vectors that define $\vec{s}$ in the two coordinate systems are

$$\mathbf{s} = \left[S_{(x)}, S_{(y)}, S_{(z)}\right]^T \tag{3.2.5}$$

in the **xyz** system and

$$\mathbf{s}' = \left[S_{(\xi)}, S_{(\eta)}, S_{(\zeta)}\right]^T \tag{3.2.6}$$

in the $\xi\eta\zeta$ system. It is clear that there is a relation between $\mathbf{s}$ and $\mathbf{s}'$, since they are uniquely defined by the same vector $\vec{s}$. Hence, observe the relation below:

$$\begin{aligned}\vec{u}_{(\xi)} &= a_{11}\vec{u}_{(x)} + a_{21}\vec{u}_{(y)} + a_{31}\vec{u}_{(z)}\\ \vec{u}_{(\eta)} &= a_{12}\vec{u}_{(x)} + a_{22}\vec{u}_{(y)} + a_{32}\vec{u}_{(z)}\\ \vec{u}_{(\zeta)} &= a_{13}\vec{u}_{(x)} + a_{23}\vec{u}_{(y)} + a_{33}\vec{u}_{(z)}\end{aligned} \tag{3.2.7}$$

Where a_{ij}, $i, j = 1,2,3$ are the direction cosines that can be expressed as

$$\begin{aligned}a_{11} &= \vec{u}_{(\xi)}.\vec{u}_{(x)} = \cos\left(\vec{u}_{(\xi)}, \vec{u}_{(x)}\right)\\ a_{21} &= \vec{u}_{(\xi)}.\vec{u}_{(y)} = \cos\left(\vec{u}_{(\xi)}, \vec{u}_{(y)}\right)\\ a_{31} &= \vec{u}_{(\xi)}.\vec{u}_{(z)} = \cos\left(\vec{u}_{(\xi)}, \vec{u}_{(z)}\right)\\ a_{12} &= \vec{u}_{(\eta)}.\vec{u}_{(x)} = \cos\left(\vec{u}_{(\eta)}, \vec{u}_{(x)}\right)\\ a_{22} &= \vec{u}_{(\eta)}.\vec{u}_{(y)} = \cos\left(\vec{u}_{(\eta)}, \vec{u}_{(y)}\right)\\ a_{32} &= \vec{u}_{(\eta)}.\vec{u}_{(z)} = \cos\left(\vec{u}_{(\eta)}, \vec{u}_{(z)}\right)\\ a_{13} &= \vec{u}_{(\zeta)}.\vec{u}_{(x)} = \cos\left(\vec{u}_{(\zeta)}, \vec{u}_{(x)}\right)\\ a_{23} &= \vec{u}_{(\zeta)}.\vec{u}_{(y)} = \cos\left(\vec{u}_{(\zeta)}, \vec{u}_{(y)}\right)\\ a_{33} &= \vec{u}_{(\zeta)}.\vec{u}_{(z)} = \cos\left(\vec{u}_{(\zeta)}, \vec{u}_{(z)}\right)\end{aligned} \tag{3.2.8}$$

Substituting from Eq.(3.2.7) into Eq.(3.2.2) yields

$$\begin{aligned}\vec{s} = &\left(a_{11}s_{(\xi)} + a_{12}s_{(\eta)} + a_{13}s_{(\zeta)}\right)\vec{u}_{(x)} + \left(a_{21}s_{(\xi)} + a_{22}s_{(\eta)} + a_{23}s_{(\zeta)}\right)\vec{u}_{(y)} +\\ &\left(a_{31}s_{(\xi)} + a_{32}s_{(\eta)} + a_{33}s_{(\zeta)}\right)\vec{u}_{(z)}\end{aligned} \tag{3.2.9}$$

By equating the right sides of Eqs.(3.2.1) and (3.2.9), it is found that

$$\begin{aligned}s_{(x)} &= a_{11}s_{(\xi)} + a_{12}s_{(\eta)} + a_{13}s_{(\zeta)}\\ s_{(y)} &= a_{21}s_{(\xi)} + a_{22}s_{(\eta)} + a_{23}s_{(\zeta)}\\ s_{(z)} &= a_{31}s_{(\xi)} + a_{32}s_{(\eta)} + a_{33}s_{(\zeta)}\end{aligned} \tag{3.2.10}$$

This is also expressed in matrix form as:

$$\mathbf{s} = \mathbf{A}\mathbf{s}' \tag{3.2.11}$$

Where the matrix **A** of direction cosines is

$$\mathbf{A} = \begin{bmatrix} a_{11} & a_{12} & a_{13} \\ a_{21} & a_{22} & a_{23} \\ a_{31} & a_{32} & a_{33} \end{bmatrix} \tag{3.2.12}$$

The matrix **A** has a special property. If the **xyz** components of unit vectors $\vec{u}_{(\xi)}, \vec{u}_{(\eta)}$,and $\vec{u}_{(\zeta)}$ are denoted by $\mathbf{u}_{(\xi)}, \mathbf{u}_{(\eta)}$,and $\mathbf{u}_{(\zeta)}$ and the **xyz** components of vectors $\vec{u}_{(x)}, \vec{u}_{(y)}$, and $\vec{u}_{(z)}$ are denoted by $\mathbf{u}_{(x)}, \mathbf{u}_{(y)}$,and $\mathbf{u}_{(z)}$, it is clear that

$$\mathbf{u}_{(x)} = \begin{bmatrix} 1 \\ 0 \\ 0 \end{bmatrix}, \quad \mathbf{u}_{(y)} = \begin{bmatrix} 0 \\ 1 \\ 0 \end{bmatrix}, \quad \mathbf{u}_{(z)} = \begin{bmatrix} 0 \\ 0 \\ 1 \end{bmatrix} \tag{3.2.13}$$

Equation (3.2.8) indicates that a_{11} is the x component of $\mathbf{u}_{(\xi)}$, a_{21} is the y component of $\mathbf{u}_{(\xi)}$,and so forth. Therefore,

$$\mathbf{u}_{(\xi)} = \begin{bmatrix} a_{11} \\ a_{21} \\ a_{31} \end{bmatrix} \qquad \mathbf{u}_{(\eta)} = \begin{bmatrix} a_{12} \\ a_{22} \\ a_{32} \end{bmatrix} \qquad \mathbf{u}_{(\zeta)} = \begin{bmatrix} a_{13} \\ a_{23} \\ a_{33} \end{bmatrix} \tag{3.2.14}$$

and the matrix **A** can be written as follows:

$$\mathbf{A} = \begin{bmatrix} \mathbf{u}_{\xi} & \mathbf{u}_{(\eta)} & \mathbf{u}_{(\zeta)} \end{bmatrix} \tag{3.2.15}$$

Since the unit vectors $\mathbf{u}_{(\xi)}, \mathbf{u}_{(\eta)}$, and $\mathbf{u}_{(\zeta)}$ are orthogonal,

$$\mathbf{A}^T \mathbf{A} = \mathbf{I} \tag{3.2.16}$$

Thus, $\mathbf{A^T = A^{-1}}$ and the matrix **A** is also orthogonal. This special property permits an easy inversion of Eq. (3.2.11), to obtain

$$\mathbf{s}' = \mathbf{A}^T \mathbf{s} \tag{3.2.17}$$

When the origins of the **xyz** and $\xi\eta\zeta$ coordinate systems do not coincide; as is the case in Fig.(3.2.1a), the analysis is applied between the **x'y'z'** and $\xi\eta\zeta$ systems. If the component

vector $\mathbf{s}'^{\mathbf{P}}$ locates a point **P** in the $\xi\eta\zeta$ coordinate system, as it does in Fig. (3.2.3), then in the **x'y'z'** system this vector is just $\mathbf{A}\,\mathbf{s}'^{\mathbf{P}}$, and in global xyz coordinate,

$$\mathbf{r}^{\mathbf{P}} = \mathbf{r} + \mathbf{A}\mathbf{s}'^{\mathbf{p}} \tag{3.2.18}$$

Where, **r** is the vector from the origin of the **xyz** system to the origin of the $\xi\eta\zeta$ system.

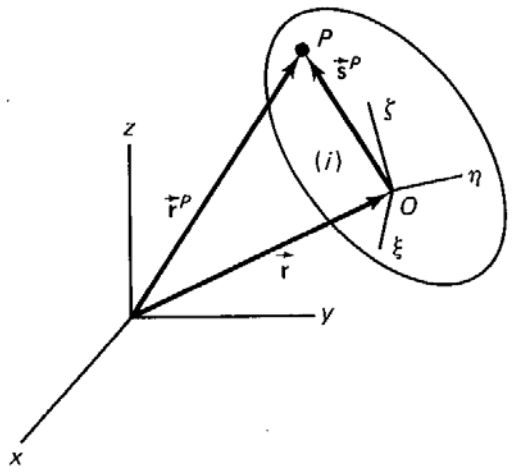

Figure 3.2.3 Translation and rotation of body in three-dimensional space

3.2.2 Euler's Theorem

At any instant of time, the orientation of a body can be specified by a transformation matrix, the elements of which may be expressed in terms of suitable sets of coordinates. As time progresses, the orientation of the body will change. Hence the transformation matrix will be a function of time. Since the motion of the body is continuous, the transformation matrix must be a continuous function of time.

3.2.3 Euler parameters

Euler's theorem states that a coordinate transformation can be accomplished by a single rotation about a suitable axis. It is therefore natural to seek a representation of the coordinate transformation in terms of parameters of this rotation, namely, the angle of rotation and the direction cosines of the orientational axis of rotation.

In Figure (3.2.4) the initial vector $\vec{s}$ can be expressed as the sum of three vectors:

$$\vec{s} = \vec{ON} + \vec{NQ} + \vec{QP} \tag{3.2.19}$$

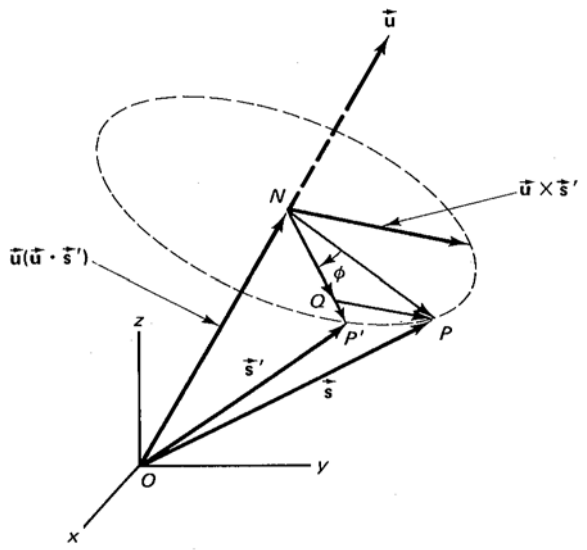

Figure 3.2.4 Vector diagram for derivation of rotation formula

The direct distance between points **O** and **N** is, $\vec{u}.\vec{s}'$ so vector $\vec{ON}$ can be written as follows:

$$\vec{ON} = \vec{u}(\vec{u}.\vec{s}') \tag{3.2.20}$$

Vector $\vec{NP}'$ can also be described as follows:

$$\vec{NP}' = \vec{s}' - \vec{ON} = \vec{s}' - \vec{u}(\vec{u}.\vec{s}') \tag{3.2.21}$$

Hence

$$\vec{NQ} = [\vec{s}' - \vec{u}(\vec{u}.\vec{s}')]\cos\phi \tag{3.2.22}$$

The magnitude of vector $\vec{NP}'$ is the same as that of vectors $\vec{NP}$ and $\vec{u} \times \vec{s}'$ .Therefore, vector $\vec{QP}$ may be expressed as

$$\vec{QP} = \vec{u} \times \vec{s}' \sin\phi \tag{3.2.23}$$

Substituting and slight rearrangement of terms, leads to the rotation formula:

$$\vec{s} = \vec{s}'\cos\phi + \vec{u}(\vec{u}.\vec{s}')(1 - \cos\phi) + \vec{u} \times \vec{s}' \sin\phi \tag{3.2.24}$$

By means of standard trigonometric relationships

$$\cos\phi = 2\cos^2\frac{\phi}{2} - 1$$
$$\sin\phi = 2\sin\frac{\phi}{2}\cos\frac{\phi}{2} \qquad (3.2.25)$$
$$1 - \cos\phi = 2\sin^2\frac{\phi}{2}$$

and the new quantities, e_0 and $\vec{e}$ .These four quantities called Euler parameters can be assigned by $e_0, \vec{e}_1, \vec{e}_2, \vec{e}_3$ as the first parameter, the second parameter, the third parameter, and the fourth parameter, respectively.

$$e_0 = \cos\frac{\phi}{2}$$
$$\vec{e} = \vec{u}\sin\frac{\phi}{2} \qquad (3.2.26)$$

The rotation formula of Eq.(3.2.24) can be put in a more useful form:

$$\vec{s} = \left(2e_0^2 - 1\right)\vec{s}' + 2\vec{e}\left(\vec{e}.\vec{s}'\right) + 2e_0\vec{e}\times\vec{s}' \qquad (3.2.27)$$

Algebraic representation of Eq. (3.2.27), using the component form $\vec{e} = \left[e_{1,} e_{2,} e_3\right]^T$ of Eq. (3.2.26, yields

$$\vec{s} = \left(2e_0^2 - 1\right)s' + 2\vec{e}\left(\vec{e}^{\,T}\vec{s}'\right) + 2e_0\left(\tilde{\vec{e}}\vec{s}'\right)$$

Or

$$\vec{s} = \left[\left(2e_0^2 - 1\right)\mathbf{I} + 2\vec{e}\vec{e}^{\,T} + 2e_0\tilde{\vec{e}}\right]\vec{s}' \qquad (3.2.28)$$

Where $\mathbf{I}$ is the 3×3 identity matrix and by the definition of skew-symmetric matrix associated with the vector $\vec{e}$ is defined as:

$$\tilde{\mathbf{e}} = \begin{bmatrix} 0 & -e_3 & e_2 \\ e_3 & 0 & -e_1 \\ -e_2 & e_1 & 0 \end{bmatrix} \qquad (3.2.29)$$

The term in brackets in Eq. (3.2.28) is thus the transformation matrix of Eq.(3.2.11); i,e

$$\mathbf{A} = \left(2e_0^2 - 1\right)\mathbf{I} + 2\left(\mathbf{e}\mathbf{e}^T + e_0\tilde{\mathbf{e}}\right) \qquad (3.2.30)$$

More explicitly,

$$\mathbf{A} = 2\begin{bmatrix} e_0^2 + e_1^2 - \frac{1}{2} & e_1e_2 - e_0e_3 & e_1e_3 + e_0e_2 \\ e_1e_2 + e_0e_3 & e_0^2 + e_2^2 - \frac{1}{2} & e_2e_3 - e_0e_1 \\ e_1e_3 - e_0e_3 & e_2e_3 + e_0e_1 & e_0^2 + e_3^2 - \frac{1}{2} \end{bmatrix} \tag{3.2.31}$$

Taking the transpose of both sides of Eq. (3.2.30) yields

$$\mathbf{A}^T = \left(2e_0^2 - 1\right)\mathbf{I} + 2\left(\mathbf{e}\mathbf{e}^T - e_0\tilde{\mathbf{e}}\right) \tag{3.2.32}$$

Equation (3.2.26) indicates that the Euler parameters are not independent since $\cos^2(\phi/2) + \mathbf{u}^T\mathbf{u}\sin^2(\phi/2) = 1$, then

$$\mathbf{p} = e_0^2 + \mathbf{e}^T\mathbf{e} = 1 \tag{3.2.33}$$

i,e.,

$$\mathbf{p} = e_0^2 + e_1^2 + e_2^2 + e_3^2 = 1$$

If the four Euler parameters are put in a 4-vector as follows:

$$\begin{aligned} \mathbf{p} &= \left[e_0, \mathbf{e}^T\right]^T \\ &= \left[e_0, e_1, e_2, e_3\right]^T \end{aligned} \tag{3.2.34}$$

The Eq. (3.2.33) is written as

$$\mathbf{p}^T\mathbf{p} - 1 = 0 \tag{3.2.35}$$

According to Euler's theorem, any vector lying along the orientational axis of rotation must have the same components in both initial and final coordinate systems.

3.2.4 Determination of Euler parameters

From the transformation matrix of Eq. (3.2.31), it is possible to derive explicit formulas for the Euler parameters in terms of the elements of the transformation matrix. Assume that the nine direction cosines of a transformation matrix are given as Eq. (3.2.12).

$$\mathbf{A} = \begin{bmatrix} a_{11} & a_{12} & a_{13} \\ a_{21} & a_{22} & a_{23} \\ a_{31} & a_{32} & a_{33} \end{bmatrix} \tag{3.2.36}$$

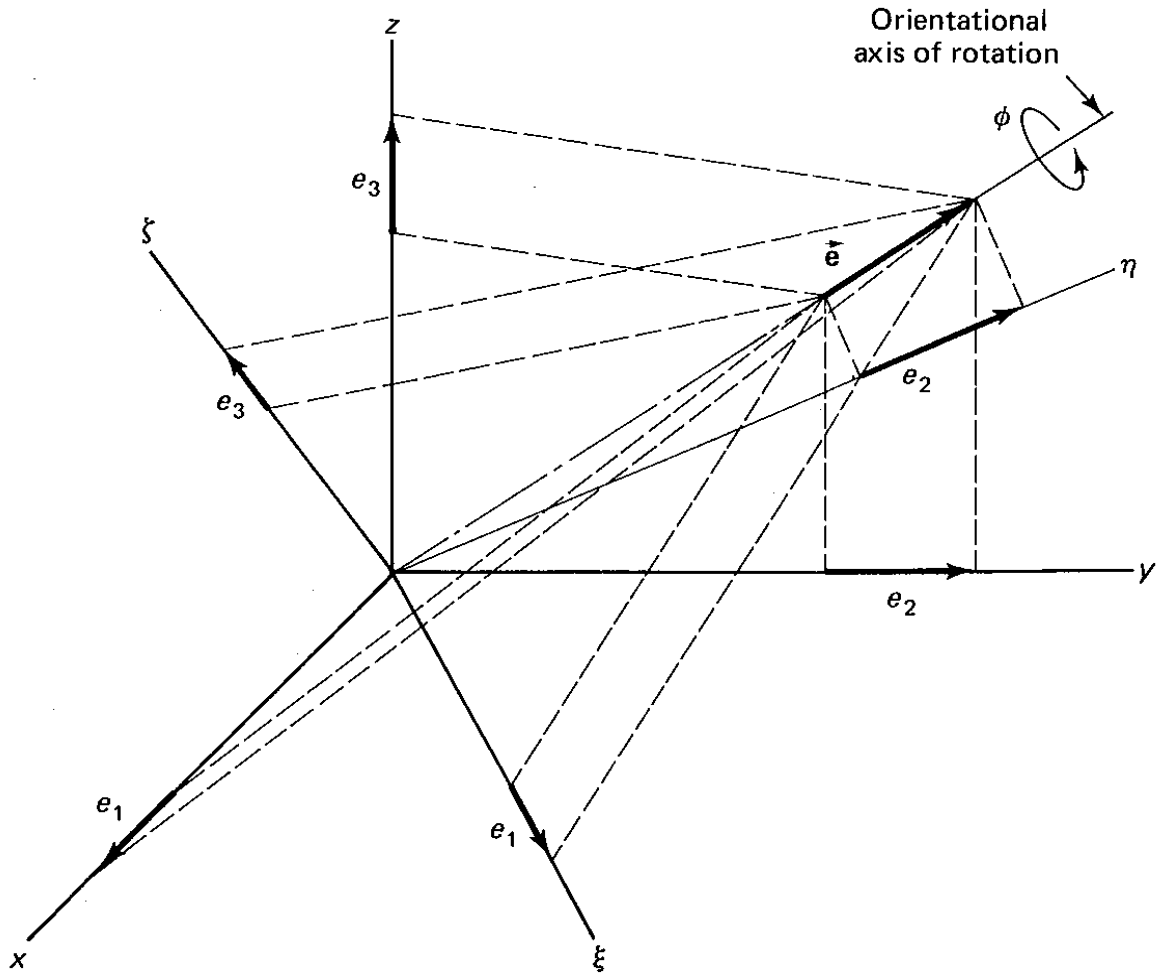

Figure 3.2.5 projection of vector $\vec{e}$ on ξ, η, ζ, x, y and z axes

The trace of **A,** denoted by $tr\mathbf{A}$**,** is defined as follows:

$$tr\mathbf{A} = a_{11} + a_{22} + a_{33} \tag{3.2.37}$$

From the transformation matrix of Eq. (3.2.31) it is found that

$$tr\mathbf{A} = 2\left(3e_0^2 + e_1^2 + e_2^2 + e_3^2\right) - 3$$

$$= 2\left(2e_0^2 + 1\right) - 3$$

$$= 4e_0^2 - 1 \tag{3.2.38}$$

Where, Eq. (3.2.33) has been employed. This equation can be written as

$$e_0^2 = \frac{tr\mathbf{A} + 1}{4} \tag{3.2.39}$$

Substituting this into the diagonal elements of **A** results in

$$a_{11} = \frac{2\left(e_0^2 + e_1^2\right) - 1}{4}$$

$$= 2\left(\frac{tr\mathbf{A} + 1}{4} + e_1^2\right) - 1$$

Or

$$e_1^2 = \frac{1 + 2a_{11} - tr\mathbf{A}}{4} \tag{3.2.40a}$$

And similarly,

$$e_2^2 = \frac{1 + 2a_{22} - tr\mathbf{A}}{4} \tag{3.2.40b}$$

and

$$e_3^2 = \frac{1 + 2a_{33} - tr\mathbf{A}}{4} \tag{3.2.40c}$$

In contrast to Euler and Bryant angles, or any other set of three rotational coordinates, there are no critical cases in which these inverse formulas are singular.

It is interesting and computationally important to note that Eqs. (3.2.39) and (3.2.40) determine only the magnitudes of the Euler parameters, in terms of only the diagonal elements of the direction cosine matrix **A**, off-diagonal terms must be used. The sign of e_0 may be selected as positive or negative. Subtracting symmetrically placed off-diagonal terms of matrix **A** in Eqs. (3.2.12) and (3.2.31) yields

$$\begin{aligned} a_{32} - a_{23} &= 4e_0e_1 \\ a_{13} - a_{31} &= 4e_0e_2 \\ a_{21} - a_{12} &= 4e_0e_3 \end{aligned} \tag{3.2.41}$$

or

$$e_1 = \frac{a_{32} - a_{23}}{4e_0}$$

$$e_2 = \frac{a_{13} - a_{31}}{4e_0}$$

$$e_3 = \frac{a_{21} - a_{12}}{4e_0} \tag{3.2.42}$$

If the sign of e_0 is inverted, the signs of e_1, e_2, and e_3 are inverted also. Changing the signs of all four parameters does not influence the transformation matrix, since the matrix is quadratic. To find the algebraic sign of e_1, e_2, and e_3, symmetrically placed off-diagonal terms of matrix **A** are added to obtain

$$\begin{aligned} a_{21} + a_{12} &= 4e_1e_2 \\ a_{31} + a_{13} &= 4e_1e_3 \\ a_{32} + a_{23} &= 4e_2e_3 \end{aligned} \tag{3.2.43}$$

At least one of the three Euler parameters e_1, e_2, and e_3 must be nonzero. Its sign may be selected as positive or negative. Then, Eq. (3.2.43) can be used to determine the magnitude and the sign of the other two parameters.

3.2.5 Identities with Euler Parameters

In this section, important formulas and identities between Euler parameters, their time derivatives, and their transformation matrices are derived. Derivation of some of the identities is shown below.

These identities are useful in the derivation of spatial constraint equations and equations of spatial motion.

The product $\mathbf{pp}^T$ is a 4×4 matrix that can be written in the form

$$\begin{aligned} \mathbf{pp}^T &= \begin{bmatrix} \mathbf{e}_0 \\ \mathbf{e} \end{bmatrix} \begin{bmatrix} \mathbf{e}_0, \mathbf{e}^T \end{bmatrix} \\ &= \begin{bmatrix} \mathbf{e}^2{}_0 & \mathbf{e}_0\mathbf{e}^T \\ \mathbf{e}_0\mathbf{e} & \mathbf{e}\mathbf{e}^T \end{bmatrix} \end{aligned} \tag{3.2.44}$$

From the algebraic vector operations, it is found that

$$\tilde{\mathbf{e}}\mathbf{e} = \mathbf{0} \tag{3.2.45}$$

and

$$\begin{aligned}\tilde{\mathbf{e}}\tilde{\mathbf{e}} &= \mathbf{e}\mathbf{e}^T - \mathbf{e}^T\mathbf{e}\mathbf{I} \\ &= \mathbf{e}\mathbf{e}^T - \left(1 - \mathbf{e}_0^2\right)\mathbf{I}\end{aligned} \tag{3.2.46}$$

A pair of 3×4 matrices **G** and **L** are defined as

$$\begin{aligned}\mathbf{G} &= \begin{bmatrix} -e_1 & e_0 & -e_3 & e_2 \\ -e_2 & e_3 & e_0 & -e_1 \\ -e_3 & -e_2 & e_1 & e_0 \end{bmatrix} \\ &= \left[-\mathbf{e}, \tilde{\mathbf{e}} + \mathbf{e}_0\mathbf{I}\right]\end{aligned} \tag{3.2.47}$$

and

$$\begin{aligned}\mathbf{L} &= \begin{bmatrix} -e_1 & e_0 & e_3 & -e_2 \\ -e_2 & -e_3 & e_0 & e_1 \\ -e_3 & e_2 & -e_1 & e_0 \end{bmatrix} \\ &= \left[-\mathbf{e}, -\tilde{\mathbf{e}} + \mathbf{e}_0\mathbf{I}\right]\end{aligned} \tag{3.2.48}$$

Each row of **G** and **L** is orthogonal to **p**; i.e.,

$$\begin{aligned}\mathbf{G}\mathbf{p} &= \left[-\mathbf{e}, \quad \tilde{\mathbf{e}} + \mathbf{e}_0\mathbf{I}\right]\begin{bmatrix} \mathbf{e}_0 \\ \mathbf{e} \end{bmatrix} \\ &= \left[-\mathbf{e}_0\mathbf{e} + \tilde{\mathbf{e}}\mathbf{e} + \mathbf{e}_0\mathbf{e}\right] = \mathbf{0}\end{aligned} \tag{3.2.49}$$

Where Eq. (3.2.45) has been used similarly,

$$\mathbf{L}\mathbf{p} = \mathbf{0} \tag{3.2.50}$$

A direct calculation reveals that the rows of **G** are orthogonal, as are also the rows of **L;** i.e.,

$$\mathbf{G}\mathbf{G}^T = \mathbf{I} \tag{3.2.51}$$

And

$$\mathbf{L}\mathbf{L}^T = \mathbf{I} \tag{3.2.52}$$

So that

$$\mathbf{G}\mathbf{G}^T = \mathbf{L}\mathbf{L}^T \tag{3.2.53}$$

However, $\mathbf{G}^T\mathbf{G}$ is of the form

$$\begin{aligned}
\mathbf{G}^T\mathbf{G} &= \begin{bmatrix} -\mathbf{e}^T \\ -\tilde{\mathbf{e}} + e_0\mathbf{I} \end{bmatrix} [-\mathbf{e}, \tilde{\mathbf{e}} + e_0\mathbf{I}] \\
&= \begin{bmatrix} \mathbf{e}^T\mathbf{e} & -\mathbf{e}^T\tilde{\mathbf{e}} - e_0\mathbf{e}^T \\ \tilde{\mathbf{e}}\mathbf{e} - e_0\mathbf{e} & -\tilde{\mathbf{e}}\tilde{\mathbf{e}} + e_0\tilde{\mathbf{e}} - e_0\tilde{\mathbf{e}} + e_0^2\mathbf{I} \end{bmatrix} \\
&= \begin{bmatrix} 1 - e_0^2 & -e_0\mathbf{e}^T \\ -e_0\mathbf{e} & -\mathbf{e}\mathbf{e}^T + \mathbf{I} \end{bmatrix} \\
&= -\begin{bmatrix} e_0^2 & e_0\mathbf{e}^T \\ e_0\mathbf{e} & \mathbf{e}\mathbf{e}^T \end{bmatrix} + \mathbf{I}^* \\
&= -\mathbf{p}\mathbf{p}^T + \mathbf{I}^*
\end{aligned} \tag{3.2.54}$$

Where Eq. (3.2.46) has been used and $\mathbf{I}^*$ is the 4×4 identity matrix. Similarly, it can be shown that

$$\mathbf{L}^T\mathbf{L} = -\mathbf{p}\mathbf{p}^T + \mathbf{I}^* \tag{3.2.55}$$

So that

$$\mathbf{G}^T\mathbf{G} = \mathbf{L}^T\mathbf{L} \tag{3.2.56}$$

A very interesting relationship can be found by evaluating the matrix product $\mathbf{G}\mathbf{L}^T$:

$$\begin{aligned}
\mathbf{G}\mathbf{L}^T &= \left[-\mathbf{e}, \quad \tilde{\mathbf{e}} + \mathbf{e}_0\mathbf{I}\right] \begin{bmatrix} -\mathbf{e}^T \\ \mathbf{e} + \mathbf{e}_0\mathbf{I} \end{bmatrix} \\
&= \mathbf{e}\mathbf{e}^T + \left(\tilde{\mathbf{e}} + \mathbf{e}_0\mathbf{I}\right)\left(\tilde{\mathbf{e}} + \mathbf{e}_0\mathbf{I}\right) \\
&= \left(2\mathbf{e}^2{}_0 - 1\right)\mathbf{I} + 2\left(\mathbf{e}\mathbf{e}^T + \mathbf{e}_0\tilde{\mathbf{e}}\right)
\end{aligned} \tag{3.2.57}$$

Comparing Eq. (3.2.57) with the transformation matrix **A** of Eq. (3.2.30) reveals that

$$\mathbf{A} = \mathbf{G}\mathbf{L}^T \tag{3.2.58}$$

Equation (3.2.58) demonstrates that the quadratic transformation matrix **A** can be treated as the results of two successive linear transformations. This is one of the most useful relationships between the **G** and **L** matrices and is a powerful property of Euler parameters.

The first and second time derivatives of Eq. (3.2.33) yields

$$\mathbf{p}^T\dot{\mathbf{p}} = \dot{\mathbf{p}}^T\mathbf{p} = \mathbf{0} \tag{3.2.59}$$

Similarly, the first time derivatives of Eq. (3.2.49) and (3.2.50) result in the identities

$$\mathbf{G}\dot{\mathbf{p}} = -\dot{\mathbf{G}}\mathbf{p} \tag{3.2.60}$$

and

$$\mathbf{L}\dot{\mathbf{p}} = -\dot{\mathbf{L}}\mathbf{p} \tag{3.2.61}$$

The product $\dot{\mathbf{G}}\dot{\mathbf{P}}$ may be calculated, using Eq. (3.2.47), as follows:

$$\dot{\mathbf{G}}\dot{\mathbf{p}} = \begin{bmatrix} -\dot{\mathbf{e}}, & \tilde{\dot{\mathbf{e}}} + \dot{\mathbf{e}}_0\mathbf{I} \end{bmatrix} \begin{bmatrix} \dot{\mathbf{e}}_0 \\ \dot{\mathbf{e}} \end{bmatrix}$$

$$= -\dot{\mathbf{e}}_0\dot{\mathbf{e}} + \dot{\mathbf{e}}_0\dot{\mathbf{e}} + \tilde{\dot{\mathbf{e}}}\dot{\mathbf{e}} = \mathbf{0} \tag{3.2.62}$$

Since the vector product of $\dot{\mathbf{e}}$ by itself is zero, similarly,

$$\dot{\mathbf{L}}\mathbf{p} = \mathbf{0} \tag{3.2.63}$$

Employing the algebraic vector operations with Eqs.(3.2.47) and (3.2.48), to show that

$$\mathbf{G}\dot{\mathbf{L}}^T = \dot{\mathbf{G}}\mathbf{L}^T \tag{3.2.64}$$

The time derivative of Eq.(3.2.58) yields

$$\dot{\mathbf{A}} = \dot{\mathbf{G}}\mathbf{L}^T + \mathbf{G}\dot{\mathbf{L}}^T = 2\mathbf{G}\dot{\mathbf{L}}^T$$

$$= 2\dot{\mathbf{G}}\mathbf{L}^T \tag{3.2.65}$$

The product $\mathbf{G}\dot{\mathbf{P}}$ can be expanded as follows

$$\mathbf{G}\dot{\mathbf{p}} = \begin{bmatrix} -\mathbf{e}, & \tilde{\mathbf{e}} + \mathbf{e}_0\mathbf{I} \end{bmatrix} \begin{bmatrix} \dot{\mathbf{e}}_0 \\ \dot{\mathbf{e}} \end{bmatrix}$$

$$= -\dot{\mathbf{e}}_0\mathbf{e} + \tilde{\mathbf{e}}\dot{\mathbf{e}} + \mathbf{e}_0\dot{\mathbf{e}} \tag{3.2.66}$$

Transforming both sides of the equation to skew- symmetric matrices, by the operation shown below

$$\tilde{\mathbf{a}} = \begin{bmatrix} 0 & -a_3 & a_2 \\ a_3 & 0 & -a_1 \\ -a_2 & a_1 & 0 \end{bmatrix} \tag{3.2.67}$$

Yields;

$$
\begin{aligned}
\widetilde{\dot{\mathbf{G}}}\mathbf{p} &= -\dot{e}_0\tilde{\mathbf{e}} + \widetilde{\dot{\mathbf{e}}}\tilde{\mathbf{e}} + e_0\tilde{\dot{\mathbf{e}}} \\
&= -\dot{e}_0\tilde{\mathbf{e}} + \tilde{\mathbf{e}}\tilde{\dot{\mathbf{e}}} - \tilde{\dot{\mathbf{e}}}\tilde{\mathbf{e}} + e_0\tilde{\dot{\mathbf{e}}} \\
&= -\dot{e}_0\tilde{\mathbf{e}} + \tilde{\mathbf{e}}\tilde{\dot{\mathbf{e}}} - \mathbf{e}\dot{\mathbf{e}}^T + \dot{\mathbf{e}}^T\mathbf{e}\mathbf{I} + e_0\tilde{\dot{\mathbf{e}}} \\
&= -\dot{e}_0\tilde{\mathbf{e}} + \tilde{\mathbf{e}}\tilde{\dot{\mathbf{e}}} - \mathbf{e}\dot{\mathbf{e}}^T - e_0\dot{e}_0\mathbf{I} + e_0\tilde{\dot{\mathbf{e}}} \\
&= [\mathbf{e}, -\tilde{\mathbf{e}} - e_0\mathbf{I}]\begin{bmatrix} -\dot{\mathbf{e}}^T \\ -\tilde{\dot{\mathbf{e}}} + \dot{e}_0\mathbf{I} \end{bmatrix} \\
&= -\mathbf{G}\dot{\mathbf{G}}^T
\end{aligned}
\tag{3.2.68}
$$

Where, the two equations (3.2.69a) and (3.2.69b) with the identity $e_0\dot{e}_0 + \mathbf{e}^T\dot{\mathbf{e}} = 0$ have been used.

$$
\widetilde{\mathbf{a}}\widetilde{\mathbf{b}} = \mathbf{b}\mathbf{a}^T - \mathbf{a}^T\mathbf{b}\mathbf{I} \tag{3.2.69a}
$$

$$
\dot{(\widetilde{\mathbf{a}}\widetilde{\mathbf{b}})} = \widetilde{\dot{\mathbf{a}}}\widetilde{\mathbf{b}} - \widetilde{\mathbf{b}}\widetilde{\dot{\mathbf{a}}} \tag{3.2.69b}
$$

Where, $\mathbf{a}$ and $\mathbf{b}$ are arbitrariy vectors.

Similarly,

$$
\widetilde{\dot{\mathbf{L}}}\mathbf{p} = \mathbf{L}\dot{\mathbf{L}}^T \tag{3.2.70}
$$

Two more identities can be derived using Eq. (3.2.60), (3.2.61), (3.2.68), and (3.2.70):

$$
\mathbf{G}\dot{\mathbf{G}}^T = -\dot{\mathbf{G}}\mathbf{G}^T \tag{3.2.71}
$$

$$
\mathbf{L}\dot{\mathbf{L}}^T = -\dot{\mathbf{L}}\mathbf{L}^T \tag{3.2.72}
$$

Furthermore, the time derivative of Eq. (3.2.59) results in

$$
\mathbf{p}^T\ddot{\mathbf{p}} + \dot{\mathbf{p}}^T\dot{\mathbf{p}} = \mathbf{0} \tag{3.2.73}
$$

The time derivative of Eq. (3.2.65) results in

$$
\begin{aligned}
\ddot{\mathbf{A}} &= 2\dot{\mathbf{G}}\dot{\mathbf{L}}^T + 2\mathbf{G}\ddot{\mathbf{L}}^T \\
&= 2\dot{\mathbf{G}}\dot{\mathbf{L}}^T + 2\ddot{\mathbf{G}}\mathbf{L}^T
\end{aligned}
\tag{3.2.74}
$$

From which it is seen that

$$
\ddot{\mathbf{G}}\mathbf{L}^T = \mathbf{G}\ddot{\mathbf{L}}^T \tag{3.2.75}
$$

3.2.6 The Concept of Angular Velocity

Consider the $\xi\eta\zeta$ coordinate system shown in Fig. (3.2.6), with its origin constrained to the origin of the non-rotating **xyz** coordinate system, but otherwise free to rotate. The global location of a point **P** that is fixed in the $\xi\eta\zeta$ coordinate system is given by the equation

$$\mathbf{s}^P = \mathbf{A}\mathbf{s}'^P \tag{3.2.76}$$

Differentiating this equation with respect to time yield

$$\dot{\mathbf{s}}^P = \dot{\mathbf{A}}\mathbf{s}'^P + \mathbf{A}\dot{\mathbf{s}}'^P \tag{3.2.77}$$

Since $\vec{s}$ is fixed in the $\xi\eta\zeta$ axes, $\dot{s}'^P = 0$ and therefore

$$\dot{\mathbf{s}}^P = \dot{\mathbf{A}}\mathbf{s}'^P \tag{3.2.78}$$

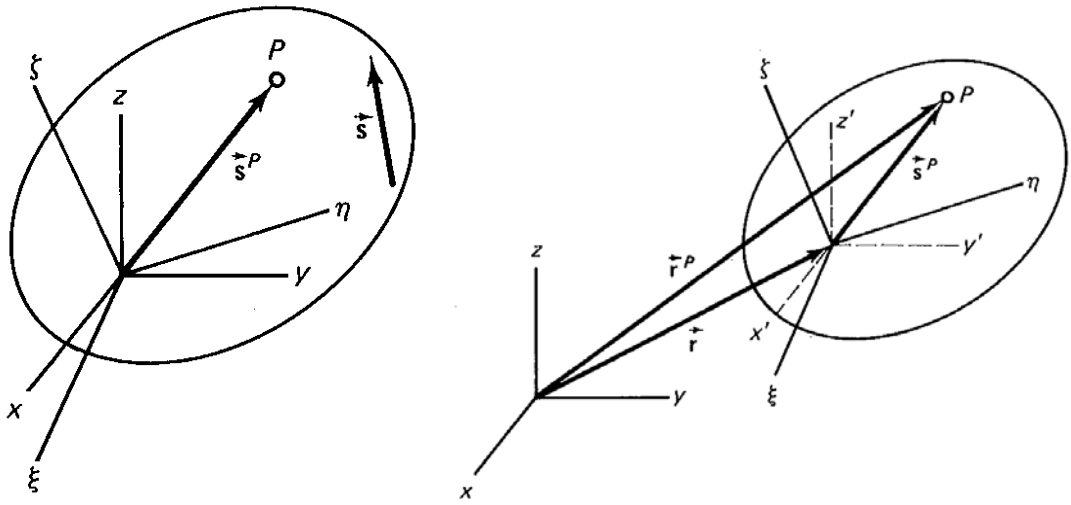

(b)

Figure 3.2.6 (a) rotating $\xi\eta\zeta$ coordinate system, (b) rotating and translating $\xi\eta\zeta$ coordinate system

Two linear relationships between $\dot{\mathbf{A}}$ and **A** may be expressed as

$$\dot{\mathbf{A}} = \Omega\mathbf{A} \tag{3.2.79}$$

Or

$$\dot{\mathbf{A}} = \mathbf{A}\Omega' \tag{3.2.80}$$

Where Ω and Ω' are two 3x3 coefficient matrices.

Differentiating the identity $\mathbf{A}^T\mathbf{A} = \mathbf{I}$ with respect to time yields

$$\dot{\mathbf{A}}^T\mathbf{A} + \mathbf{A}^T\dot{\mathbf{A}} = \mathbf{0} \tag{3.2.81a}$$

Substituting Eq. (3.2.79) into Eq. (3.2.81a) results in

$$\mathbf{A}^T\Omega^T\mathbf{A} + \mathbf{A}^T\Omega\mathbf{A} = \mathbf{0} \tag{3.2.81b}$$

Premultiplying Eq. (3.2.81b) by $\mathbf{A}$ and then postmultiplying the result by $\mathbf{A}^T$ yield $\Omega^T + \Omega = 0$, or

$$\Omega = -\Omega^T \tag{3.2.82}$$

Equation (3.2.82) indicates that Ω is a skew-symmetric matrix. Assume that Ω is composed of the elements of a 3-vector ω so that $\Omega = \tilde{\omega}$ .Then Eq. (3.2.79) becomes

$$\dot{\mathbf{A}} = \tilde{\omega}\mathbf{A} \tag{3.2.83}$$

Similarly, substituting Eq. (3.2.80) into Eq. (3.2.81a) results in

$$\Omega'^T\mathbf{A}^T\mathbf{A} + \mathbf{A}^T\mathbf{A}\Omega' = \mathbf{0} \tag{3.2.84}$$

Or

$$\Omega' = -\Omega'^T \tag{3.2.85}$$

Therefore Ω' is also a skew-symmetric matrix. Assume that Ω' is composed of the elements of a 3-vector ω' so that $\Omega' = \tilde{\omega}'$ .Then Eq. (3.2.80) becomes

$$\dot{\mathbf{A}} = \mathbf{A}\tilde{\omega}' \tag{3.2.86}$$

Comparing Eq. (3.2.83) and Eq. (3.2.86) gives

$$\tilde{\omega}\mathbf{A} = \mathbf{A}\tilde{\omega}' \tag{3.2.87}$$

Therefore, Ω and Ω' are the global and local components of the same vector $\vec{\omega}$ .The vector $\vec{\omega}$ is defined as the angular velocity of the $\xi\eta\zeta$ coordinate system. The components of vector $\vec{\omega}$ may be expressed as

$$\omega = \begin{bmatrix}\omega_{(x)} & \omega_{(y)} & \omega_{(z)}\end{bmatrix}^T \tag{3.2.88}$$

or

$$\omega' = \begin{bmatrix}\omega_{(\xi)} & \omega_{(\eta)} & \omega_{(\zeta)}\end{bmatrix}^T \tag{3.2.89}$$

By substituting Eq. (3.2.83) in Eq. (3.2.78), it is found that

$$\dot{\mathbf{s}}^P = \tilde{\omega}\mathbf{A}\mathbf{s}'^P$$

$$= \tilde{\omega}\mathbf{s}^P \tag{3.2.90}$$

In vector form Eq. (3.2.90) is expressed as

$$\dot{\mathbf{s}}^P = \tilde{\omega} \times \vec{s}^P \tag{3.2.91}$$

For a $\xi\eta\zeta$ coordinate system that rotates and translates relative to the nonmoving **xyz** axes, the velocity of a point **P** that is fixed in the $\xi\eta\zeta$ system can be determined. As shown in Fig. (3.2.6b), we may employ a translating coordinate system such as $x'y'z'$ whose origin coincides with the origin of the $\xi\eta\zeta$ coordinate axes. The $\xi\eta\zeta$ system rotates relative to the $x'y'z'$ system, which only translates relative to the **xyz** system. Point **P** can be located in the **xyz** system by the relation

$$\mathbf{r}^P = \mathbf{r} + \mathbf{s}^P \tag{3.2.92}$$

The time derivative of this equation gives the velocity of point **P** as

$$\begin{aligned} \dot{\mathbf{r}}^P &= \dot{\mathbf{r}} + \dot{\mathbf{s}}^P \\ &= \dot{\mathbf{r}} + \tilde{\omega}\vec{s}^P \end{aligned} \tag{3.2.93}$$

3.2.7 Time Derivative of Euler Parameters

Identities between the time derivatives of Euler parameters and angular velocity vectors Ω and Ω', are going to be derived in this section. These identities can be used for conversion from Ω or Ω' to $\dot{\mathbf{p}}$ and vice versa.

Postmultiplying Eq. (3.2.83) by $\mathbf{A}^T$ yields

$$\dot{\mathbf{A}}\mathbf{A}^T = \tilde{\omega} \tag{3.2.94}$$

From Eqs.(3.2.65) and (3.2.58), Eq. (3.2.94) becomes $\mathbf{2\dot{G}L}^T\mathbf{LG}^T = \tilde{\omega}$, which, upon application of Eq. (3.2.55) and (3.2.49), results in $\mathbf{2\dot{G}G}^T = \tilde{\omega}$ .Finally, substituting Eqs. (3.2.71) and (3.2.68) into this last equation gives $2\mathbf{G}\tilde{\dot{\mathbf{p}}} = \tilde{\omega}$, or

$$\omega = 2\mathbf{G}\dot{\mathbf{p}} \tag{3.2.95}$$

In expanded form,

$$\begin{bmatrix} \omega_{(x)} \\ \omega_{(y)} \\ \omega_{(z)} \end{bmatrix} = 2 \begin{bmatrix} -e_1 & e_0 & -e_3 & e_2 \\ -e_2 & e_3 & e_0 & -e_1 \\ -e_3 & -e_2 & e_1 & e_0 \end{bmatrix} \begin{bmatrix} \dot{e}_0 \\ \dot{e}_1 \\ \dot{e}_2 \\ \dot{e}_3 \end{bmatrix} \tag{3.2.96}$$

Premultiplying Eq. (3.2.95) by $\mathbf{G}^T$ yields $\mathbf{G}^T \omega = \mathbf{2G}^T \mathbf{G}\dot{\mathbf{p}}$, which upon application of Eqs. (3.2.54) and (3.2.59), results in the inverse transformation

$$\dot{\mathbf{p}} = \frac{1}{2} \mathbf{G}^T \omega \tag{3.2.97}$$

Similarly, it can be shown that

$$\omega' = 2\mathbf{L}\dot{\mathbf{p}} \tag{3.2.98}$$

In expanded form, Eq. (3.2.98) is

$$\begin{bmatrix} \omega_{(\xi)} \\ \omega_{(\eta)} \\ \omega_{(\zeta)} \end{bmatrix} = 2 \begin{bmatrix} -e_1 & e_0 & e_3 & -e_2 \\ -e_2 & -e_3 & e_0 & e_1 \\ -e_3 & -e_2 & -e_1 & e_0 \end{bmatrix} \begin{bmatrix} \dot{e}_0 \\ \dot{e}_1 \\ \dot{e}_2 \\ \dot{e}_3 \end{bmatrix} \tag{3.2.99}$$

The inverse transformation of Eq. (3.2.98) is found to be

$$\dot{\mathbf{p}} = \frac{1}{2} \mathbf{L}^T \omega' \tag{3.2.100}$$

Differentiating Eq. (3.2.95) with respect to time yields $\dot{\omega} = \mathbf{2G}\ddot{\mathbf{p}} + \mathbf{2}\dot{\mathbf{G}}\dot{\mathbf{p}}$, which, upon application of Eq. (3.2.62), becomes

$$\dot{\omega} = 2\mathbf{G}\ddot{\mathbf{p}} \tag{3.2.101}$$

Similarly, differentiating Eq. (3.2.98) with respect to time and using Eq. (3.2.63) results in

$$\dot{\omega}' = 2\mathbf{L}\ddot{\mathbf{p}} \tag{3.2.102}$$

Vectors $\dot{\omega}$ and $\dot{\omega}'$ are the global and local components of a vector $\vec{\dot{\omega}}$ defined as the angular acceleration of the $\xi\eta\zeta$ coordinate system. It can be shown that the inverses of Eqs. (3.2.101) and (3.2.102) are

$$\ddot{\mathbf{p}} = \frac{1}{2} \mathbf{G}^T \dot{\omega} - \frac{1}{4} \left(\omega^T \omega \right) \mathbf{p} \tag{3.2.103}$$

Or

$$\ddot{\mathbf{p}} = \frac{1}{2}\mathbf{L}^T\dot{\omega}' - \frac{1}{4}\left(\omega'^T\omega'\right)\mathbf{p} \tag{3.2.104}$$

It is clear that $\omega^T\omega = \omega'^T\omega' = \omega^2$, where ω is the magnitude of $\vec{\omega}$. Furthermore, it can be shown that the scalar product $\omega^T\omega - \omega^2 = 0$ yields

$$4\dot{\mathbf{p}}^T\dot{\mathbf{p}} - \omega^2 = \mathbf{0} \tag{3.2.105}$$

3.3 Kinematic Constraints

The multibody systems are made of two major groups namely links and kinematic joints. Joints are represented by a set of kinematic constraints. The functionality of a kinematic joint relays upon the relative motion allowed between the connected components, which implies the existence of a gap, that is, a clearance between the mating parts, and thus surface contact, shock transmission and the development of different regimes of friction and wear.

A kinematic joint imposes certain conditions on the relative motion between the adjacent bodies that it comprises. When these conditions are expressed in analytical form, they are called constraint equations. In a simple way, a constraint is any condition that reduces the number of degrees of freedom in a system.

Constraint equations are assigned a superscript with two indices in this thesis. The first index denotes the type of constraint, and the second index defines the number of independent equations in the expression.

The kinematic joint in the multibody system can be described by Algebraic constraint equations, denoted as **Φ.** In the proceeding sections, constraint equations of some of commonly used lower-pair kinematic joints are derived. The purpose here is to derive analytical conditions with which to define a library or kinematic connections for the mechanism designed in this paper. For the purpose of this thesis work, only the spherical, revolute and translational kinematic joints are discussed in detail in the proceeding sections.

3.3.1 Spherical Joint

Spherical joint, also known as by ball and socket joint, illustrated in Fig. (3.3.1), constrains the relative translations between two adjacent bodies *i* and *j* , allowing only three relative rotations. Therefore, the center of the spherical joint, point **P**, has constant coordinates with

respect to any of the local coordinates systems (in the Figure 3.3.1 below, $\xi_i\eta_i\zeta_i$ and $\xi_j\eta_j\zeta_j$) of the connected bodies, *i.e.*, a spherical joint is defined by the condition that the point P_i on body i coincides with the point P_j on body j. There are three algebraic equations for the joint; they can be found from the vector equation $\mathbf{r}_i + \mathbf{s}_i^P - \mathbf{s}_j^P - \mathbf{r}_j = 0$, as follows

$$\Phi^{(s,3)} \equiv \mathbf{r}_i + \mathbf{A}_i\mathbf{s}_i'^P - \mathbf{A}_j\mathbf{s}_j'^P - \mathbf{r}_j = 0 \tag{3.3.1}$$

Where, $\mathbf{A}_i$ and $\mathbf{A}_j$ are the transformation matrices.

There are three relative degrees of freedoms between two bodies that are connected by a spherical joint.

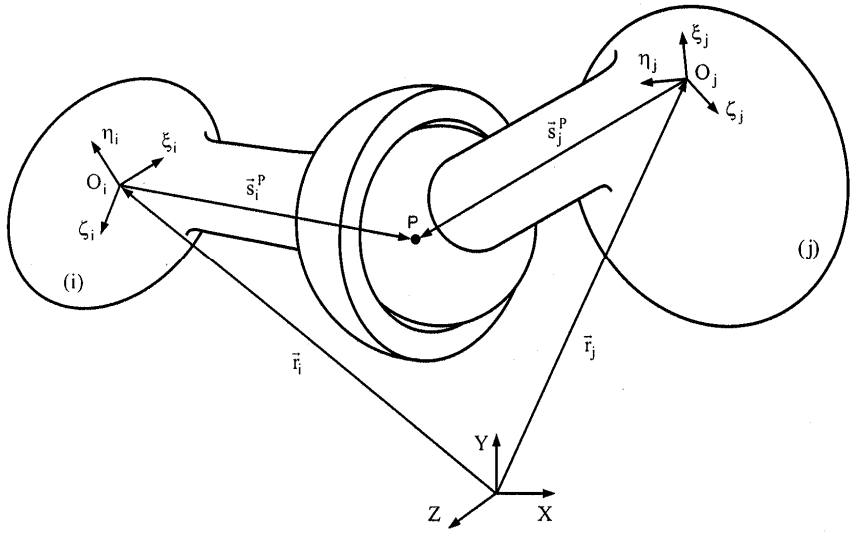

Figure 3.3.1 A spherical joint

3.3.2 Revolute Joint

A three-dimensional revolute between bodies i and j, shown in Fig.(3.3.2) is built with a journal-bearing that allows a relative rotation about a common axis, but precludes relative translation along this axis. Any point located on the revolute joint axis has constant coordinates, when expressed in the local coordinate systems of the connected bodies. Thus, Eq. (3.3.1) can be imposed on an arbitrary point **P** on the joint axis. Two other points Q_i on body i and Q_j on body j are also arbitrarily chosen on the joint axis. It is clear that vectors $\mathbf{s}_i$ and $\mathbf{s}_j$ must remain parallel. Therefore, there are five constraint equations for a three-dimensional revolute joint [**21**].

$$\Phi^{(r,5)} = \begin{cases} \mathbf{r}_i + \mathbf{A}_i \mathbf{s}_i^{'P} - \mathbf{r}_j - \mathbf{A}_j \mathbf{s}_j^{'P} = 0 \\ \widetilde{\mathbf{s}}_i \mathbf{s}_j = 0 \end{cases} \tag{3.3.2}$$

It is worth nothing that the cross product in Eq. (3.3.2) only has two independent constraints, being the third a linear dependency of the first two. The five scalar constraint equations yield only one relative degree of freedom for this joint, that is, rotation about the common axis of the revolute joint. There is only one relative degree of freedom between two bodies connected by a revolute joint.

The constraint formulation for a revolute joint may be simplified for special cases. Consider as an example the configuration in Fig. (3.3.2b), where the body-fixed coordinates are placed in such a way that the ζ_i and ζ_j axes are parallel to the revolute-joint axis. In such a case, the two unit vectors $\mathbf{u}_i^{'} = [0, \quad 0, \quad 1]^T$ and $\mathbf{u}_j^{'} = [0, \quad 0, \quad 1]^T$ must remain parallel at all times; i.e,

$$\Phi^{(p1,2)} \equiv \widetilde{\mathbf{u}}_i \mathbf{u}_j = 0 \tag{3.3.3}$$

This equation replaces the $\widetilde{\mathbf{s}}_i \mathbf{s}_j = 0$ constraints in Eq. (3.3.2). For this or other, similar special cases, only one point on the joint axis (point **P**) needs to be defined.

For the special case of Fig.(3.3.2b) below, another method can be used to keep the ζ_i and ζ_j axes parallel. Since these axes are parallel to the joint axis, the joint axis is the relative orientational axis of rotation [**7**].

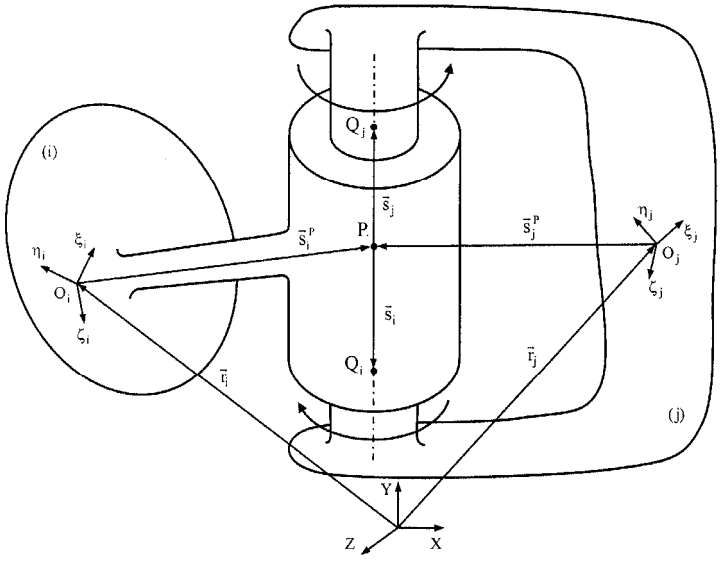

(a)

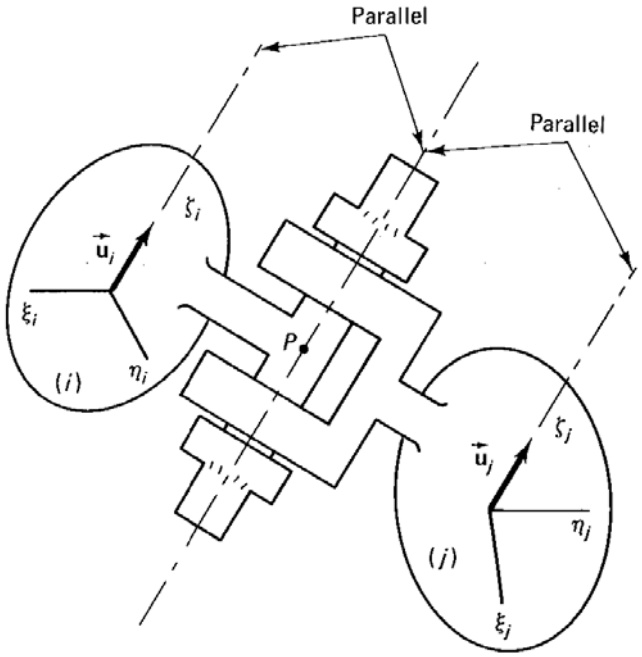

(b)

Figure 3.3.2 A revolute joint: (a) general case, (b) special case when the ζ_i axis, the ζ_j axis, and the joint axis are parallel.

3.3.3 Translational (Prismatic) Joint

A translational joint is similar to a cylindrical joint with the exception that the two bodies cannot rotate relative to each other. Therefore, the cylindrical vector, $\vec{\mathbf{h}}_i$ and $\vec{\mathbf{h}}_j$ on bodies i and j as shown in Fig. (3.3.3) must remain perpendicular. Therefore there are five constraint equations for a translational joint [**7**];

$$\begin{aligned} \Phi^{(p1,2)} &\equiv \tilde{\mathbf{s}}_i \mathbf{s}_j = 0 \\ \Phi^{(p2,2)} &\equiv \tilde{\mathbf{s}}_i \mathbf{d} = 0 \\ \Phi^{(n1,1)} &\equiv \mathbf{h}_i^T \mathbf{h}_j = 0 \end{aligned} \tag{3.3.4}$$

The vectors $\vec{\mathbf{h}}_i$ and $\vec{\mathbf{h}}_j$ are located so they are perpendicular to the line of translation. The relative number of degrees of freedom between two bodies that are connected by a translational joint is one.

If $\xi_i\eta_i\zeta_i$ and $\xi_j\eta_j\zeta_j$ are parallel, and ζ_i, and ζ_j are also parallel to the joint axis, then the constraint $\mathbf{h}_i^T\mathbf{h}_j = 0$ of Eq. (3.3.4) can be replaced by similar constraint, but without defining any additional points such as R_i and R_j. Since the ξ_i axis is perpendicular to the η_j axis, then unit vector on these axes must remain perpendicular at all times.

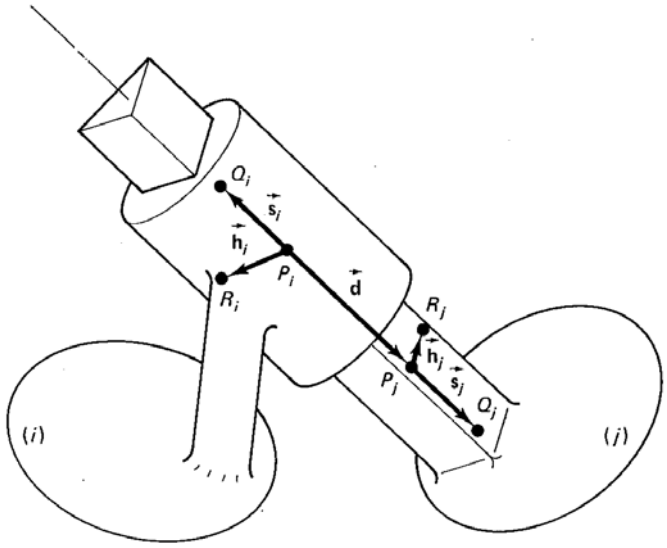

Figure 3.3.3 A translational joint

3.4 Formulation of Equations of Motion for spatial Multibody Systems

3.4.1 Introduction

In order to analyze the dynamic response of a constrained multibody system, it is first necessary to formulate the equations of motion that govern its behavior. The kinematic joints control the relative motion between the bodies, while the force elements represent the internal forces that develop between bodies due to their relative motion. The forces applied over the system components may be the result of springs, dampers, actuators or external forces. The kinematic constraints considered in this work are assumed to be holonomic, arising from geometric constraints on the generalized coordinates. Holonomic constraints, also called geometric restrictions, are algebraic equations imposed to the system that are expressed as functions of the displacement and, possibly, time. If the time *t* does not appear explicitly in the constraint equation, then the system is said to be scleronomic. A simple example of scleronomic constraint equations is the revolute joint between any two bodies in a slider-crank mechanism.

Otherwise, when the constraint is holonomic and *t* appears explicitly, the system is said to be rheonomic. When the constraint equation contains inequalities or relations between velocity components that are not integrable in closed form, they are said to be nonholonomic constraints. Nonholonomic constraints are also still kinematic constraints since they impose restrictions to the velocity and acceleration (Nikravesh, 1988; Shabana, 1989).

3.4.2 Vector of Coordinates

Let Fig. (3.4.1) represents a rigid body *i* to which a body-fixed coordinate system $[\xi\eta\zeta]_i$ is attached at its center of mass. When Cartesian coordinates are used, the position and orientation of the rigid body must be defined by a set of translational and rotational coordinates. The position of the body with respect to global coordinate system **XYZ** is defined by the coordinate vector $\mathbf{r}_i = [x \quad y \quad z]_i^T$ that represents the location of the local reference frame $[\xi\eta\zeta]_i$. The orientation of the body is described by the rotational coordinate's vector $\mathbf{p}_i = [e_0 \quad e_1 \quad e_2 \quad e_3]_i^T$, which includes the Euler parameters for the rigid body [**7**]. Therefore, the vector of coordinates that describes completely the rigid body *i* is,

$$\mathbf{q}_i = \begin{bmatrix} \mathbf{r}_i^T & \mathbf{p}_i^T \end{bmatrix}_i^T \tag{3.4.1}$$

or

$$\mathbf{q}_i = [\mathbf{q}_1^T, \mathbf{q}_2^T, ..., \mathbf{q}_{nb}^T]_i^T \tag{3.4.2}$$

Where,

$$\mathbf{r}_i = [\mathbf{r}_1^T, \mathbf{r}_2^T, ..., \mathbf{r}_{nb}^T]_i^T \tag{3.4.3a}$$

$$\mathbf{p}_i = [\mathbf{p}_1^T, \mathbf{p}_2^T, ..., \mathbf{p}_{nb}^T]_i^T \tag{3.4.3b}$$

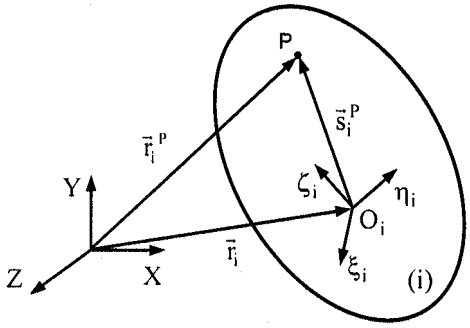

Figure 3.4.1 Definition of the Cartesian coordinates for a rigid body

According to this definition, a spatial multibody system with *nb* bodies is described by a set of dependent vector of generalized coordinates.

A point **P** on body i can be defined by position vector $\mathbf{s}_i^P$, which represents the location of point **P** with respect to the body-fixed reference frame $[\xi\eta\zeta]_i$, and by the global position vector $\mathbf{r}_i$, that is,

$$\mathbf{r}_i^P = \mathbf{r}_i + \mathbf{s}_i^P = \mathbf{r}_i + \mathbf{A}_i \mathbf{s}_i'^P \tag{3.4.4}$$

Where, $\mathbf{A}_i$ is the transformation matrix for body i that defines the orientation of the referential $[\xi\eta\zeta]_i$ with respect to the referential frame **XYZ**. The transformation matrix is expressed as function of the four Euler parameters as [**7**], $\mathbf{A}_i$ becomes

$$\mathbf{A}_i = 2\begin{bmatrix} e_0^2 + e_1^2 - \frac{1}{2} & e_1e_2 - e_0e_3 & e_1e_3 + e_0e_2 \\ e_1e_2 + e_0e_3 & e_0^2 + e_2^2 - \frac{1}{2} & e_2e_3 - e_0e_1 \\ e_1e_3 - e_0e_2 & e_2e_3 + e_0e_1 & e_0^2 + e_3^2 - \frac{1}{2} \end{bmatrix} \tag{3.4.5}$$

Notice that the vector $\mathbf{s}_i^P$ is expressed in global coordinates whereas the vector $\mathbf{s}_i'^P$ is defined in the body i fixed coordinate system. The velocities and accelerations of body i use the angular velocities ω_i' and accelerations $\dot{\omega}_i'$ instead of the time derivatives of the Euler parameters, which simplifies the mathematical formulation and do not have critical singular cases (Nikravesh and Chung, 1982). When Euler parameters are employed as rotational coordinates, the relation between their time derivatives $\dot{\mathbf{p}}_i$, and the angular velocities is expressed by[**7**],

$$\dot{\mathbf{p}}_i = \frac{1}{2}\mathbf{L}^T \omega'_i \tag{3.4.6}$$

Where the auxiliary matrix **L** is function of Euler parameters [**7**],

$$\mathbf{L} = \begin{bmatrix} -e_1 & e_0 & e_3 & -e_2 \\ -e_2 & -e_3 & e_0 & e_1 \\ -e_3 & e_2 & -e_1 & e_0 \end{bmatrix} \tag{3.4.7}$$

The velocities and accelerations of body i are given by vectors,

$$\dot{\mathbf{q}}_i = \begin{bmatrix} \dot{\mathbf{r}}_i^T & \omega_i'^T \end{bmatrix}_i^T \tag{3.4.8}$$

$$\ddot{\mathbf{q}}_i = \begin{bmatrix} \ddot{\mathbf{r}}_i^T & \dot{\omega}_i'^T \end{bmatrix}_i^T \tag{3.4.9}$$

3.4.3 Vector of Forces

The derivation of equations to calculate the forces (or moments) of the force elements in spatial motion is identical to the planar motion. If the resultant force and moment acting on body i are $\vec{f}_i$ and $\vec{n}_i$, they must be transformed into the coordinate system in which the equations of motion are derived. For the translational equations of motion shown in Fig.(3.4.2) below, the force must be defined in terms of its **XYZ** components; i.e., $\mathbf{f}_i$.If the rotational equations of motion given by Eq.(3.4.10) are used, then the moment $\vec{n}_i$ must be defined in terms of its $\xi\eta\zeta$ components; i.e., **n**. . However, if Euler parameters are used and the equations of motion are expressed in terms of these coordinates, then the moment $\vec{n}_i$ must be transformed to a coordinate system associated with the Euler parameters.

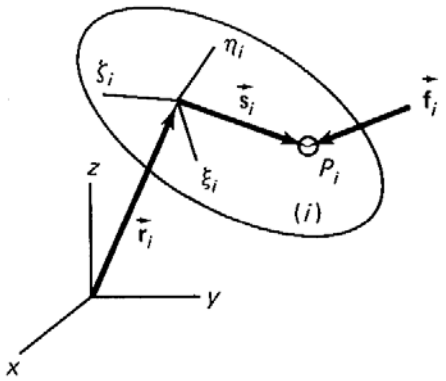

Figure 3.4.2 Applied force

It is possible to convert the three rotational equations of motion represented by

$$\mathbf{J}'_i\dot{\omega}'_i + \tilde{\omega}'_i\mathbf{J}'_i\omega'_i = \mathbf{n}'_i \tag{3.4.10}$$

to four rotational equations of motion associated with the Euler parameters. In this case the moment $\vec{n}_i$ must be expressed in terms of four components denoted by:

$$\mathbf{n}_i^* = 2L_i^T\mathbf{n}'_i \tag{3.4.11}$$

The objective is to find the transformation between $\mathbf{n}'_i$ (or $\mathbf{n}_i$) and $\mathbf{n}_i^*$. As long as two vectors are described in the same coordinate system in which the vectors are described in the same coordinate system, their scalar product yields a scalar quantity independent of the coordinate system in which the vectors are expressed. In Eq. (3.4.11), $\mathbf{n}'_i$ is expressed in the same coordinate as ω'_i. When Euler parameters are used, the moment $\mathbf{n}_i^*$ must be expressed in the same coordinate system as $\dot{\mathbf{p}}_i$ .Hence,

$$\dot{\mathbf{p}}_i^T\mathbf{n}_i^* = \omega'^T_i\mathbf{n}'_i \tag{3.4.12}$$

If the global components of these vectors are considered, then Eq. (3.4.12) is also equal to $\omega_i^T\mathbf{n}_i$, and therefore it can be found that

$$\mathbf{n}_i^* = 2G_i^T\mathbf{n}_i \tag{3.4.13}$$

The inverse transformations are

$$\mathbf{n}_i' = \frac{1}{2} L_i \mathbf{n}_i^* \tag{3.4.14}$$

and

$$\mathbf{n}_i = \frac{1}{2} G_i \mathbf{n}_i^* \tag{3.4.15}$$

3.4.4 Equations of Motion for a Constrained Body

For a constrained mechanical system containing body i, it is assumed that there are m independent constraint equations,

$$\Phi(\mathbf{q},t) = \left[\Phi_1(\mathbf{q},t), \Phi_2(\mathbf{q},t), ..., \Phi_m(\mathbf{q},t)\right]^T = 0$$

or

$$\Phi(\mathbf{r},\mathbf{p},t) = \left[\Phi_1(\mathbf{r},\mathbf{p},t), \Phi_2(\mathbf{r},\mathbf{p},t), ..., \Phi_m(\mathbf{r},\mathbf{p},t)\right]^T = 0 \tag{3.4.16}$$

Where $\mathbf{q}$ contains the coordinates of all of the bodies in the system, including the coordinates of i:

$$\mathbf{q}_i = \begin{bmatrix} \mathbf{r}_i \\ \mathbf{p}_i \end{bmatrix} \tag{3.4.17}$$

The constraint reaction forces could be described in terms of the Jacobian matrix of the system and a vector of Lagrange multipliers:

$$\mathbf{g}^* = \Phi_{\mathbf{q}}^T \lambda \tag{3.4.18}$$

This equation was obtained with the assumption that the vectors of forces $\mathbf{g}$ and $\mathbf{g}^{(*)}$ were defined in a coordinate system consistent with $\mathbf{q}$.

The constrained translational equation of motion for body i can be written as:

$$\mathbf{N}_i \ddot{\mathbf{r}} = \mathbf{f}_i + \mathbf{f}_i^{(c)} \tag{3.4.19}$$

From Eq. (3.4.18) it is found that the joint reaction forces can be expressed in terms of the Jacobian matrix of the constraint equations and the vector of Lagrange multipliers as

$$\mathbf{f}_i^{(c)} = \Phi_{ri}^T \lambda \tag{3.4.20}$$

$$\mathbf{M}_i \ddot{\mathbf{r}} - \Phi_{ri}^T \lambda = \mathbf{f}_i \tag{3.4.21}$$

This represents the translational equations of motion for constrained body i.

Where $\mathbf{M_i}$ is the global mass matrix, containing the mass and moment of inertia of all bodies and $\ddot{\mathbf{r}}_i$ is the vector that contains the translational accelerations, $\mathbf{f}$ is the generalized force vector; a force vector that contains the external and Coriolis forces acting on the bodies of the system (which contains all external forces and moments), and $\mathbf{f}^{(c)}$ is the vector of constraint reaction equations. The rotational equations of motion for this body are derived in three forms.

Formulation I. Substitution of Eqs.(3.2.98) and (3.2.102) into Eq. (3.4.10) yield

$$2\mathbf{J}_i'\mathbf{L}_i\ddot{\mathbf{p}}_i + 4\mathbf{L}_i\dot{\mathbf{L}}_i^T\mathbf{J}_i'\mathbf{L}_i\dot{\mathbf{p}}_i = \mathbf{n}_i' \tag{3.4.22}$$

Premultiplying of this equation by $2\mathbf{L}_i^T$ gives

$$\mathbf{J}_i^*\ddot{\mathbf{p}}_i + 2\mathbf{L}_i^T\mathbf{L}_i\mathbf{H}_i\dot{\mathbf{p}}_i = \mathbf{n}_i^* \tag{3.4.23}$$

Where

$$\mathbf{J}_i^* = 4\mathbf{L}_i^T\mathbf{J}_i'\mathbf{L}_i \tag{3.4.24}$$

$$\mathbf{H}_i = 4\dot{\mathbf{L}}_i^T\mathbf{J}_i'\mathbf{L}_i \tag{3.4.25}$$

Using Eq. (3.2.59) and defining

$$\sigma_i = 8\dot{\mathbf{p}}_i^T\mathbf{L}_i^T\mathbf{J}_i'\mathbf{L}_i\dot{\mathbf{p}}_i \tag{3.4.26}$$

$$= -8\mathbf{p}_i^T\dot{\mathbf{L}}_i^T\mathbf{J}_i'\mathbf{L}_i\dot{\mathbf{p}}_i \tag{3.4.27}$$

Equation (3.4.23) can be written as

$$\mathbf{J}_i^*\ddot{\mathbf{p}}_i + \sigma_i\mathbf{p}_i + 2\mathbf{H}_i\dot{\mathbf{p}}_i = \mathbf{n}_i^* \tag{3.4.28}$$

This represents the rotational equations of motion in terms of $\ddot{\mathbf{p}}_i$ for unconstrained body. However, since the four Euler parameters are not independent, Eq. (3.2.73), i.e,

$$\mathbf{p}_i^T\ddot{\mathbf{p}} + \dot{\mathbf{p}}_i^T\dot{\mathbf{p}}_i = 0 \tag{3.4.29}$$

must be considered with Eq.(3.4.28).Equations (3.4.28) and (3.4.29) in matrix form are

$$\begin{bmatrix} \mathbf{J}^* & \mathbf{p} \\ \mathbf{p}^T & 0 \end{bmatrix}_i \begin{bmatrix} \ddot{\mathbf{p}} \\ \sigma \end{bmatrix}_i + \begin{bmatrix} 2\mathbf{H}\dot{\mathbf{p}} \\ \dot{\mathbf{p}}^T\dot{\mathbf{p}} \end{bmatrix}_i = \begin{bmatrix} \mathbf{n}^* \\ 0 \end{bmatrix}_i \tag{3.4.30}$$

The artificial variable σ_i was defined in such a way as to have an exact inverse to 5×5 matrix at the left in Eq. (3.4.30). In Eq. (3.4.28), σ_i can be interpreted as a Lagrange multiplier associated with the constraint equation $\mathbf{p}_i^T\mathbf{p}_i - 1 = 0$. The rotational equations of motion from Eq.(3.4.28) for a constrained body i are written as

$$\mathbf{J}_i^* \ddot{\mathbf{p}}_i + \sigma_i \mathbf{p}_i + 2\mathbf{H}_i\dot{\mathbf{p}}_i = \mathbf{n}_i^* + \mathbf{n}_i^{*(c)} \tag{3.4.31}$$

Since $\mathbf{n}_i^*$ and $\mathbf{n}_i^{*(c)}$ are described in the same coordinate system as $\mathbf{p}_i$, Eq. (3.4.20) yields

$$\mathbf{n}_i^{*(c)} = \Phi_{\mathbf{p}i}^T \lambda$$

Therefore,

$$\mathbf{J}_i^* \ddot{\mathbf{p}}_i + \sigma_i \mathbf{p}_i + 2\mathbf{H}_i\dot{\mathbf{p}}_i - \Phi_{\mathbf{p}i}^T \lambda = \mathbf{n}_i^* \tag{3.4.32}$$

Equations (3.4.32) and (3.4.29) are the rotational equations of motion for a constrained body.

Formulation II. Equation (3.4.22) for a constrained body is written as

$$2\mathbf{J}_i'\mathbf{L}_i\ddot{\mathbf{p}}_i + \mathbf{L}_i\mathbf{H}_i\dot{\mathbf{p}}_i = \mathbf{n}_i' + \mathbf{n}_i'^{(c)} \tag{3.4.33}$$

The transformation of moments is given by Eq.(3.4.14)as

$$\mathbf{n}_i'^{(c)} = \frac{1}{2}L_i\mathbf{n}_i^{*(c)}$$

$$= \frac{1}{2}L_i\Phi_{\mathbf{p}i}^T\lambda \tag{3.4.34}$$

Therefore,

$$2\mathbf{J}_i'\mathbf{L}_i\ddot{\mathbf{p}}_i + \mathbf{L}_i\mathbf{H}_i\dot{\mathbf{p}}_i - \frac{1}{2}\mathbf{L}_i\Phi_{\mathbf{p}i}^T\lambda = \mathbf{n}_i' \tag{3.4.35}$$

Equations (3.4.35) and (3.4.29) together can be used as the rotational equation of motion for a constrained body.

In Equations (3.4.22), the matrix $\mathbf{J}'$ is called the inertia tensor (inertia matrix) for the body given by

$$\mathbf{J}_i^{'} = \begin{bmatrix} \mathbf{J}_{\xi\xi} & \mathbf{J}_{\xi\eta} & \mathbf{J}_{\xi\zeta} \\ \mathbf{J}_{\eta\xi} & \mathbf{J}_{\eta\eta} & \mathbf{J}_{\eta\zeta} \\ \mathbf{J}_{\zeta\xi} & \mathbf{J}_{\zeta\eta} & \mathbf{J}_{\zeta\zeta} \end{bmatrix}_i \tag{3.4.36}$$

Formulation III. Equation (3.4.10) can be written for a constrained body as

$$\mathbf{J}_i^{'}\dot{\omega}_i^{'} + \tilde{\omega}_i^{'}\mathbf{J}_i^{'}\omega_i^{'} = \mathbf{n}_i^{'} + \mathbf{n}_i^{'(c)} \tag{3.4.37}$$

Or

$$\mathbf{J}_i^{'}\dot{\omega}_i^{'} + \tilde{\omega}_i^{'}\mathbf{J}_i^{'}\omega_i^{'} - \frac{1}{2}\mathbf{L}_i\Phi_{\mathbf{p}i}^{T}\lambda = \mathbf{n}_i^{'} \tag{3.4.38}$$

In this equation the constraint equations, and hence the Jacobian matrix, are expressed in terms of Euler parameters.

3.4.5 Formulation of Spatial Constrained Multi-body Systems

This section presents the formulation of the general equations of motion to the spatial dynamic analysis of multibody systems. Due to its simplicity and computational easiness, Cartesian coordinates and Newton-Euler's method are used to formulate the equations of motion of the spatial multi-body systems.

For a system of *nb* constrained bodies with the *m* independent constraint equations Eq. (3.4.16), two different formulations are obtained. The second-time derivative of the constraint equations, i.e,

$$\Phi_{\mathbf{q}}\ddot{\mathbf{q}} = \gamma \tag{3.4.39}$$

Where,

$$\gamma = -\left(\Phi_q\dot{\mathbf{q}}\right)_q\dot{\mathbf{q}} - \Phi_{tt} - 2\Phi_{qt}\dot{\mathbf{q}}$$

is appended to the equations of motion. The total number of equations becomes equal to the total number of accelerations and Lagrange multipliers. For a constrained multibody system, the kinematical joints are described by a set of holonomic algebraic constraints involving generalized coordinates. The Euler parameter generalized coordinates of each body must satisfy the normalization constraint of Eq. (3.2.35):

$$\Phi_i^{\mathbf{p}} = \mathbf{p}_i^T \mathbf{p}_i - 1 = 0 \,, i = 1,..., nb \tag{3.4.40}$$

The vector of Euler parameter normalization constraint equation is thus

$$\Phi^{\mathbf{p}} = \left[\Phi_i^{\mathbf{p}},...,\Phi_{nb}^{\mathbf{p}}\right]^T = 0 \tag{3.4.41}$$

If we generally assume that the system has *nb* bodies, *m* joints, *l* drivers, and p normalization constraints, we can write the kinematic constraints in Eq.(3.4.42b) below.

The combined system of kinematic, driving and an Euler parameter normalization constraint equation that determines the position and orientation of the system is

$$\Phi(\mathbf{q},t) = \begin{bmatrix} \Phi^{\mathbf{K}}(\mathbf{q}) \\ \Phi^{\mathbf{D}}(\mathbf{q},t) \\ \Phi^{\mathbf{p}}(\mathbf{q}) \end{bmatrix} = 0 \tag{3.4.42a}$$

or

$$\Phi(\mathbf{q},t) = \begin{bmatrix} \Phi^{(\mathbf{jnt_1},\mathbf{i_1}\mathbf{j_1})}(\mathbf{q}_{i1},\mathbf{q}_{j1}) \\ . \\ . \\ \Phi^{(\mathbf{jnt_m},\mathbf{i_m}\mathbf{j_m})}(\mathbf{q}_{im},\mathbf{q}_{jm}) \\ \Phi_t^{(drv_1,i_1j_1)}(\mathbf{q}_{i1},\mathbf{q}_{j1},t) \\ . \\ . \\ \Phi_t^{(drv_\mathbf{m},i_1j_l)}(\mathbf{q}_{il},\mathbf{q}_{jl},t) \\ \Phi^{(par_1,i_1j_1)}(\mathbf{q}_{i1},\mathbf{q}_{j1}) \\ . \\ . \\ \Phi^{(par_\mathbf{m},i_\mathbf{p}j_\mathbf{p})}(\mathbf{q}_{ip},\mathbf{q}_{jp}) \end{bmatrix} = 0 \tag{3.4.42b}$$

Where **Φ** (**q**, t) = **0** are the non-linear loop-closure constraint equations expressed in an implicit form. **Φ** can be taken as a measure of the violation of the constraint for a given configuration, **q;** if the violation is zero, the mechanism is assembled. The explicit dependence of **t** implies that driver function may enter **Φ,** whereas constraints imposed by the joints will not have this dependence of **t.**

To solve the non-linear position equations in Eq. (3.4.42), the Jacobian matrix of the system must be computed. The two different formulations are discussed below in detail.

FORMULATION I. Equation (3.4.21), (3.4.32), and (3.4.29) are written for all *nb* bodies and then Eq. (3.4.29) is appended to them to obtain $8 \times nb + m$ equations, as follows:

$$\begin{bmatrix} \mathbf{M}^* & \mathbf{P}^T & \Phi_{\mathbf{q}}{}^T \\ \mathbf{P} & 0 & 0 \\ \Phi_{\mathbf{q}} & 0 & 0 \end{bmatrix} \begin{bmatrix} \ddot{\mathbf{q}} \\ \sigma \\ -\lambda \end{bmatrix} + \begin{bmatrix} \mathbf{b}^* \\ \mathbf{c} \\ 0 \end{bmatrix} = \begin{bmatrix} \mathbf{g}^* \\ 0 \\ \gamma \end{bmatrix} \tag{3.4.43}$$

Where ,

$$\Phi_{\mathbf{q}} = \left[\Phi_{\mathbf{r}1}, \Phi_{\mathbf{p}1}, \ldots, \Phi_{\mathbf{r}nb}, \Phi_{\mathbf{p}nb}\right], \quad \mathbf{M}^* = \begin{bmatrix} \mathbf{N}_i & & & & \\ & \mathbf{J}_1^* & & 0 & \\ & & \ddots & & \\ & & & \ddots & \\ & 0 & & & \mathbf{N}_{nb} \\ & & & & & \mathbf{J}_{nb}^* \end{bmatrix}$$

$$\mathbf{P} = \begin{bmatrix} 0^T & \mathbf{p}_1^T & & & \\ & & & 0 & \\ & & \ddots & & \\ & & & \ddots & \\ & 0 & & & 0^T & \mathbf{J}_{nb}^* \end{bmatrix}, \quad \ddot{\mathbf{q}} = \begin{bmatrix} \ddot{\mathbf{r}}_1 \\ \ddot{\mathbf{p}}_1 \\ \vdots \\ \ddot{\mathbf{r}}_{nb} \\ \ddot{\mathbf{p}}_{nb} \end{bmatrix}$$

$$\sigma = \begin{bmatrix} \sigma_1 \\ . \\ . \\ . \\ \sigma_b \end{bmatrix}, \quad \mathbf{b}^* = \begin{bmatrix} 0 \\ 2\ddot{\mathbf{H}}_1\dot{\mathbf{p}}_1 \\ . \\ . \\ . \\ 0 \\ 2\ddot{\mathbf{H}}_{nb}\dot{\mathbf{p}}_{nb} \end{bmatrix}, \quad \mathbf{c} = \begin{bmatrix} \dot{\mathbf{p}}_1^T\dot{\mathbf{p}}_1 \\ . \\ . \\ . \\ \dot{\mathbf{p}}_{nb}^T\dot{\mathbf{p}}_{nb} \end{bmatrix}, \quad \mathbf{g}^* = \begin{bmatrix} \mathbf{f}_1 \\ \mathbf{n}_1^* \\ . \\ . \\ . \\ \mathbf{f}_{nb} \\ \mathbf{n}_{nb}^* \end{bmatrix}$$

and

$$\lambda = [\lambda_1, \lambda_2, ..., \lambda_m]^T$$

Note that the square matrix at the left in Eq.(3.4.43) is symmetric.

FORMULATION II. In the second formulation, the acceleration equation as given by Eq. (3.4.39) is written in terms of the angular acceleration of each body, $\dot{\omega}_i'$, instead of $\ddot{\mathbf{p}}_i$. This conversion is performed first by writing Eq. (3.4.39) as

$$\left[\Phi_{\mathbf{r}1}, \Phi_{\mathbf{p}1}, ..., \Phi_{\mathbf{r}nb}, \Phi_{\mathbf{p}nb}\right] \begin{bmatrix} \ddot{\mathbf{r}}_1 \\ \ddot{\mathbf{p}}_1 \\ . \\ . \\ . \\ \ddot{\mathbf{r}}_{nb} \\ \ddot{\mathbf{p}}_{nb} \end{bmatrix} = \gamma \tag{3.4.44}$$

From the identity $\ddot{\mathbf{p}}_i = \frac{1}{2}\mathbf{L}_i^T\dot{\omega}_i' - \frac{1}{4}\omega^2\mathbf{p}_i$, a typical term $\Phi_{\mathbf{p}i}\ddot{\mathbf{p}}_i$ in Eq. (3.4.44) can be written as

$$\Phi_{\mathbf{p}i}\ddot{\mathbf{p}}_i = \Phi_{\mathbf{p}i}\left(\frac{1}{2}\mathbf{L}_i^T\dot{\omega}_i' - \frac{1}{4}\omega_i^2\mathbf{p}_i\right)$$

$$= \frac{1}{2}\Phi_{\mathbf{p}i}\mathbf{L}_i^T\dot{\omega}_i' - \frac{1}{4}\omega_i^2\Phi_{\mathbf{p}i}\mathbf{p}_i \tag{3.4.45}$$

Hence, Eq. (3.4.44) is written as

$$\left[\Phi_{\mathbf{r}1},\frac{1}{2}\Phi_{\mathbf{p}1}\mathbf{L}_1^T,...,\Phi_{\mathbf{r}nb},\frac{1}{2}\Phi_{\mathbf{p}nb}\mathbf{L}_{nb}^T\right]\begin{bmatrix}\ddot{\mathbf{r}}_1\\ \dot{\omega}_i'\\ .\\ .\\ .\\ \ddot{\mathbf{r}}_{nb}\\ \dot{\omega}_{nb}'\end{bmatrix}=\gamma^{\neq} \tag{3.4.46}$$

Where the terms $-\frac{1}{4}\omega_i^2\Phi_{\mathbf{p}i}\mathbf{p}_i, i=1,...,nb$, have been moved to the right side of the equation. A detailed explanation of this new form of the Jacobian matrix is given in the next section below. Appending Eq. (3.4.44) to Eqs.(3.4.21) and (3.4.38) for all nb bodies yields

$$\begin{bmatrix}\mathbf{M} & \Phi_{\mathbf{q}}^T\\ \Phi_{\mathbf{q}} & 0\end{bmatrix}\begin{bmatrix}\dot{\mathbf{h}}\\ -\lambda\end{bmatrix}+\begin{bmatrix}\mathbf{b}\\ 0\end{bmatrix}=\begin{bmatrix}\mathbf{g}\\ \gamma^{\neq}\end{bmatrix} \tag{3.4.47}$$

Where ,

$$\mathbf{M}=\begin{bmatrix}\mathbf{N}_1 & & & & & \\ & \mathbf{J}_1' & & 0 & & \\ & & . & & & \\ & & & . & & \\ & & & & . & \\ & 0 & & & \mathbf{N}_{nb} & \\ & & & & & \mathbf{J}_{nb}'\end{bmatrix}$$

$$\dot{\mathbf{h}}=\begin{bmatrix}\ddot{\mathbf{r}}_1\\ \dot{\omega}_1'\\ .\\ .\\ .\\ \ddot{\mathbf{r}}_{nb}\\ \dot{\omega}_{nb}'\end{bmatrix},\qquad \mathbf{b}=\begin{bmatrix}0\\ \tilde{\omega}_1'\mathbf{J}_1'\omega_1'\\ .\\ .\\ .\\ 0\\ \tilde{\omega}_{nb}'\mathbf{J}_{nb}'\omega_{nb}'\end{bmatrix},\qquad \mathbf{g}=\begin{bmatrix}\mathbf{f}_1\\ \mathbf{n}_1'\\ .\\ .\\ .\\ \mathbf{f}_{nb}\\ \mathbf{n}_{nb}'\end{bmatrix}$$

Note that the square matrix at the left in this equation is symmetric.

Although the Euler parameters are ideal for representing the angular orientation of a body in space, they yield too many equations when their time derivatives are used explicitly in the equations of motion, as shown in Eq. (3.4.30). For a constrained body, the equations of motion given in Eq. (3.4.38) contains only three equations and also take advantage of the Euler parameters (the constraint equations and hence the Jacobian matrix are described in terms of Euler parameters). This advantage becomes apparent when Eqs. (3.4.38) and (3.4.43) are compared. Equation.(3.4.43) contains 2xnb fewer equations than Eq.(3.4.38).

In Eq. (3.4.43), the kinematic constraints are kept in terms of Euler parameters, as follows:

$$\begin{aligned} \Phi &\equiv \Phi(\mathbf{q}) \\ &\equiv \Phi(\mathbf{r}_1, \mathbf{p}_1, ..., \mathbf{r}_{nb}, \mathbf{p}_{nb}) = 0 \end{aligned} \tag{3.4.48}$$

The velocity equations are written as

$$\dot{\Phi}(\mathbf{q}, t) = \Phi_q \dot{\mathbf{q}} + \Phi_t = 0 \tag{3.4.49a}$$

Where,

$$\Phi_{\mathbf{q}} = \left[\frac{\partial \Phi_i}{\partial \mathbf{q}_j} \right]$$

or

$$\dot{\Phi} \equiv \Phi_{\mathbf{q}} \dot{\mathbf{q}}$$

$$= \left[\Phi_{\mathbf{r}1}, \Phi_{\mathbf{p}1}, \ldots, \Phi_{\mathbf{r}nb}, \Phi_{\mathbf{p}nb}\right] \begin{bmatrix} \dot{\mathbf{r}}_1 \\ \dot{\mathbf{p}}_1 \\ . \\ . \\ . \\ \dot{\mathbf{r}}_{nb} \\ \dot{\mathbf{p}}_{nb} \end{bmatrix}$$

$$= \left[\Phi_{\mathbf{r}1}, \frac{1}{2}\Phi_{\mathbf{p}1}\mathbf{L}_1^T, \ldots, \Phi_{\mathbf{r}nb}, \frac{1}{2}\Phi_{\mathbf{p}nb}\mathbf{L}_i^T\right] \begin{bmatrix} \dot{\mathbf{r}}_1 \\ \omega_1' \\ . \\ . \\ . \\ \dot{\mathbf{r}}_{nb} \\ \omega_{nb}' \end{bmatrix} \qquad (3.4.49b)$$

Differentiating Eq. (3.4.49b) with respect to time yields the acceleration equation:

$$\ddot{\Phi}(\mathbf{q},t) = \Phi_q \ddot{\mathbf{q}} + \dot{\Phi}_q \dot{\mathbf{q}} + \dot{\Phi}_t \equiv 0 \qquad (3.4.50)$$

Where, $\Phi_q(\mathbf{q},t) = \dfrac{\partial \Phi(q,t)}{\partial \mathbf{q}}$ is the constraint Jacobian matrix. The Jacobian matrix is a matrix of the partial derivatives of the constraints, **Φ,** with respect to the coordinates; **q. Φ_t** is a vector of the partial derivatives of **Φ** with respect to time.

The modified Jacobian matrix of Eq. (3.4.50) is the same as that of Eq. (3.4.46). The modified Jacobian matrix and the modified vector $\gamma^{\neq}$ can be obtained in explicit forms for the constraint equations of spatial kinematics.

The vectors **q,** $\dot{\mathbf{q}}$, and $\ddot{\mathbf{q}}$ are of dimension n representing the generalized position, velocity, and acceleration of the system, **M** is the generalized mass matrix, **λ** is the vector of Lagrange multipliers, and **g(q,** $\dot{\mathbf{q}}$ **,** t) is the vector of generalized external forces plus all the velocity dependent inertia terms (centrifugal and coriolis).

Table (3.4.1) shows the components of the Jacobian matrix and vector $\gamma^{\neq}$ for some of the most common constraints. This table provides sufficient information to assemble in the form of Eq.(3.4.47), the complete set of equations of motion for mechanical systems with the more commonly used constraints.

Table 3.4.1 Components in expansion of the most common constraints

Φ	$\Phi^{(m)}_{ri}$	$\frac{1}{2}\Phi^{(m)}_{\mathbf{p}i}\mathbf{L}_i^T$	$\Phi^{(m)}_{rj}$	$\frac{1}{2}\Phi^{(m)}_{\mathbf{p}j}\mathbf{L}_j^T$	$\gamma^{\neq}$
$\Phi^{(n1,1)}$	$\mathbf{0}^{\mathbf{T}}$	$-\mathbf{s}_i^T\,\tilde{\mathbf{s}}_i\,\mathbf{A}_i$	$\mathbf{0}^{\mathbf{T}}$	$-\mathbf{s}_i^T\,\tilde{\mathbf{s}}_j\,\mathbf{A}_j$	$-2\dot{\mathbf{s}}_i^T\,\dot{\mathbf{s}}_j+\dot{\mathbf{s}}_i^T\tilde{\boldsymbol{\omega}}_i\,\mathbf{s}_j+\dot{\mathbf{s}}_j^T\tilde{\boldsymbol{\omega}}_j\mathbf{s}_i$
$\Phi^{(n2,1)}$	$-\mathbf{s}_i^T$	$-\left(\mathbf{d}+\mathbf{s}_i^{\,B}\right)^T\tilde{\mathbf{s}}_i\,\mathbf{A}_i$	$\mathbf{s}_i^T$	$-\mathbf{s}_i^T\,\tilde{\mathbf{s}}_j^{\,\mathbf{B}}\,\mathbf{A}_j$	$-2\dot{\mathbf{d}}^T\dot{\mathbf{s}}_i-\mathbf{d}^T\tilde{\boldsymbol{\omega}}_i\mathbf{s}_i+\mathbf{s}_i^T\left(\tilde{\boldsymbol{\omega}}_i\dot{\mathbf{s}}_i^{\mathbf{B}}-\tilde{\boldsymbol{\omega}}_j\dot{\mathbf{s}}_j^{\mathbf{B}}\right.$
$\Phi^{(p1,1)}$	$\mathbf{0}^{\mathbf{T}}$	$\tilde{\mathbf{s}}_j\,\tilde{\mathbf{s}}_i\,\mathbf{A}_i$	$\mathbf{0}^{\mathbf{T}}$	$-\mathbf{s}_i\,\tilde{\mathbf{s}}_j\,\mathbf{A}_j$	$-2\dot{\tilde{\mathbf{s}}}_i\,\dot{\mathbf{s}}_j+\tilde{\mathbf{s}}_j\,\tilde{\boldsymbol{\omega}}_i\,\dot{\mathbf{s}}_i-\tilde{\mathbf{s}}_i\,\tilde{\boldsymbol{\omega}}_j\dot{\mathbf{s}}_j$
$\Phi^{(p2,1)}$	$-\tilde{\mathbf{s}}_i$	$\left(\tilde{\mathbf{s}}_i\,\tilde{\mathbf{s}}_i^{\mathbf{B}}+\tilde{\mathbf{d}}\,\tilde{\mathbf{s}}_i\right)\mathbf{A}_i$	$\tilde{\mathbf{s}}_i$	$-\mathbf{s}_i\,\tilde{\mathbf{s}}_j^{\,\mathbf{B}}\,\mathbf{A}_j$	$-2\dot{\tilde{\mathbf{s}}}_i\,\dot{\mathbf{d}}+\tilde{\mathbf{s}}_i\,\left(\tilde{\boldsymbol{\omega}}_i\,\dot{\mathbf{s}}_i^{B}-\tilde{\boldsymbol{\omega}}_j\dot{\mathbf{s}}_j^{\mathbf{B}}\right)+\tilde{\mathbf{d}}\tilde{\boldsymbol{\omega}}_i\dot{\mathbf{s}}_i$
$\Phi^{(s,3)}$	$\mathbf{I}$	$-\tilde{\mathbf{s}}_i^{\mathbf{P}}\mathbf{A}_i$	$\mathbf{-I}$	$\tilde{\mathbf{s}}_j^{\mathbf{P}}\mathbf{A}_j$	$-\tilde{\boldsymbol{\omega}}_i\dot{\mathbf{s}}_i^{\mathbf{P}}+\tilde{\boldsymbol{\omega}}_j\,\dot{\mathbf{s}}_j^{\mathbf{P}}$
$\Phi^{(s\text{-}s,1)}$	$-2\,d^T$	$-2\,d^T\,\tilde{\mathbf{s}}_i^{\mathbf{P}}\mathbf{A}_i$	$2\,d^T$	$-2\,d^T\,\tilde{\mathbf{s}}_j^{\mathbf{P}}\mathbf{A}_j$	$-2\,\dot{\mathbf{d}}^T\dot{\mathbf{d}}+2\mathbf{d}^T\left(\tilde{\boldsymbol{\omega}}_i\dot{\mathbf{s}}_i^{\mathbf{P}}-\tilde{\boldsymbol{\omega}}_j\dot{\mathbf{s}}_j^{\mathbf{P}}\right)$

CHAPTER 4-OPTIMAL DYNAMIC SIMULATION OF SPATIAL FOUR-BAR MECHANISMS

4.1 Introduction

Dynamics simulation tools have shown manifold increases in terms of their usage in the design, analysis, parametric refinement and ultimately model-based control of a variety of multi-body systems such as automobile industry, heavy machinery, biomechanics, aerospace and robots etc. In the absence of efficient, general-purpose, closed-form analytical methods, numerical simulation methods have taken a premier position for simulation of such multi-body systems.

A very important task in a design process is how to make a mechanism which will satisfy desired characteristics of motion of a member (link), i.e. a mechanism in which one part will surely perform desired motion.

A four-bar linkage consists of four rigid members or links attached to one another using different types of joints. The four rigid members are as follows: the fixed member, the crank, the follower and the coupler. Since most mechanism tasks require transferring a single input to a single output, the four-bar linkage is used often (Erdman, 1984).

It is observed that the configuration of constrained multi-body systems can be described by a variety of sets of coordinates. The suitable selection of a set of configuration coordinates is of particular importance due to its impact both on the ease of formulation and the subsequent computational efficiency. In our case, we will focus our attention on the use of sets of Cartesian coordinates and reference point coordinates. These coordinates are useful in the principle of multi-body dynamics for the required equation of motion formulation.

For the four-bar planar mechanism, the number of generalized coordinates is 9; i.e., three coordinates (two positions and one orientation angle) for each of the three moving links. The number *m* of constraint equations is 8, two for each of the four revolute joints. The mechanism thus has (9-8=1) one degree of freedom. Whereas, in the four-bar spatial mechanism; each body is described by seven generalized coordinates (three positions and four orientational Euler parameters) where the dimension of the matrix becomes very bulky.

The application of the laws of dynamics to constrained multi-body systems leads to a set of differential algebraic equations (DAE). These can be transformed to second order ordinary

differential equations (ODE) by proper differentiation of the kinematic constraint equations, by use of an independent set of coordinates. A stable and accurate integration of both DAE and ODE is of great importance for the solution of the equations of motion. Although analytical solutions may be found for some simple cases, the number and complexity of the equations resulting from the majority of multi-body systems requires numerical solutions. Because the theory of ordinary differential equations has been known for a long time, the stability, convergence, and accuracy of many methods have been studied in great detail. As a consequence, many of the computer programs currently available for the computer-aided analysis and design of multi-body systems rely on well-established methods for the solution of ODE.

From the viewpoint of the user of established computer software, such as the MSC.ADAMS program, essentially all the algebraic and numerical complexity is hidden in the implementation of computer intensive calculations. This interesting circumstance in an illustration of a situation in which equation of spatial dynamics that are virtually intractable from the point of view of the human analyst are practically implementable on modern high-speed digital computers, whose ever-increasing power makes spatial kinematic and dynamic analysis practical. Manual application methods would lead to extensive algebraic manipulations that are extremely time consuming and prone to error when carried out analytically by the engineer. However, the basic formulations should be clear in order to avoid analytical and numerical difficulties.

Once geometric and material property information is defined and entered into a computer data base, implementation of the analytical methods presented in this section for calculating the locations of centroids, moments, and products of inertia is a relatively simple matter.

The solution of the problem for constrained multi-body systems can be obtained using the Lagrange's multipliers technique which leads to a set of differential and algebraic equations (DAE), in which the coordinates and the Lagrange multipliers are unknown quantities. The numerical solution of the set of DAE is not a straightforward problem (Brenan *et al*., 1989). One of the most used methods to solve this problem consists of converting the system of DAE into a set of ordinary differential equations (ODE) by appending the second derivative with respect to time of the constraint equations (Gear, 1981; Nikravesh, 1988). In general, dynamic simulation means integration of the resulting non-linear DAEs or ODEs from the formulations to obtain the motion trajectories of the rigid bodies considering the inertial properties and the external loads.

4.2 Method of Lagrange Multipliers

The dynamics of mechanical systems with closed loops can be formulated as a system of ODEs whose solutions are required to satisfy additional holonomic (algebraic) equations resulting from cutting the loops (Featherstone, 1987).

i. The two principal approaches adopted for the forward dynamics simulation of index-3 DAEs are: Direct elimination of the surplus variables using the position-level algebraic constraints to explicitly reduce the index-3 DAE to an ODE in a minimal set of generalized coordinates. The resulting ODE can then be integrated using ODE methods without worrying about the stability issues.

ii. Converted ODE approach wherein all the algebraic position and velocity level constraints are differentiated and represented at the acceleration level to obtain an augmented index-1 DAE.

The Lagrange multiplier method permits determining the motor forces and the reactions that appear at the joints of a multibody system and makes optimum use of the relationship that exists between the Lagrange multipliers and the forces associated with the constraint equations.

For kinematically constrained mechanical systems the equations of motion can written as:

$$\Phi = \Phi(\mathbf{q},t) = \Phi(\mathbf{r},\mathbf{p},t) = 0 \tag{4.2.1}$$

$$\dot{\Phi} = \Phi_q \dot{\mathbf{q}} + \Phi_t = 0 \tag{4.2.2}$$

$$\ddot{\Phi} = \Phi_q \ddot{\mathbf{q}} - \gamma = 0 \tag{4.2.3}$$

$$\mathbf{M}\ddot{\mathbf{q}} - \Phi_q^T \lambda - \mathbf{g} = 0 \tag{4.2.4}$$

Where

$$\gamma = -\left(\Phi_q \dot{\mathbf{q}}\right)_q \dot{\mathbf{q}} - 2\Phi_{qt}\dot{\mathbf{q}} - \Phi_{tt} \tag{4.2.5}$$

In Eq. (4.2.4) the first term represents the inertia forces; the second, the forces produced by the constraints; and the third is the external forces plus additional velocity-dependent inertia forces. Each column of matrix Φ_q^T, multiplied by the corresponding λ, represents the vector of forces associated with the constraint.

In the case of spatial motion, it is assumed that the constraints of Eq. (4.2.1) contain both kinematic constraints and mathematical constraints. Therefore, the Jacobian matrix in Eqs. (4.2.2) to (4.2.4) contains the **P** and $\Phi_{\mathbf{q}}$ matrices of Eq. (3.4.43).

Equation (4.2.4) represents n equations and $(n+m)$unknowns: the n elements of vector **q** and the n elements of vector λ . In order to have a sufficient number of equations, it is necessary to supply m more equations. The obvious choice is to use the algebraic constraint Eq. (4.2.1) which along with Eq. (4.2.4) constitutes a set of differential algebraic equations DAEs of index three. In order to avoid DAEs, one can use the acceleration kinematic equations which are obtained by differentiating the constraint Eq. (4.2.1) twice with respect to time:

$$\Phi_q \ddot{\mathbf{q}} = -\dot{\Phi}_t - \dot{\Phi}_q \dot{\mathbf{q}} \equiv \gamma \tag{4.2.6}$$

The acceleration equation as given by Eq. (4.2.6) is written in terms of the angular acceleration of each body $\dot{\omega}_i'$, instead of $\ddot{\mathbf{p}}_i'$ .Therefore, considering the identity $\ddot{\mathbf{p}}_i = \frac{1}{2}\mathbf{L}_i^T \dot{\omega}_i' - \frac{1}{4}\omega^2 \mathbf{p}_i$, Eq. (3.4.46) can be written as

$$\left[\Phi_{\mathbf{r}1}, \frac{1}{2}\Phi_{\mathbf{p}1}\mathbf{L}_1^T, \ldots, \Phi_{\mathbf{r}b}, \frac{1}{2}\Phi_{\mathbf{p}nb}\mathbf{L}_{nb}^T\right] \begin{bmatrix} \ddot{\mathbf{r}}_1 \\ \dot{\omega}_i' \\ \cdot \\ \cdot \\ \cdot \\ \ddot{\mathbf{r}}_{nb} \\ \dot{\omega}_{nb}' \end{bmatrix} = \gamma^{\neq} \tag{4.2.7}$$

Appending Eq. (4.2.7) to Eqs.(4.2.4) and (3.4.38) for all *nb* bodies yields

$$\begin{bmatrix} \mathbf{M} & \Phi_{\mathbf{q}}^T \\ \Phi_{\mathbf{q}} & 0 \end{bmatrix} \begin{bmatrix} \dot{\mathbf{h}} \\ -\lambda \end{bmatrix} + \begin{bmatrix} \mathbf{b} \\ 0 \end{bmatrix} = \begin{bmatrix} \mathbf{g} \\ \gamma^{\neq} \end{bmatrix} \tag{4.2.8}$$

But, if we consider the Euler parameters to be explicit the equation below already derived in section (3.4.5) can be used.

$$\begin{bmatrix} \mathbf{M}^* & \mathbf{P}^T & \Phi_{\mathbf{q}}{}^T \\ \mathbf{P} & 0 & 0 \\ \Phi_{\mathbf{q}} & 0 & 0 \end{bmatrix} \begin{bmatrix} \ddot{\mathbf{q}} \\ \sigma \\ -\lambda \end{bmatrix} + \begin{bmatrix} \mathbf{b}^* \\ \mathbf{c} \\ 0 \end{bmatrix} = \begin{bmatrix} \mathbf{g}^* \\ 0 \\ \gamma \end{bmatrix} \tag{4.2.9}$$

Equation (4.2.8) is a system of $(n+m)$ equations with $(n+m)$ unknowns, whose matrix is symmetrical and also very sparse in many practical cases. The system of Eq. (4.2.8) or (4.2.9) can be used for the simultaneous solution of the accelerations and Lagrange multipliers.

The main advantage of the dynamic formulation in dependent coordinates using Lagrange multipliers, besides the conceptual simplicity of the method, is permitting the calculation of forces associated with the constraints (which depend on the Lagrange multipliers) with a minimum additional effort. The solution of Eq. (4.2.8) yields λ directly without the need for a special call to an inverse dynamic module.

The resulting set of generalized accelerations $\ddot{\mathbf{q}}$ must be numerically integrated to determine the generalized coordinates and velocities used to evaluate the system at the following time step. A number of comments could be accompanied with this form of the equations of motion:

i. The coefficient matrix is symmetric due symmetry of **M**.
ii. The coefficient matrix is very sparse, because **M** is block diagonal and also the constraint Jacobian, $\Phi_{\mathbf{q}}$ is sparse.

4.3 Stiff Differential Equation Method

The method of solving a mixed system of algebraic and differential equations of motion is presented in this section.This method considers the algebraic constraint equations to be a special form of differential equation in which the time derivatives of the variables do not appear. This assumption has proved to cause the system equations to be come numerically stiff.Therefore, a stiff numerical integration method must be applied to solve the equations.This algorithm has served as a forerunner in the development of the numerical methods in the area of mechanical systems.The algorithm has been formulated into a computer program for three-dimensional motion known as MSC.ADAMS.This is the motivation to discuss this algorithm in this thesis work.

Standard numerical integration algorithm are designed to solve systems of differential equations of the form

$$\dot{\mathbf{y}} = \mathbf{f}(\mathbf{y}, t) \tag{4.3.1}$$

The modified approach taken here allows for the simultaneous solution of mixed algebraic and differential equations of the form

$$\mathbf{g}(\mathbf{y}, \dot{\mathbf{y}}, t) = 0 \tag{4.3.2}$$

Where some components of $\dot{\mathbf{y}}$ may not appear in some of the equations.When none of the components of $\dot{\mathbf{y}}$ appear in an equation, that is an algebraic equation; otherwise it is a differential equation.

The k^{th} order Gear algorithm and its corresponding corrector formula are modified to solve a mixed system of algebraic and differential equations given as

$$\mathbf{g}(\mathbf{z}, t) = 0 \tag{4.3.3}$$

Where $\mathbf{z} = \left[\mathbf{y}^T, \dot{\mathbf{y}}^T\right]^T$ .The Newton-Raphson formula for this equation is

$$\mathbf{g}_{\mathbf{z}}^{(l_n)} \Delta \mathbf{z}^{(l_n)} = -\mathbf{g}^{(l_n)} \tag{4.3.4}$$

Where l_n is the iteration number.When the substitution $\mathbf{z} = \left[\mathbf{y}^T, \dot{\mathbf{y}}^T\right]^T$ is made in Eq.(4.3.4), it is found that

$$\mathbf{g}_{\mathbf{y}}^{(l_n)} \Delta \mathbf{y}^{(l_n)} + \mathbf{g}_{\dot{\mathbf{y}}}^{(l_n)} \Delta \dot{\mathbf{y}}^{(l_n)} = -\mathbf{g}^{(l_n)} \tag{4.3.5}$$

For the l_n^{th} and $(l_n + 1)^{st}$ Newton-Raphson iterations, it can be written as

$$\left(\mathbf{y}^{i+1}\right)^{(l_n)} - hb_{-1}\left(\dot{\mathbf{y}}^{(i+1)}\right)^{(l_n)} - \sum_{j=0}^{k-1}\left(a_j \mathbf{y}^{i-j}\right) = 0 \tag{4.3.6}$$

$$\left(\mathbf{y}^{i+1}\right)^{(l_n+1)} - hb_{-1}\left(\dot{\mathbf{y}}^{(i+1)}\right)^{(l_n+1)} - \sum_{j=0}^{k-1}\left(a_j \mathbf{y}^{i-j}\right) = 0 \tag{4.3.7}$$

The summation terms in these equations are not a function of the iteration number instead they are a function of the information from the i^{th} and previous steps, so they remain constant at each iteration. Subtracting Eq.(4.3.6) from Eq.(4.3.7) yields

$$\left(\mathbf{y}^{i+1}\right)^{(l_n+1)} - \left(\mathbf{y}^{(i+1)}\right)^{(l_n)} - hb_{-1}\left(\dot{\mathbf{y}}^{(i+1)}\right)^{(l_n+1)} + hb_{-1}\left(\dot{\mathbf{y}}^{i+1}\right)^{(l_n)} = 0$$

Or

$$\Delta\dot{\mathbf{y}}^{(l_n)} = \frac{1}{hb_{-1}}\Delta\mathbf{y}^{(l_n)} \tag{4.3.8}$$

Which holds true for the $i+1^{st}$ or any other time step.Substitution of Eq.(4.3.8) into Eq.(4.3.5) results in the corrector formula

$$\left(\mathbf{g}_{\mathbf{y}}^{(l_n)} + \frac{1}{hb_{-1}}\mathbf{q}_{\dot{\mathbf{y}}}^{(l_n)}\right)\Delta\mathbf{y}^{(l_n)} = -\mathbf{g}^{(l_n)} \tag{4.3.9}$$

If Eq.(4.3.2) is of the form

$$\mathbf{g}(\mathbf{y},\dot{\mathbf{y}},t) = \mathbf{W}\dot{\mathbf{y}} + \mathbf{w}(\mathbf{y}.t) = 0 \tag{4.3.10}$$

Where $\mathbf{W}$ is a constant matrix or a time-dependent matrix, then Eq.(4.3.10) can be written in a simpler form as

$$\left(\mathbf{w}_{\mathbf{y}}^{(l_n)} + \frac{1}{hb_{-1}}\mathbf{W}\right)\Delta\mathbf{y}^{(l_n)} = -\mathbf{g}^{(l_n)} \tag{4.3.11}$$

At each time step, the iterative corrector process of Eq.(4.3.9) or Eq.(4.3.11) is continued until all of the Newton difference $\Delta\mathbf{y}^{(l_n)}$ are below a specified tolerance level.At each Newton-Raphson iteration, arrays $\mathbf{y}$ and $\dot{\mathbf{y}}$ are updated:

$$\begin{aligned}\mathbf{y}^{(l_n+1)} &= \mathbf{y}^{(l_n)} + \Delta\mathbf{y}^{(l_n)}\\ \dot{\mathbf{y}}^{(l_n+1)} &= \dot{\mathbf{y}}^{(l_n)} + \frac{1}{hb_{-1}}\Delta\mathbf{y}^{(l_n)}\end{aligned} \tag{4.3.12}$$

The total-system equations of motion of Eq.(4.2.4) and Eq.(4.2.1) are written as

$$\begin{aligned}&\mathbf{M}\dot{\mathbf{s}} - \Phi_{\mathbf{q}}^{T}\lambda = \mathbf{g}\\ &\dot{\mathbf{q}} = \mathbf{s}\\ &\Phi(\mathbf{q}) = 0\end{aligned} \tag{4.3.13}$$

Equations (4.3.13) may be expressed in the form of Eq.(4.3.10), where

$$\mathbf{W} = \begin{bmatrix}\mathbf{M} & \mathbf{0} & \mathbf{0}\\ \mathbf{0} & \mathbf{I} & \mathbf{0}\\ \mathbf{0} & \mathbf{0} & \mathbf{0}\end{bmatrix} \tag{4.3.14}$$

$$\mathbf{w} = \begin{bmatrix}\Phi_{\mathbf{q}}^{T}\lambda - \mathbf{g}\\ -\mathbf{s}\\ \Phi\end{bmatrix} \tag{4.3.15}$$

$$\mathbf{y} = \left[\mathbf{s}^T, \mathbf{q}^T, \lambda^T\right]^T \tag{4.3.16}$$

and

$$\dot{\mathbf{y}} = \left[\dot{\mathbf{s}}^T, \dot{\mathbf{q}}^T, \dot{\lambda}^T\right]^T \tag{4.3.17}$$

The corrector formula of Eq.(4.3.11) can be employed to solve for the unknown $\mathbf{y}$ at every time step. In this case, Eq.(4.3.11) provides $2n+m$ equations in $2n+m$ unknowns.

It was noted at the beginning of this section that treating algebraic equations as special forms of differential equations yield numerically stiff systems.This causes artificially high-frequency components in the solution. The high-frequency components of the response do mot represent the physical sysytem-they are introduced into the solution numerically.Because of this presence of high-frequency components in the respnse, the time increment h must be chosen relatively small. For small values of h, the term $\frac{1}{h}$ in the algorithm can become substantially large.

4.4 Body of Matrix Equations

Under this section, the dynamic analysis of a four-bar spatial mechanism formulation will be discussed according to the constraint joints presented in section (3.3).The assembling procedures for the equations of motion for this mechanism will be also discussed.

Consider the four-bar spatial linkage mechanism shown in Fig. (4.4.1). The system is composed of three moving rigid bodies of length r_2, r_3 and r_4 with their respective masses m_2, m_3 and m_4 .The mechanism can be parameterized in terms of the Cartesian coordinates of the mass center of each link, together with the angles that each link makes in the space.

The Cartesian coordinates employ a body-fixed coordinate system for each body. The body-fixed systems are described by a set of coordinates $\mathbf{q}_i$.

The main complexity in analyzing the spatial mechanisms is defining the orientation of a body in space. The fundamental difference between planar and spatial kinematic analysis is the use of angular velocity and acceleration variables in spatial analysis that are not time derivatives of generalized coordinates. Euler parameter orientation generalized coordinates are defined, and their properties are developed for use in kinematic and dynamic analysis.

We can choose a reference point on each link in which the body-fixed frame is attached. The most convenient reference point is the center of mass of each body. Hence, the local coordinates

coincide with the center of mass for each moving links and with the global system xyz for the fixed link.

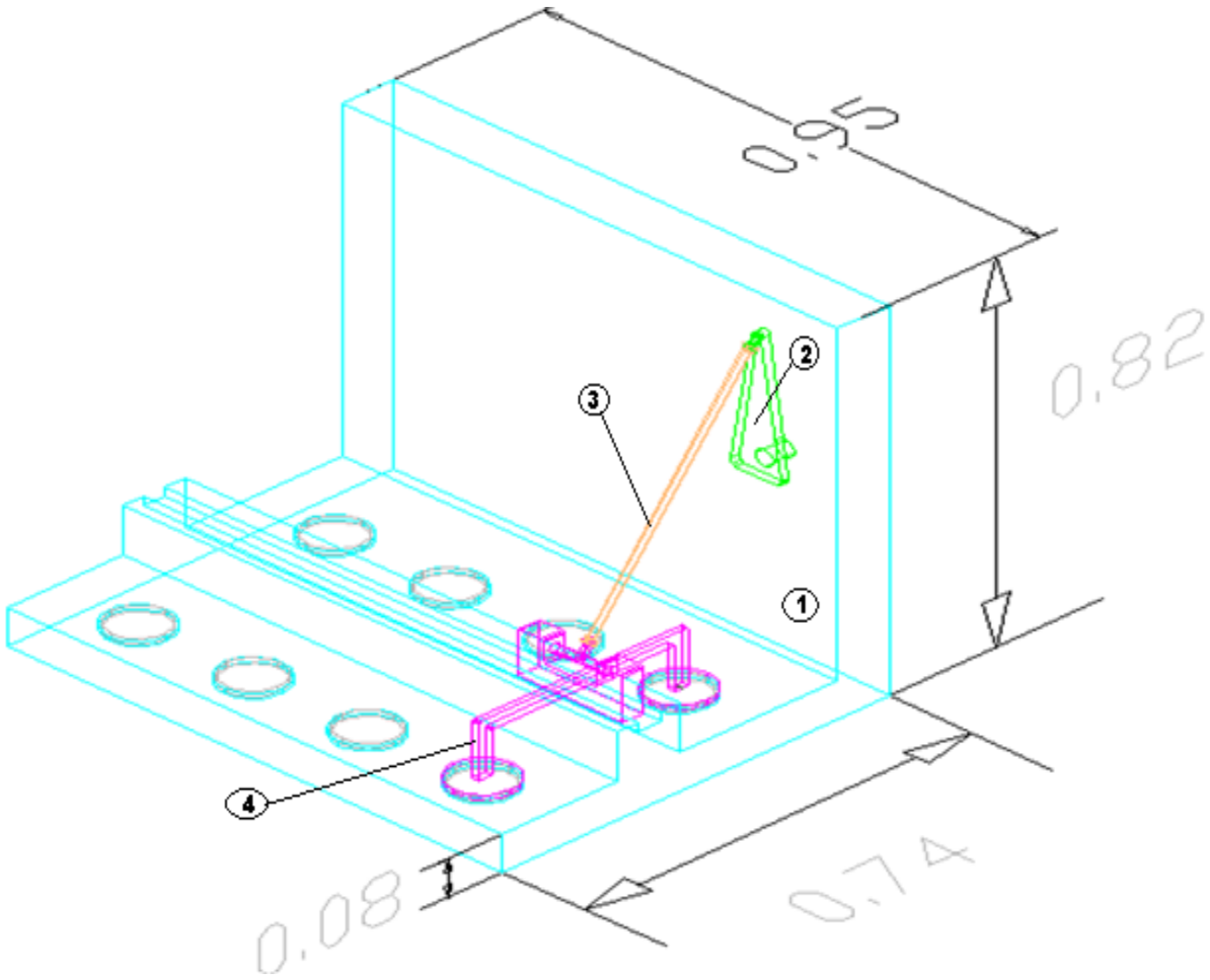

Figure 4.4.1 Assembly drawing of a spatial four-bar lens polishing mechanism

The above spatial four-bar slider mechanism constraint equations are represented as follows using reference point coordinates. Let's consider the crank (body2) that has connection through a revolute joint with the ground (body1). A small cylindrical link which connects the crank and the ground doesn't change its position with respect to x-y-z reference frame. Four rigid bodies describe the model under consideration. The model also includes one revolute joint that connects the ground and the crank, one spherical joint between the crank and the coupler (body3), another

second spherical joint between the coupler and the slider-block (body4), and one translational joint that connects the ground and the slider-block system.The slider-block system contains the system linkages to accomplish the the polishing operation of the mechanism.The detail design of each linkages of this mechanism is described in chapter five.

The initial configuration is taken with the crank rotates at some average angular velocity of 50.4rad/sec about z-axis. The coupler has a spatial motion in space.The coupler is a linkage combination of a cylindrical and two sockets attached at its extreme tips.The slider-block system model shown in Fig. (4.4.1) is constrained to move in the xz plane.

4.4.1 Mass Matrix

From equation (4.2.8), the mass matrix for the mechanism is depicted as

$$\mathbf{M} = \left[\mathbf{N}_2, \quad \mathbf{N}_3, \quad \mathbf{N}_4, \quad \mathbf{J}_2, \quad \mathbf{J}_3, \quad \mathbf{J}_4\right] \tag{4.4.1}$$

Where,

$$\mathbf{N}_b = \begin{bmatrix} m^{nb} & 0 & 0 \\ 0 & m^{nb} & 0 \\ 0 & 0 & m^{nb} \end{bmatrix} \tag{4.4.2}$$

$$\mathbf{J}_b = \begin{bmatrix} J_{11}^{\ nb} & J_{12}^{nb} & J_{13}^{nb} \\ & J_{22}^{nb} & J_{23}^{nb} \\ sym & & J_{33}^{nb} \end{bmatrix} \tag{4.4.3}$$

In which m^k is the mass of link nb, J_{kk}^{nb} are the mass moments of inertia and J_{kl}^{nb}, are the products of inertia and $nb = 2,3,4$.

4.4.2 External Vectors of Forces and Torques

The set of external forces **g** that act on the rigid bodies of the system are computed. Contribution to the force system are made from the weight of the three rigid bodies plus forces due to compliant constraints, like springs, dampers and actuators, if they are implemented in the system. The number of bodies in the system determines the dimension of the external force array. The array contains the X**,** Y and Z components of the external forces as well as the resultant moments applied to each body. Therefore, in this case, eighteen entries are required:

$$\mathbf{g} = \left[\mathbf{f}_{2,x}, \mathbf{f}_{2,y}, \mathbf{f}_{2,z}, \mathbf{T}_{2,x}, \mathbf{T}_{2,y}, \mathbf{T}_{2,z}, \mathbf{f}_{3,x}, \mathbf{f}_{3,y}, \mathbf{f}_{3,z}, \mathbf{T}_{3,x}, \mathbf{T}_{3,y}, \mathbf{T}_{3,z}, \mathbf{f}_{4,x}, \mathbf{f}_{4,y}, \mathbf{f}_{4,z}, \mathbf{T}_{4,x}, \mathbf{T}_{4,y}, \mathbf{T}_{4,z}\right]^T \tag{4.4.3}$$

But, the only external force is considered the gravitational force along the negative Y-axis. This is expressed as:

$$\begin{aligned}\mathbf{f}_{2g,y} &= -m_2\mathbf{g}\\ \mathbf{f}_{3g,y} &= -m_3\mathbf{g}\\ \mathbf{f}_{4g,y} &= -m_4\mathbf{g}\end{aligned} \tag{4.4.4}$$

The overall external force vector **g** is of Eq.(4.4.3) is obtained by assembling the force and moment contributions(in this case the input woking torque imposed at the crank) from Eq.(4.4.4) and any contribution from the compliant constraints.

4.4.3 Jacobian Matrix

The Jacobian matrix is the matrix of partial derivatives of the constraint equations **Φ** with respect to the vector of the system dependent coordinates **q**. It will be assumed that there are at least as many equations as there are unknown variables or coordinates. When the Jacobian matrix entries are evaluated, the number of constraint equations determines the number of rows in the Jacobian matrix and the number of columns is dependent upon the number of generalized coordinates. Since this formulation specifies the use of Cartesian coordinates, seven columns are required for each body in the system. This matrix takes the following form:

$$\Phi_{\mathbf{q}} = \begin{bmatrix} \frac{\partial\Phi_1}{\partial\mathbf{q}_1} & \frac{\partial\Phi_1}{\partial\mathbf{q}_2} & \cdots\cdots & \frac{\partial\Phi_1}{\partial\mathbf{q}_n} \\ \frac{\partial\Phi_2}{\partial\mathbf{q}_1} & \frac{\partial\Phi_2}{\partial\mathbf{q}_2} & \cdots\cdots & \frac{\partial\Phi_2}{\partial\mathbf{q}_n} \\ \cdots\cdots & \cdots\cdots & \cdots\cdots & \cdots\cdots \\ \frac{\partial\Phi_m}{\partial\mathbf{q}_1} & \frac{\partial\Phi_m}{\partial\mathbf{q}_2} & \cdots\cdots & \frac{\partial\Phi_m}{\partial\mathbf{q}_n} \end{bmatrix} \tag{4.4.4}$$

In equation (4.4.4), *m* is the number of constraint equations and *n* the number of dependent coordinates. The constraint Jacobian matrix $\Phi_{\mathbf{q}}$ has a dual use. In addition to relating the velocities to the rate of change of the constraint function Φ , the rows of $\Phi_{\mathbf{q}}$ act as basis vectors for constraint forces. Thus, when we solve for the constraint forces, we actually just need to solve for the coefficient vector **λ** (whose components are the Lagrange multipliers) that contains the magnitudes of the forces that correspond to each of these basis vectors. The total force acting on the system is the sum of the external forces and the constraint forces**.**

Finally, the elements of the constraint accelerations right-hand side vector must be computed. The same number of entries is required as the number of constraint equations in the system.

Performing all derivations and evaluations of the key sub-matrices and vectors required by the dynamic analysis formulation, the governing equations of motion can be assembled according to the Eqs.(4.2.8) or (4.2.9).

4.5 Introduction to Optimization

Optimization can be described as the process of seeking the best result under a given set of circumstances. The best result can be either the minimum or the maximum value of something, depending on the evaluation criteria and what is to be accomplished. In the case of spatial mechanisms, the common approach is to minimize the error between the desired output and the achieved output.

The optimization problem takes form by creating a mathematical function (objective function) that represents the system that is to be minimized. Within this function there are variables that the designer can manipulate in order to change the value of the objective function. These variables are known as design variables. Typically they have practical limits that the designer will place on them. These limits are called constraints and must be expressed in the objective function in terms of the design variables.

A general approach to mechanism optimization can be outlined in four steps.

1. Choose the type of mechanism to be designed.
2. Select an approach for analysis.
3. Set up an objective function that will measure the quality of the design with respect to the objectives and constraints.
4. Search to find the optimal set of values for the design variables that produce the best result and satisfy all design constraints.

There are three types of variables in optimization problems: Pre-set variables are constants, such as the modulus of elasticity or π. Design variables are independent, and generally express some aspect of the topology of the structure, its configuration or cross-section. Behavioral variables are dependent on variation of the design variables and behavioral relationships such as elasticity. Examples of behavioral variables for a structural system are stress, strain, and strain energy (Kirsch, 1981).

4.5.1 Formal Definition of the Optimization Problem

An optimization problem or mathematical programming problem can be stated in the following form [**19**]:

$$\text{Find} \qquad \mathbf{X} = \begin{Bmatrix} X_1 \\ X_2 \\ . \\ . \\ X_n \end{Bmatrix} = \{X_1, \quad X_2 \quad . \quad . \quad X_n\}^T \tag{4.5.1}$$

That minimizes the function $\Gamma(X, \theta)$ (where θ is an independent set of input motion variables having a predetermined range), subject to inequality constraints

$$\mathrm{K_j}(\mathbf{X}, \theta) < 0\,, \quad j = 1,2,.....,m \tag{4.5.2}$$

and equality constraints

$$l_j(\mathbf{X}, \theta) = 0\,,\ j = m+1, m+2,....., p \tag{4.5.3}$$

Where, $\boldsymbol{X}$ is the design vector, and $\Gamma(\mathbf{X}, \theta)$ is the objective function. The design vector is composed of the design variables, which may be written in transposed form as $\{X_1, X_2,....., X_n\}^T$. The vector $\theta = \{\theta_1, \theta_2,....., \theta_q\}^T$, made up of a set of independent parameters, may typically be comprised of time or position values. In mechanism design, the independent parameters representing the mechanism inputs often appear in the design equations.

4.5.2 Objective Function

As with any linkage synthesis problem, only a limited number of output positions can be reached exactly. By using optimization, a mechanism can be synthesized that will minimize the structural error at any number of desired positions. A logical and popular way to form the objective function is by computing the sum of the squares of the structural error at the given design points. In this case, the structural error is defined as the difference between the desired and the actual output position of the mechanism. Therefore, if the position of a point *P* is a known function of the input angle at each of the *n* prescribed positions (desired output), then

$$P_i = \beta(\theta_i), i = 1,2,...,n \tag{4.5.4}$$

so that the objective function (O. F.) to be minimized is

$$O.F = \Gamma(\mathbf{X},\theta) = \sum_{i=1}^{n} \{\beta(\theta_i) - \alpha(\mathbf{X},\theta_i)\}^2 \tag{4.5.5}$$

Where, $\alpha(\mathbf{X},\theta_i)$, $i = 1,2,...,n$, are the output positions actually generated by the mechanism (actual output).

A number of methods exist for determining the optimum combination of imperfections. The first is iteration. By calculating the value of the objective function for a large number of possible combinations of the design variables, it is possible to find an approximate optimum value. Another method used for analysis is the pre-selection of constraints believed to be critical (active) at the optimum and solution of the optimization problem based upon these constraints. This method can be accurate if the correct constraints are chosen.The general method of optimization used with mechanisms is mathematical programming. It is intended to solve a generally defined problem using numerical search algorithms. This method is efficient in solving problems with a single, global optimum value for the objective function within the design space. The algorithm considered for optimization discussion in this thesis is the generalized reduced gradient (GRG).This algorithm has applied to discuss the designed lens-polishing mechanism optimization in chapter five using the MSC.ADAMS software package.

4.5.3 Non-linear Programming Methods

The two main optimization algorithms built-in MSC.ADAMS are sequential quadratic programming (SQP) and generalized reduced gradient (GRG) methods. For small to medium sized nonlinear constrained problems, studies have concluded that the (GRG) and (SQP) methods are the most robust and efficient. From these two algorithms, a specific emphasis is given to the GRG method in this thesis work.

4.5.4 Generalized Reduced Gradient (GRG) Mathematical Formulation

This section presents a concise description of the GRG method as it has been implemented in MSC.ADAMS2005 to discuss the representative numerical mechanism in chapter five. The intent is to give an understanding to discuss the method for application to the optimal design of the mechanism.

Recall the equality constrained nonlinear programming problem given by

$$\text{Minimize: } \Gamma(\mathbf{X},\theta) \qquad \{X_1, X_2, ..., X_n\}^T, \ \theta = \{\theta_1, \theta_2, ..., \theta_q\}^T \tag{4.5.6}$$

$$\text{Subject to: } l_j(\mathbf{X},\theta)=0 \qquad j=1,2,...,m \tag{4.5.7}$$

$$X_{n_l} \le X_n \le X_{n_u} \quad n=1,2,...,N \tag{4.5.8}$$

The basic concept of the GRG method is to convert the equality constrained problem into an unconstrained problem and then utilize an unconstrained search procedure. The method requires the division of the variables into two classes: dependent variables X_D, and independent variables X_I.

$$\nabla^2\Gamma(\mathbf{X}_I)=\left[\frac{\partial\Gamma}{\partial X_{1I}},\frac{\partial\Gamma}{\partial X_{2I}},...\frac{\partial\Gamma}{\partial X_{NI}}\right] \tag{4.5.9}$$

$$\nabla^2\Gamma(\mathbf{X}_D)=\left[\frac{\partial\Gamma}{\partial X_{1D}},\frac{\partial\Gamma}{\partial X_{2D}},...\frac{\partial\Gamma}{\partial X_{ND}}\right] \tag{4.5.10}$$

The independent variables become the decision variables and dependent variables are slaves to the decision variables, used only to satisfy the constraints. In the computation of the reduced gradient, the Jacobian of the constraints is also partitioned with respect to the dependent and independent variables:

$$J_{X_I}=\begin{bmatrix} \frac{\partial l_1}{\partial \mathbf{X}_{1I}} & \frac{\partial l_1}{\partial \mathbf{X}_{2I}} & \cdot & \cdot & \cdot & \frac{\partial l_1}{\partial \mathbf{X}_{NI}} \\ & & & & & \cdot \\ & & & \cdot & & \cdot \\ & & & & \cdot & \cdot \\ & & & & & \cdot \\ & & & & & \cdot \\ \frac{\partial l_{ND}}{\partial \mathbf{X}_{1D}} & \frac{\partial l_{ND}}{\partial \mathbf{X}_{2D}} & \cdot & \cdot & \cdot & \frac{\partial l_{ND}}{\partial \mathbf{X}_{ND}} \end{bmatrix} \tag{4.5.11}$$

$$J_{X_D} = \begin{bmatrix} \frac{\partial l_1}{\partial \mathbf{X}_{1D}} & \frac{\partial l_1}{\partial \mathbf{X}_{2D}} & \cdots & \frac{\partial l_1}{\partial \mathbf{X}_{ND}} \\ \vdots & \vdots & & \vdots \\ \frac{\partial l_{ND}}{\partial \mathbf{X}_{1D}} & \frac{\partial l_{ND}}{\partial \mathbf{X}_{2D}} & \cdots & \frac{\partial l_{ND}}{\partial \mathbf{X}_{ND}} \end{bmatrix} \tag{4.5.12}$$

The differential of the objective function can be written as a function of the partitioned gradients

$$d\Gamma = \nabla^T \Gamma(\mathbf{X}_I) d\mathbf{X}_I + \nabla^T \Gamma(\mathbf{X}_D) d\mathbf{X}_D \tag{4.5.13}$$

The differential of the constraints can be written as function of the partitioned Jacobian and differential displacement vectors, which by definition of this method is zero.

$$d\vec{l} = \bar{J}_{X_I} d\mathbf{X}_I + \bar{J}_{X_D} d\mathbf{X}_D \equiv 0 \tag{4.5.14}$$

Solving for the dependent variable differential change in terms of the independent variables gives,

$$d\mathbf{X}_D = -\bar{J}_{X_D}^{-1} \bar{J}_{X_I} d\mathbf{X}_I \tag{4.5.15}$$

Which when substituted into Eq. (4.5.13) and rearranging gives the reduced gradient

$$\nabla_r^T \Gamma(\mathbf{X}_I) = \nabla^T \Gamma(\mathbf{X}_I) - \nabla^T \Gamma(\mathbf{X}_D) \bar{J}_{X_D}^{-1} \bar{J}_{X_I} \tag{4.5.16}$$

The reduced gradient is the rate of change of the objective function with respect to the independent variables with the dependent variables adjusted to maintain feasibility. Changing the values of the independent variables will force a change in the dependent variables to maintain feasibility, at least over small changes where the constraints are linear. For nonlinear functions, changes in independent variable values beyond finite values will cause the linear approximation of the constraints to become invalid. Therefore, the dependent variables must be adjusted by a nonlinear technique during each line search step to restore feasibility. The method most

commonly employed is the Newton-Raphson (N-R) method to readjust the dependent variables to satisfy the constraints. The finite adjustment of the dependent variables is given by

$$\Delta \mathbf{X}_D = -\bar{J}_{X_D}^{-1} \mathbf{r}_e \tag{4.5.17}$$

Where $\mathbf{r_e}$ is the residual error vector of the constraints and $\bar{J}_{X_D}^{-1}$ is the inverse of the dependent Jacobian, already computed in Eq.(4.5.12). Because the N-R method requires a square Jacobian for inversion, the number of dependent variables must equal the number of equality constraints. The implementation of the GRG method generally consists of a number of line searchsteps in the (feasible) reduced gradient direction, each step followed by a N-R readjustment of the dependent variables to maintain feasibility. The GRG method is sometimes referred to as the 'saw-tooth'.

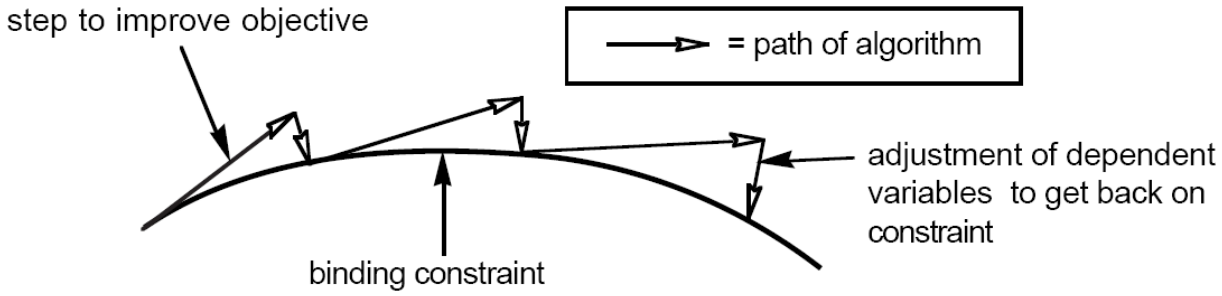

Figure 4.5.1 GRG nonlinear constraint satisfaction

CHAPTER 5-THE DESIGN OF LENS-POLISHING SPATIAL FOUR-BAR MECHANISM USING ADAMS SOFTWARE PACKAGE

5.1 Some Points about the MSC. ADAMS† Software Package

In the late 1970s engineers began using newly available computer programs that automate the process of creating the mathematical models and solving the equations. These programs are generically referred to as general-purpose multi-body dynamics programs, allowing detailed models of literally any mechanical system to be created and simulated rapidly with relative ease (Schiehlen, 1986; Kortüm and Sharp, 1993; Richard and Gosselin, 1993; Sharp, 1994).

Early simulations were based on mathematical models whose equations were laboriously and painstakingly derived by hand and solved using purpose-written computer programs. The development of these simulation programs and verification of their outputs against experimental tests was undertaken at considerable expense.

Multibody simulation programs are now widely used throughout the automotive industry, and they are also used to solve dynamics problems that arise in areas such as bio-mechanics, machine dynamics, rail vehicle dynamics, robotics, and in spacecraft dynamics and control.

ADAMS is a complete set of integrated software modules for simulating large displacement, three-dimensional motions of a wide range of mechanical systems. The first version of ADAMS was commercially released in the USA in 1980. It was first demonstrated by simulating a three-dimensional mechanical dynamic system and the predictions from the simulations were confirmed through experimental verification (Orlandea et al, 1977; Orlandea and Chace, 1977). Since then, ADAMS has been demonstrated and verified in a broad and diverse range of applications. The degree-of-freedom that one part has relative to another part depends on the specific features of the joint.

---

† ADAMS is an acronym for **A**utomatic **D**ynamic **A**nalysis of **M**echanical **S**ystems. In addition to its widespread use in Australia and North America, ADAMS is also used widely in Europe and Asia.

The ADAMS software generates the mathematical equations that describe the dynamics of the mechanical system, and the software then proceeds to find solutions for each time step in the simulation. The simulation builds a picture of how for each time-step each part in the model moves in 3-dimensional space (translates and rotates). When the simulation is completed all motions and forces are available to the user for review and for further analysis either within ADAMS or using other engineering software.

ADAMS is an extremely powerful tool providing the user with sufficient features enabling almost any conceivable and imaginable mechanical system to be built and fully tested. A model is built by creating assembling parts, connecting them with joints, and driving them with motion generators. We can also define forces, such as springs or friction, and apply them between individual parts in our full system design. The mass properties for each part must be defined. We can give also our ADAMS model parametric properties, enabling us to select design variables, sweep it through a range of values, and initiate a set of parametric simulations to study design sensitivities.

The software checks our model and automatically formulates and solves the equation of motion for kinematic, static, or dynamic simulations. The purpose of simulation is to assess the behavior of a system before its construction so as to

- dimension its mechanical elements
- optimize its performances
- design a controller(sensor, if necessary)
- identify possible problems on an existing system

The Basic elements are bodies, defined by mass m_i ; position of center of mass r_{gi} ; body fixed reference frame (coordinate system); inertia tensor $\mathbf{I}_{gi}$; auxiliary body fixed frames (attachment points); ground fixed reference body.

Cartesian coordinates are used in MSC.ADAMS to configure the parameters (position and orientation) of each body. The main advantage of this coordinate system is that; very systematic, hence easy to program. The drawbacks are; large number of equations (but simple and sparse), constraints (DAE_s need more robust integration methods).

Forces, torques and motions can be applied so the system moves in a particular fashion. It is also possible to implement control systems. The user only needs to define the parametric data; the

equations of motion are automatically applied when the finalized model is sent to the solver program. Program scripts can be utilized by the solver program to customize and guide the simulation process. The solver automatically integrates the equation of motion for a certain time step which is determined by the solver and outputs data in the form of result sets for each time step.

ADAMS enables users to produce virtual prototypes, realistically simulating the full motion behavior of complex mechanical systems and quickly analyze multiple design variations in search for an optimal design. This reduces the number of costly physical prototypes, improves design quality and dramatically reduces product development time.

The MSC.ADAMS is a family of products each developed for a specific purpose. The MSC.ADAMS products are:

ADAMS/View: This software lets you build models of mechanical systems and simulate the full motion behavior of the models and can be used to quickly analyze multiple design variations in search for an optimal design. It is a 3-D interactive environment in which the parametric properties of the mechanical system are defined.

ADAMS/Solver: This software is a powerful numerical analysis application that solves the equations of motion for kinetic, static, and dynamic simulations.

ADAMS/Post Processor: This software is a powerful post processing tool that lets you view the results of simulation performed using other products.

The above three MSC.ADAMS products are mainly used to build the model of my interest in this thesis work. In addition to the above MSC.ADAMS family, the following products are also developed for a specific purpose.

ADAMS/Aircraft	ADAMS/Car	ADAMS/Flex	
ADAMS/Insight	ADAMS/Rail	ADAMS/Vibration	
ADAMS/Real-time	ADAMS/Ride	ADAMS/Chassis	ADAMS/Controls
ADAMS/Driveline	ADAMS/Durability	ADAMS/Engine	ADAMS/Tire

In MSC.ADAMS, like all other computer aided engineering (CAE) software, there are four main steps in simulation of a model. These are preprocessing (modeling), solution, post processing and optimization.

ADAMS/Solver to solve our model and ADAMS/Post Processor to see the results of our simulation and finally thought parametric design; will be able to optimize our design. Although

we rarely change our working environment out of ADAMS/View but we should know that these products are used throughout the simulation and we indirectly interact with them.

Table 5.1.1 Design process steps in MSC.ADAMS software package

Build	▪ Model mechanism elements including moving parts, joints and connections. ▪ Verify the model parts and connections that have been created properly.
Test	▪ Perform simulations. ▪ Measure the required parameters. ▪ Apply proper input loads.
Review	▪ Import test data/design variables to compare with simulation data.
Improve	▪ **Refine:** • Parameterize the critical point locations. ▪ **Iterate:** • Study the effect of design parameters on design objective. • Find sensitivity of design objectives to parameters in any critical point. ▪ **Optimize:** • Optimize the design to achieve the best performance by the best combination of design parameters.
Compare	▪ Compare your real test data/ design variables with simulation data.

5.2 Problem Descriptions of the Lens-polishing Spatial Mechanism

The advantage that is of our interest here is the ability of spatial slider-crank mechanism to perform the functions of robot manipulators that are used as lens polishing mechanisms. The motivation here is to design the mechanism which does the work of rotary lens-polishing robots; that are too much expensive to afford. Lenses are used in different optical instruments such as telescopes, military fire control instruments and so on.

Here, a spatial four-bar mechanism will be designed to polish military optical instruments (in our case the objective lens of one machine gun is considered) which are very useful in every maintenance areas of the Ethiopian Defence Industries. These lenses have contacts with the mechanical supports which may cause rust due to cold weather and dusts go through the lens surfaces. Polishing of these lenses manually (by hand) has the disadvantage of not cleaning at the required time since the motion of the hand is slow to polish properly and fastly. The other

disadvantages is breakage from hand during polishing operation may occurred in addition to the hand's imprints that reduces the ability of lenses in observing targets after assembling them to their mechanical supports.

The bottom surfaces of the two polishing pads are covered with spongy material to suck the white alcohol that is used as a polishing agent. Very thin circular leathers (dog skins) are used to retain these polishing agent and spongy materials together in the bottom surfaces of the pads.These materials are used to avoid scratches on the lens surfaces to be polished.Moreover, the polishing pads are built from light materials (aluminum) to avoid scratches and breakages on the lens surfaces. The eight holes on the wooden-block according to the lenses' dimensions to be polished could be made to be easily adjustable on the working slots of a table. Of course, the two polishing pads and wooden blocks with the holes for different diameters of lenses can be designed in such a way that to be fitted and removed easily to the connecting bar and polishing table, respectively. As an illustrative example, the mechanism below is designed to polish eight lenses which have 5cm radius each. The clearance between the lenses' upper surfaces and the polishing pads is taken to be 4mm as an initial data which is nearly the thickness of the polishing materials tied to the bottom surface of the two polishing pads. In general; designing this mechanism will reduce cost and ease of production (easily in machine shops) as compared to polishing rotary robots. Detail design parameters for the lens-polishing mechanism are given in Tables (5.2.1) to (5.2.9) below.

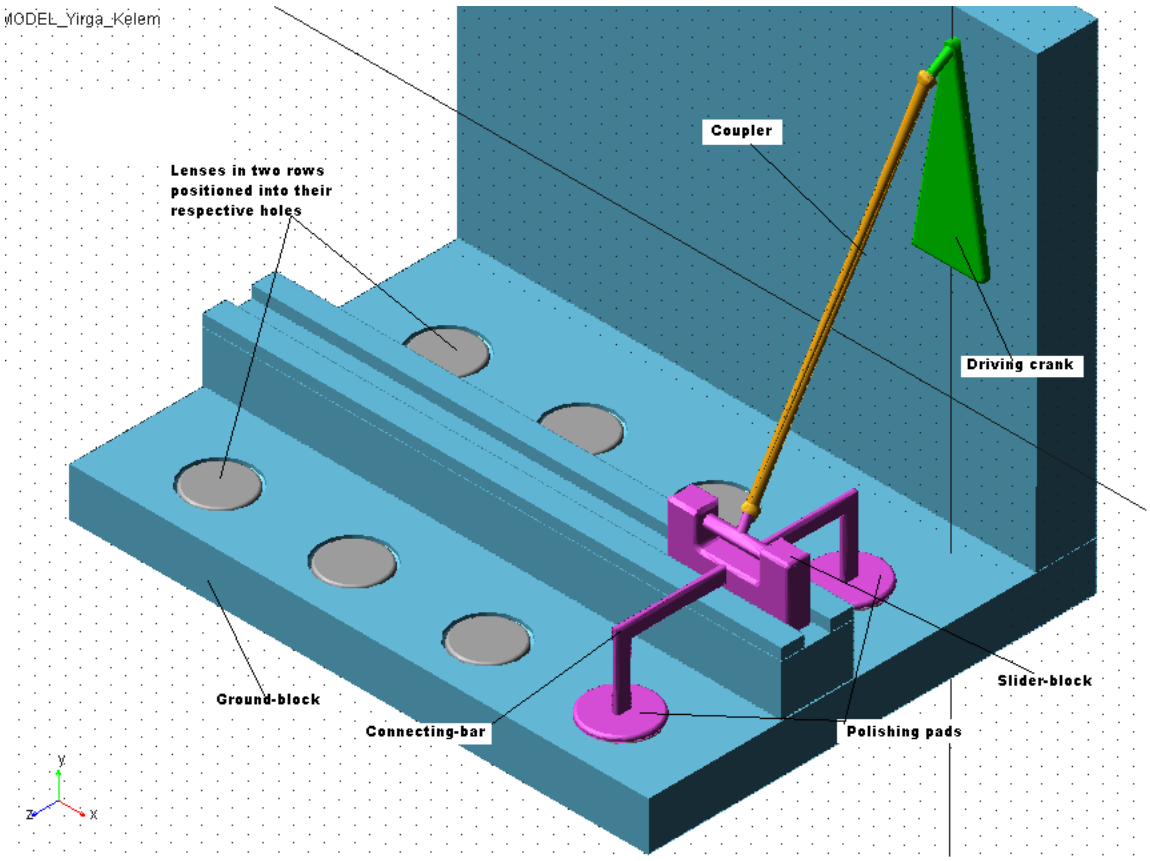

Figure 5.2.1 Linkage parameters of spatial four-bar lenses polishing mechanism

This mechanism is used to demonstrate the application of the methodologies previously presented. Four rigid bodies describe the mechanism under consideration. The model also includes one revolute joint that connects the ground and the driving crank, one spherical joint between the crank and the coupler, and another one spherical joint that connects the slider-block system and the coupler link, and one translational joint that connects the ground-block (fixed link) and the slider-block system. A body fixed coordinate systems is attached to the center of mass of each body, and xyz represents the global coordinate system. The gravitational acceleration is considered as acting in the negative Y direction and the crank is driven by constant input torque.

The crank, which is the driving link, rotates about the z-axis with a constant average working torque of 10.25Nm. The minimum input working torque is computed by considering the effort of a normal person's hand to overcome the inertia loads on the links in absence of actuating motor's power. For some linkages, an optimal positions and velocities will be obtained

in the optimization section using generalized reduced gradient (GRG) algorithm. As it is shown in the model, the crank is made of three sub-links which are joined each other with a weld at two positions. The same color (green) is given for the three bodies (two cylindrical and one plate link in the middle) to show that these links act as one unit driving crank for the whole mechanism, and the coupler is assigned by a maize color. The same fashion is followed to the slider-block, connecting-bar, and polishing pads assigned by a magenta color. Ground-block linkage is represented by a skyblue colour. Knowingly, the slider-block, connecting-bar and polishing-pads are part of the sliding-block system. The detail material properties of the linkages in the spatial mechanism are given in Table (5.2.5).

Table 5.2.1 Geometric parameters of each linkage for the spatial four-bar mechanism

Types of links	Length(m)	Width/depth(m)	radius(m)	Fillet radius(m)
Cylindrical link near the driving crank	0.04	---	0.018	---
Plate	0.300	0.015	0.010	0.005
Cylindrical link b/n the coupler & plate	0.050	---	0.007	---
Coupler Cylindrical link	0.56	---	0.008	---
Cylindrical link b/n the coupler slider block	0.035	---	0.007	---
Cylindrical link that connects the extruded box	0.2	---	0.010	---
Left and right polishing pads	0.008	----	0.056	0.004
Each hole	----	0.010	0.055	0.004
Each lens	0.012	---	0.05	0.004
Slider-block	See Tab.(5.2.3)	See Tab.(5.2.3)	---	0.005
connecting bar	See Tab.(5.2.4)	See Tab. (5.2.4)	---	0.004
Ball and socket	---	See Tab. (5.2.2)	See Tab. (5.2.2)	---

Table 5.2.2 Geometric parameters of each linkage for the spatial four-bar mechanism

Joint pairs	outer radius(m)	Hole depth(m)	Hole radius(m)	Radial clearance(m)
Upper and lower balls	0.008	---	---	---
Upper and lower sockets	0.013	0.01	0.0085	0.0005

Table 5.2.3 Location coordinates for the extruded slider-block with length of 0.04m along z-axis

Corner points	X	Y	Z
1	-0.130	-0.035	0.300
2	-0.130	-0.035	0.340
3	-0.080	-0.035	0.340
4	-0.080	-0.035	0.300
5	-0.080	-0.085	0.300
6	-0.080	-0.085	0.340
7	0.020	-0.085	0.340
8	0.020	-0.085	0.300
9	0.020	-0.035	0.300
10	0.020	-0.035	0.340
11	0.070	-0.035	0.340
12	0.070	-0.035	0.300
13	0.070	-0.135	0.300
14	0.070	-0.135	0.340
15	-0.130	-0.135	0.340
16	-0.130	-0.135	0.300

Table 5.2.4 Location coordinates for the extruded connecting-bar with length of 0.012m along x-axis

Corner points	X	Y	Z
1	-0.042	-0.086	0.520
2	-0.030	-0.086	0.520

3	-0.030	-0.086	0.120
4	-0.042	-0.086	0.120
5	-0.042	-0.111	0.145
6	-0.030	-0.111	0.145
7	-0.042	-0.111	0.495
8	-0.030	-0.111	0.495
9	-0.030	-0.211	0.145
10	-0.030	-0.211	0.120
11	-0.042	-0.211	0.120
12	-0.042	-0.211	0.145
13	-0.030	-0.211	0.520
14	-0.030	-0.211	0.495
15	-0.042	-0.211	0.495
16	-0.042	-0.211	0.520

Table 5.2.5 Material properties used in the dynamic simulation of the four-bar spatial lens-polishing mechanism

Links	Material type	Density(kg/m^3)	Poisson's ratio	Young's modulus(GPa)
Driving crank	steel	7801	0.29	207
coupler	aluminum	2740	0.33	71.71
Slider-block system	aluminum	2740	0.33	71.71
Ground-block (working table)	wood	438	0.33	11

Table 5.2.6 Mass and inertia properties of the spatial four-bar lens polishing mechanism

Links	Mass(kg)	$I_{x'x'}$	$I_{y'y'}$	$I_{z'z'}$	$I_{x'y'}$	$I_{y'z'}$	$I_{z'x'}$
Crank	2.88	0.0229	0.0215	0.0018	0	0	0
Coupler	0.33	0.00961	0.00961	0.0000112	0	0	0
Slider-block system	2.59	0.0325	0.0318	0.0141	0	0	0

Table 5.2.7 Key points for modeling of the spatial four-bar lens polishing mechanism

Hot points	X	Y	Z
1	0	0.22	-0.04
2	0	0.22	0
3	0.05	0.2	0
4	-0.05	0.2	0
5	0	0.5	0
6	0.0086	0.48	0.054
7	-0.03	-0.018	0.299
8	-0.03	-0.055	0.32
9	0.08	-0.055	0.32
10	0.02	-0.055	0.32
11	-0.03	-0.086	0.12
12	-0.042	-0.107	0.3
13	-0.13	-0.135	0.34
14	-0.0375	-0.216	0.5075
15	-0.0375	-0.216	0.13125

Table 5.2.8 Joints and linkages definitions used in the spatial four-bar lens polishing mechanism

Model Input Data for the Lens Polishing Mechanism	
Bodies	

Four links	nc=28
Constraints	
Revolute joint(crank, ground-block)	5
Spherical joint-1(crank, coupler or connecting rod)	3
Spherical joint-2 (coupler, slider)	3
Translational joint(slider, ground-block)	5
Distance constraint(coupler, slider)	1
Ground constraint	6
Euler parameter normalization constraint	4
Degree of freedom for the mechanism DOF=28-27=1	nh=27

The four- bar spatial mechanism is modeled with twenty eight vector coordinates, which result from the four rigid bodies and twenty seven kinematic constraints. Consequently, this system has one-degrees of freedom as illustrated in Table (5.2.8). It is very difficult to take out the equations manually from a lot of kinematic equations by avoiding the redundant equations. But, ADAMS will understand and solve simply the already designed model in the ADAMS/View.

The motion of the multi-body system can be defined by requiring that the orientation of the driving crank be some function of time. This is equivalent to imposing a driving constraint so that the remaining degrees of freedom are determined.

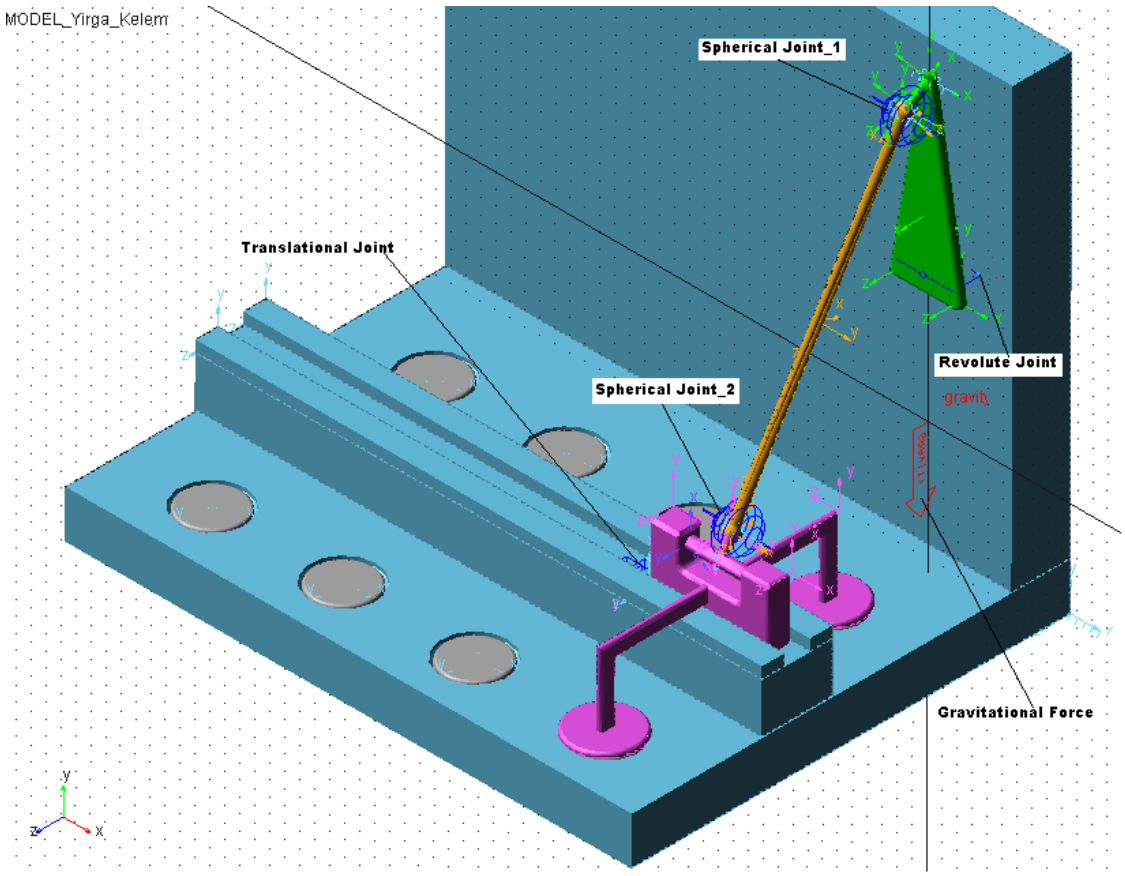
MODEL_Yirga_Kelem
Spherical Joint_1
Translational Joint
Revolute Joint
gravity
Spherical Joint_2
Gravitational Force

(a)

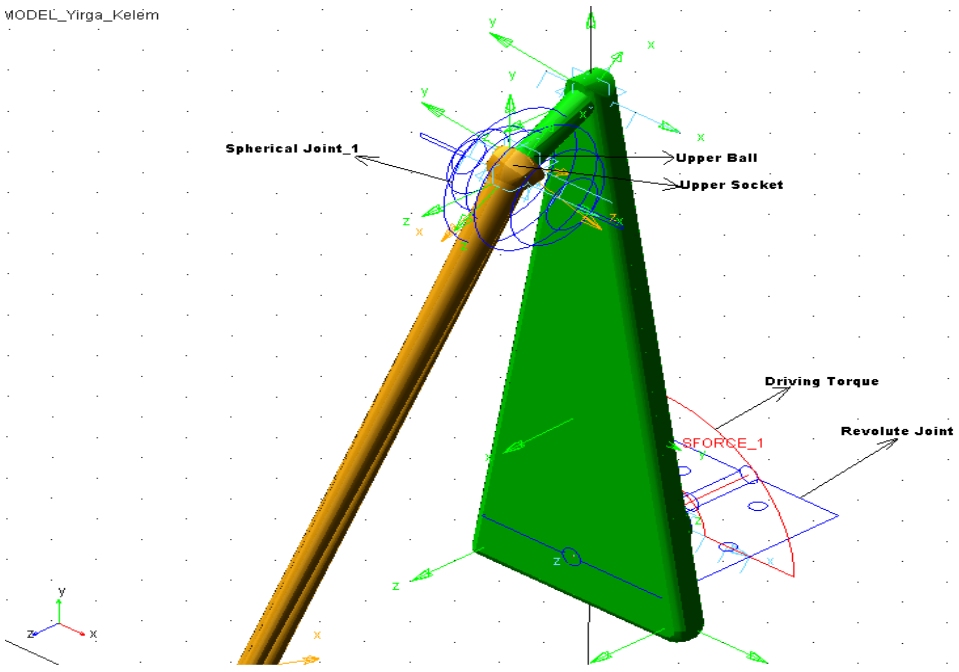
MODEL_Yirga_Kelem
Spherical Joint_1
Upper Ball
Upper Socket
Driving Torque
Revolute Joint
SFORCE_1

(b)

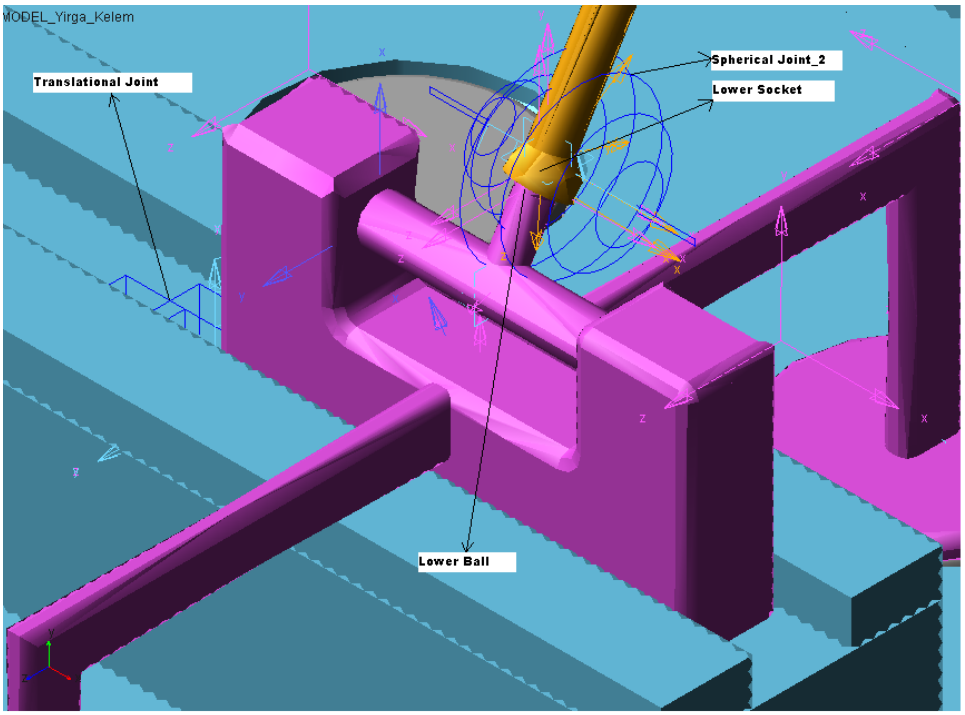

(c)

Figure 5.2.2 Different joints and input torque at equilibrium position (t=0) under gravitational force: (a) all joint descriptions, (b) upper section zoomed-in, and (c) lower section zoomed-in

The analysis of results is carried out for the first 2.5seconds. The time integrator use in MSC.ADAMS is stiff method for solving algebraic and differential equations of motion. The dynamic run is executed for the nominal coupler length of $l = 0.56m$ with input actuating torque of $T_{in} = 10.25Nm$ on the driving crank which rotates it with 50.4rad/sec. Output plots of the most important linkages and joints are given in the next chapter with a time step of $\Delta t = 0.01s$.

CHAPTER 6–DISCUSSION OF RESULTS AND OPTIMIZATION

6.1 Discussion of Results

Output plots of center of mass for each main linkage positions, orientations (in terms of Euler normalization parameters), velocities, and accelerations are presented in this section. The CM-angular velocities, CM-accelerations, translational momentums and angular momentums about CM of crank and coupler linkages are going to be discussed. Finally, the Lagrange multipliers for each joint are going to be discussed too.

The initial configuration of the spatial four bar mechanism is illustrated in Figure (5.2.1) and (5.2.2). The system is released from the initial position with input working torque and under the action of gravity force, which is taken to act in the negative y direction. So, the heights of centers of mass of all bodies dominate the total potential system energy and control the dynamic system's behavior.

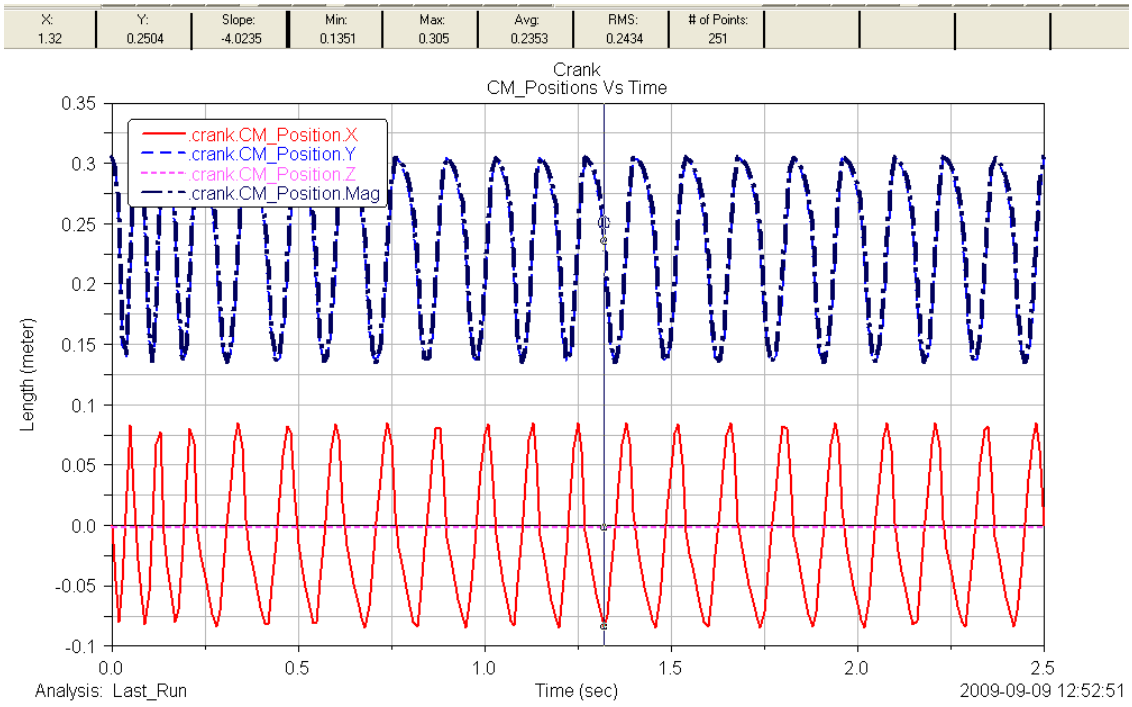

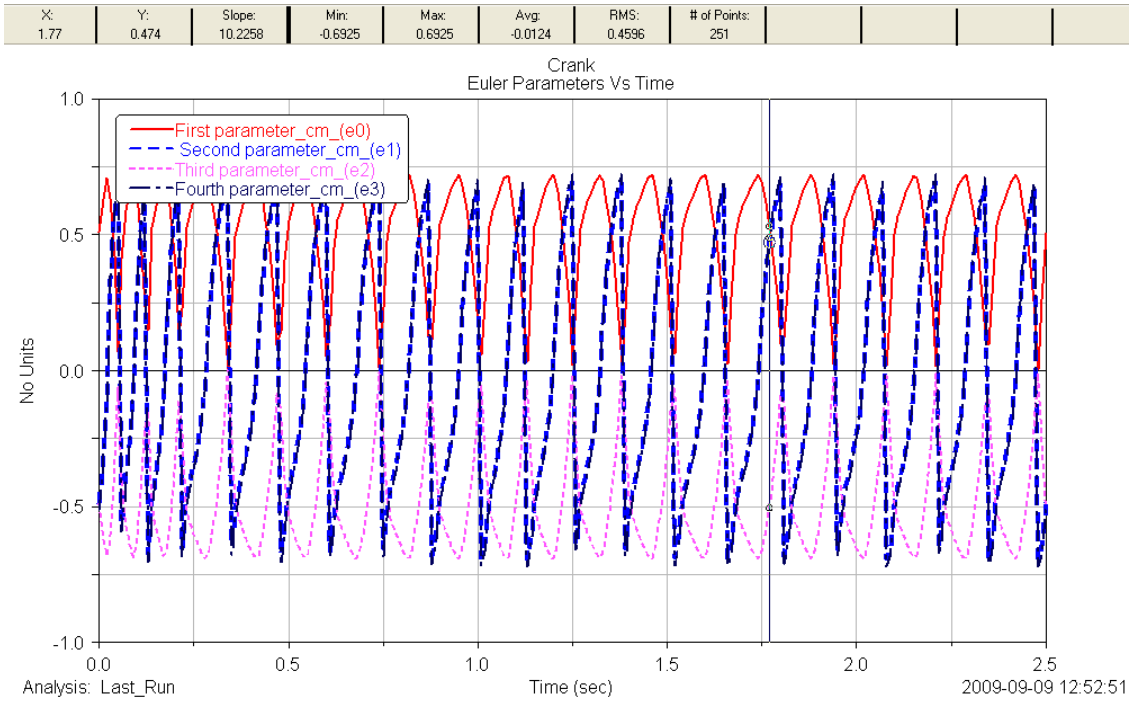
X: 1.77
Y: 0.474
Slope: 10.2258
Min: -0.6925
Max: 0.6925
Avg: -0.0124
RMS: 0.4596
# of Points: 251
Crank
Euler Parameters Vs Time
First parameter_cm_(e0)
Second parameter_cm_(e1)
Third parameter_cm_(e2)
Fourth parameter_cm_(e3)
No Units
1.0
0.5
0.0
-0.5
-1.0
0.0
0.5
1.0
1.5
2.0
2.5
Time (sec)
Analysis: Last_Run
2009-09-09 12:52:51

(a)

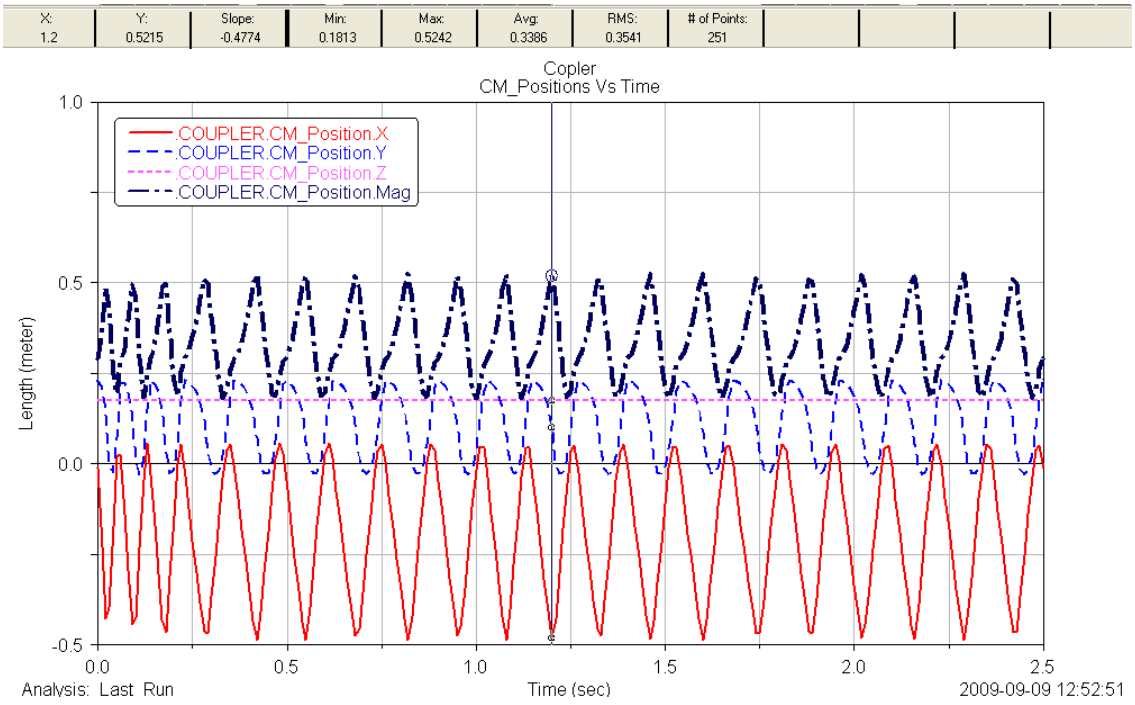
X: 1.2
Y: 0.5215
Slope: -0.4774
Min: 0.1813
Max: 0.5242
Avg: 0.3386
RMS: 0.3541
# of Points: 251
Copler
CM_Positions Vs Time
.COUPLER.CM_Position.X
.COUPLER.CM_Position.Y
.COUPLER.CM_Position.Z
.COUPLER.CM_Position.Mag
Length (meter)
1.0
0.5
0.0
-0.5
0.0
0.5
1.0
1.5
2.0
2.5
Time (sec)
Analysis: Last Run
2009-09-09 12:52:51

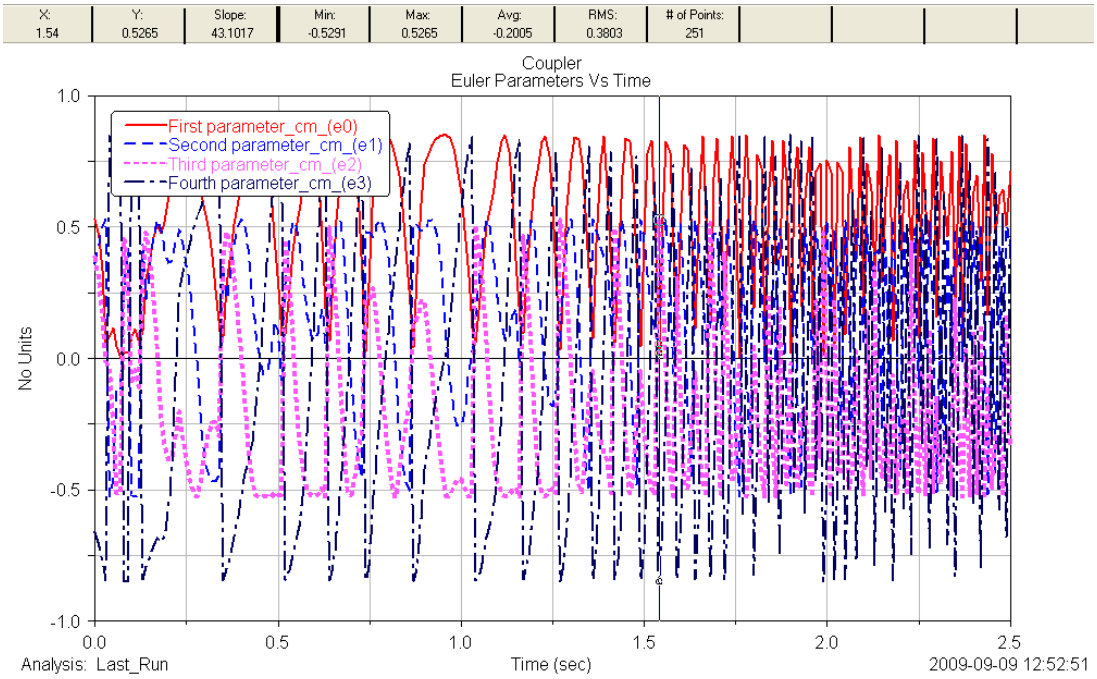

(b)

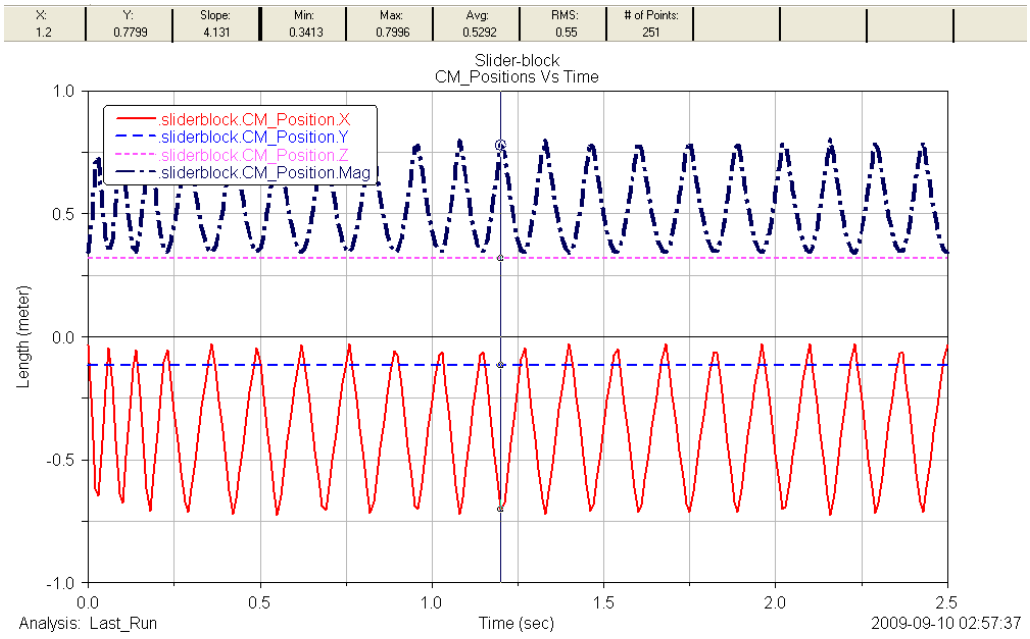

(c)

Figure 6.1.1 Positions and angular orientations of the (a) crank; (b) coupler; (c) slider-block versus time

Figure (6.1.1) presents the locations and orientations of the crank, coupler, and slider-block where the orientations are in terms of Euler parameters for the first 2.5 seconds for each linkage. All the output plots are given for the center of mass of each links. The Euler normalization parameters should fulfill Eq. (3.2.35) for each orientation change at any instant of time. The crank position is given for the x and y positions whereas the z is at the global reference frame (coincident with the origin). It also evident that the coupler is positioned in a space (x, y, and z) with its respective orientations but the slider and polishing pads translates only in the x-direction due to the prismatic joint connected to the slider-block.Whereas; if the translational joint is removed from its connecting position the mechanism will have unpredictable general motion in the space due to the spherical joints at the coupler extreme ends.

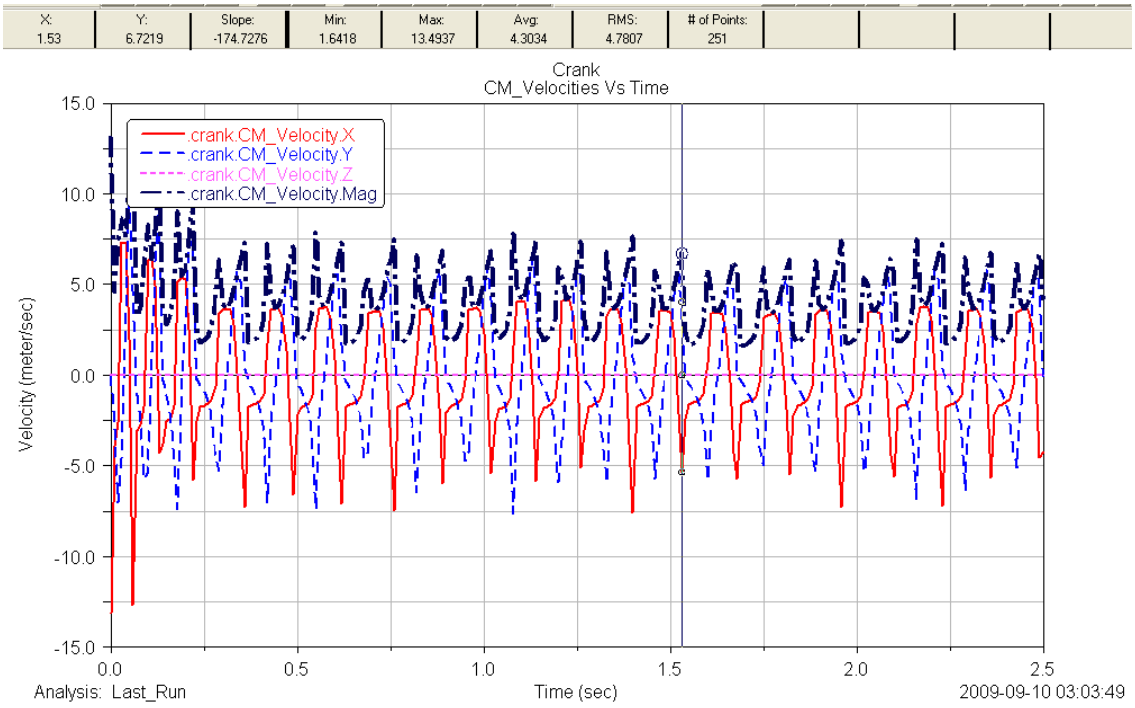

(a)

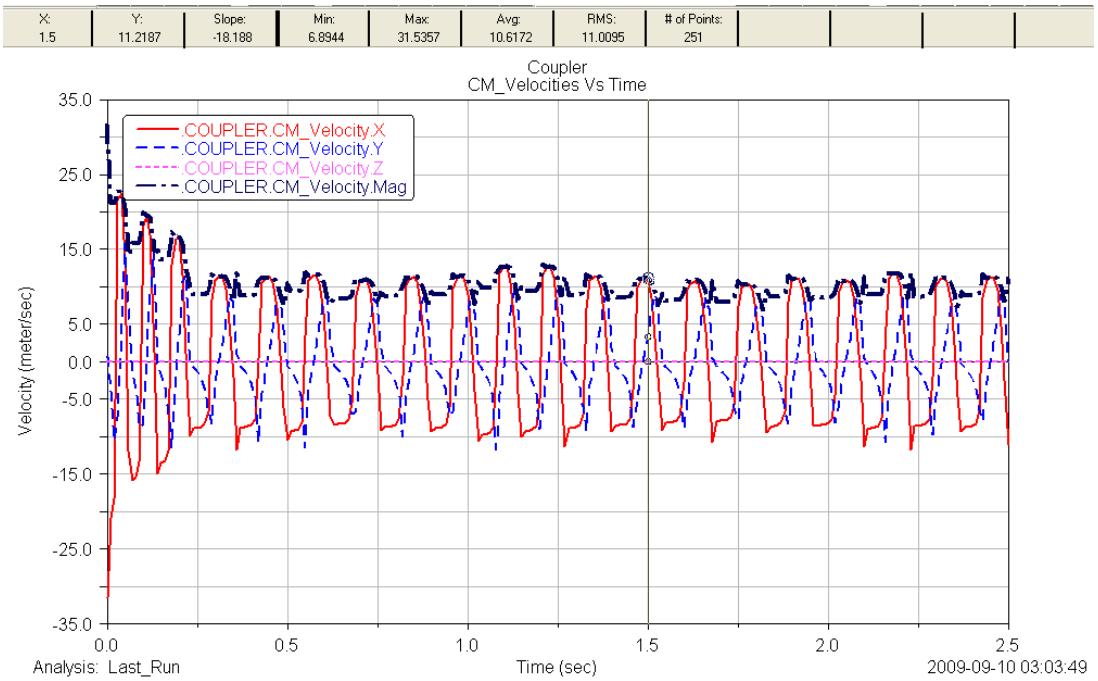

(b)

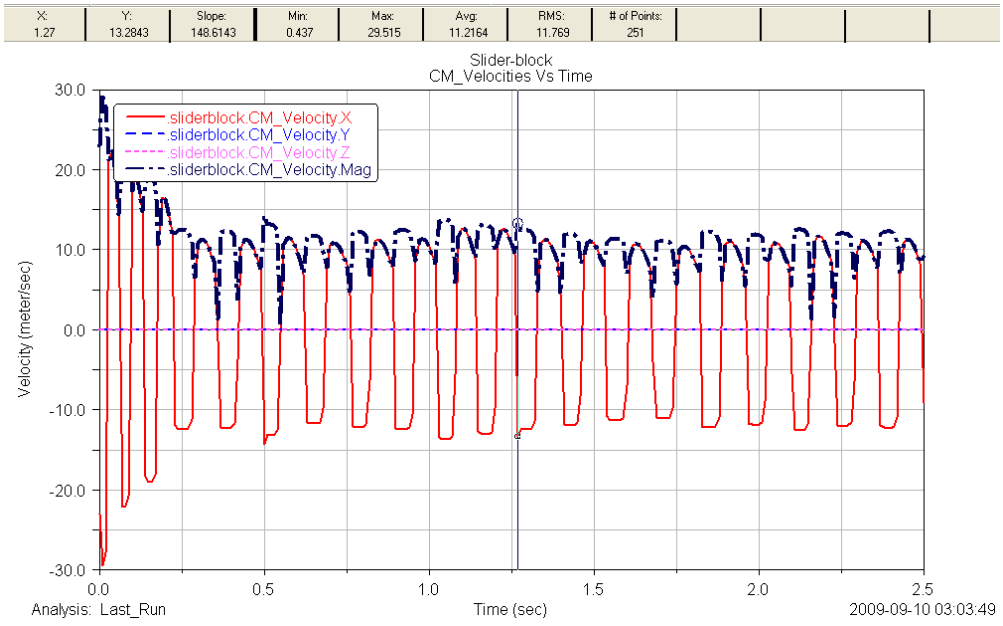

(c)

Figure 6.1.2 Output results of CM-velocities for (a) crank; (b) coupler; (c) slider-block; versus Time

Figure (6.1.2) shows that the output plots for CM-velocities of the slider-block and the polishing pads are the same for the first 2.5 seconds; this is evident that they represent parts of the same system. But the crank and coupler follow their own quite different velocity outputs. The crank CM rotates with an average velocity of magnitude 4.3 m/s, the coupler CM rotates with an average velocity of magnitude 10.62m/s, and the slider block system of magnitude 11.22m/s. The types of joints between two linkages are the determinant ones to allow the speed of the links. As it is shown in the above Fig.(6.1.2); the speeds of the coupler and the slider block system are about twice greater than the driving crank's velocity.

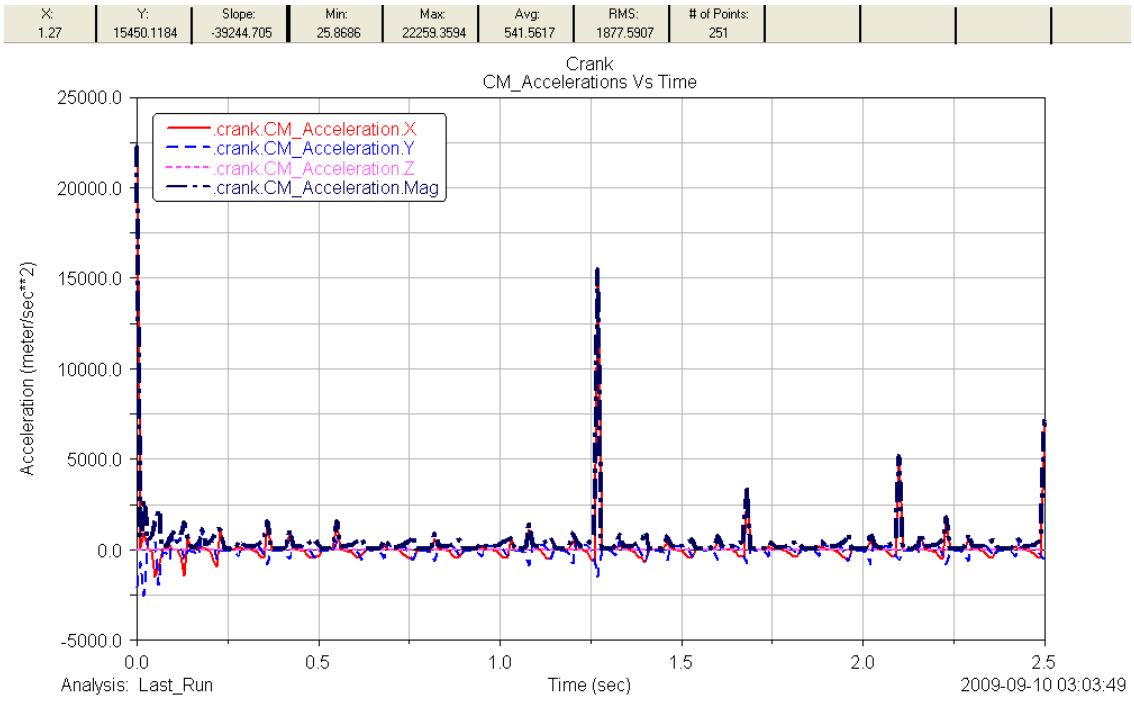

(a)

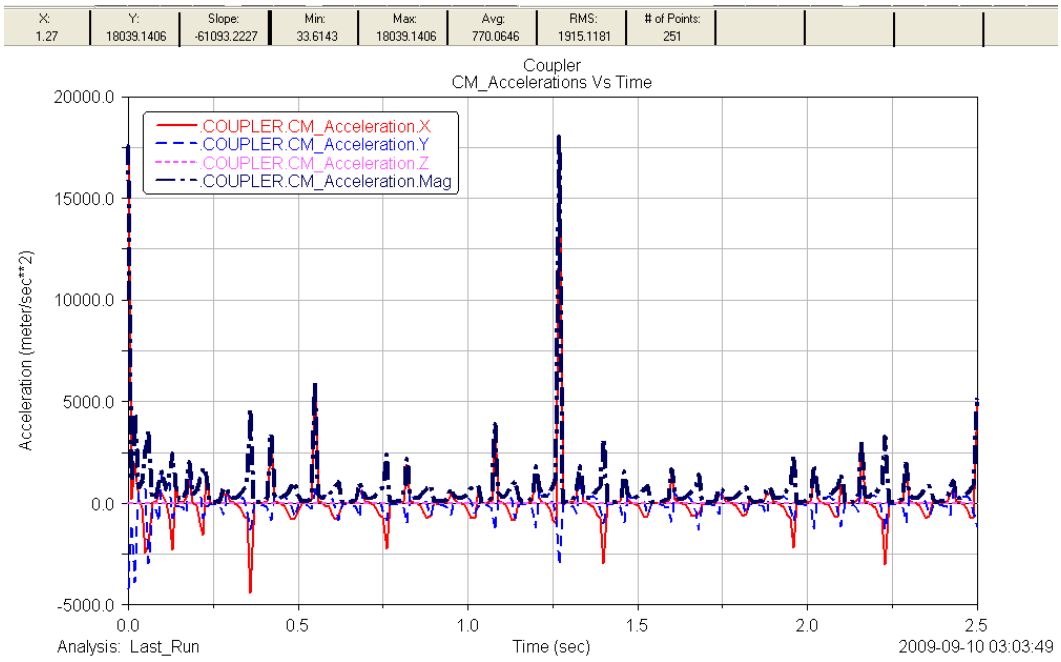

(b)

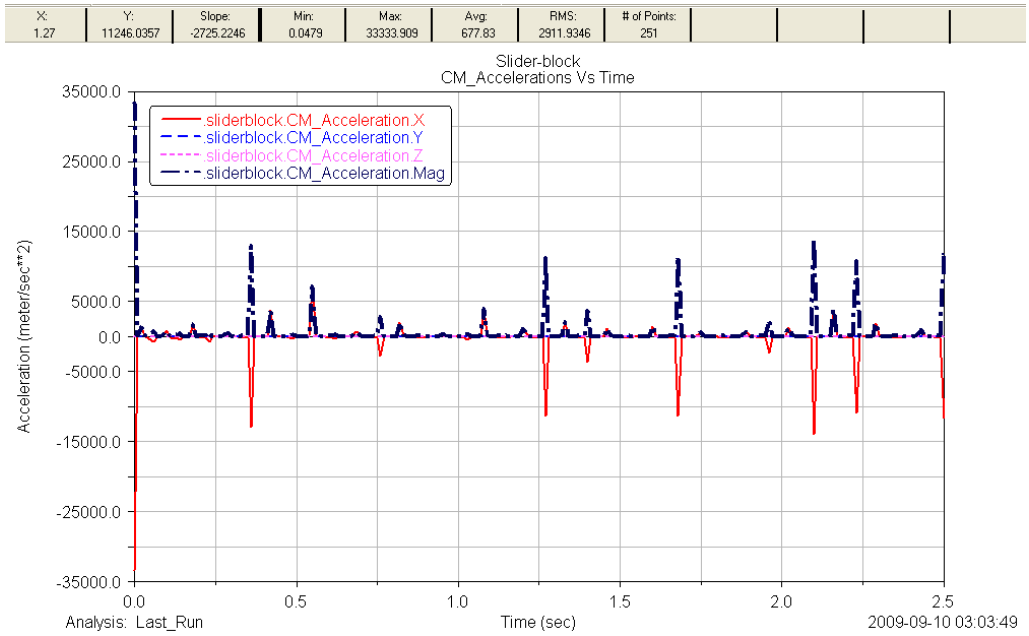

(c)

Figure 6.1.3 Output results of CM-accelerations for (a) crank; (b) coupler; (c) slider-system versus Time

Figure (6.1.3) shows that the output plots for CM-accelerations of slider-block and lens polishing pads is the same for the first 2.5 seconds. This shows that the polishing pads and slider-block are parts of the same system called the slider-system.Whereas; the crank and coupler follow their own quite different acceleration outputs. The acceleration output results for the crank (541.6m/s^2), coupler (770.1m/s^2), slider-system (677.8m/s^2) are obtained as shown in Fig.(6.1.3).

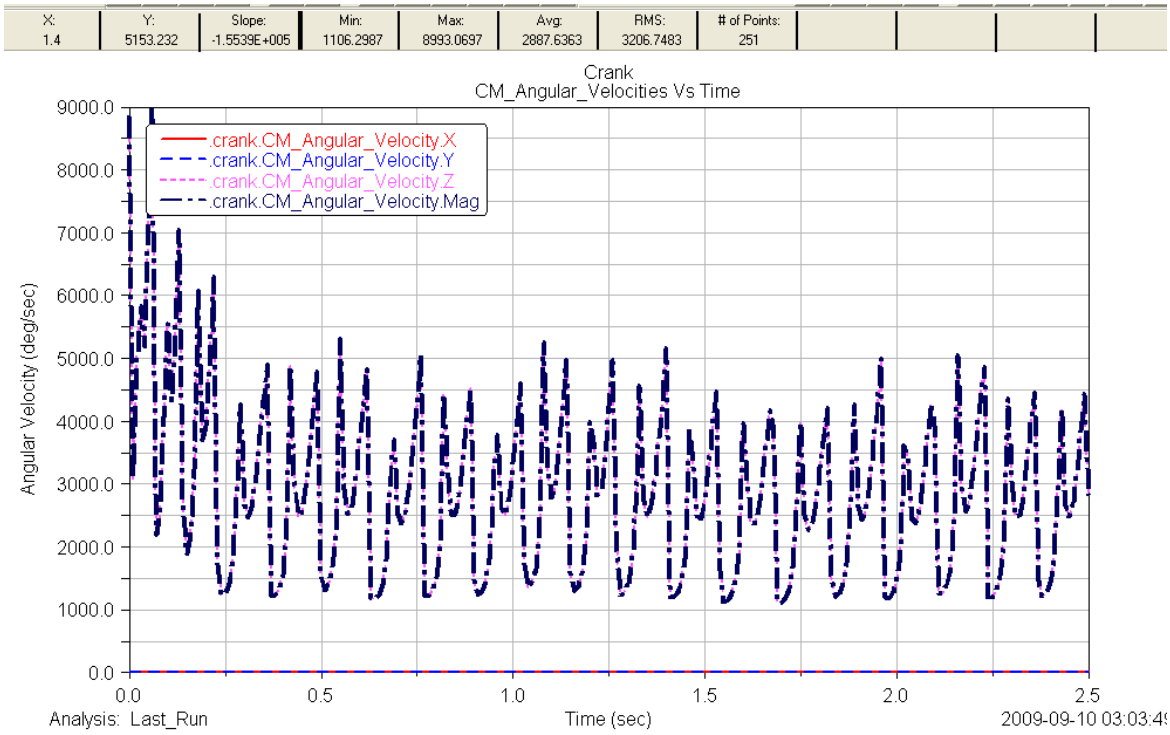

(a)

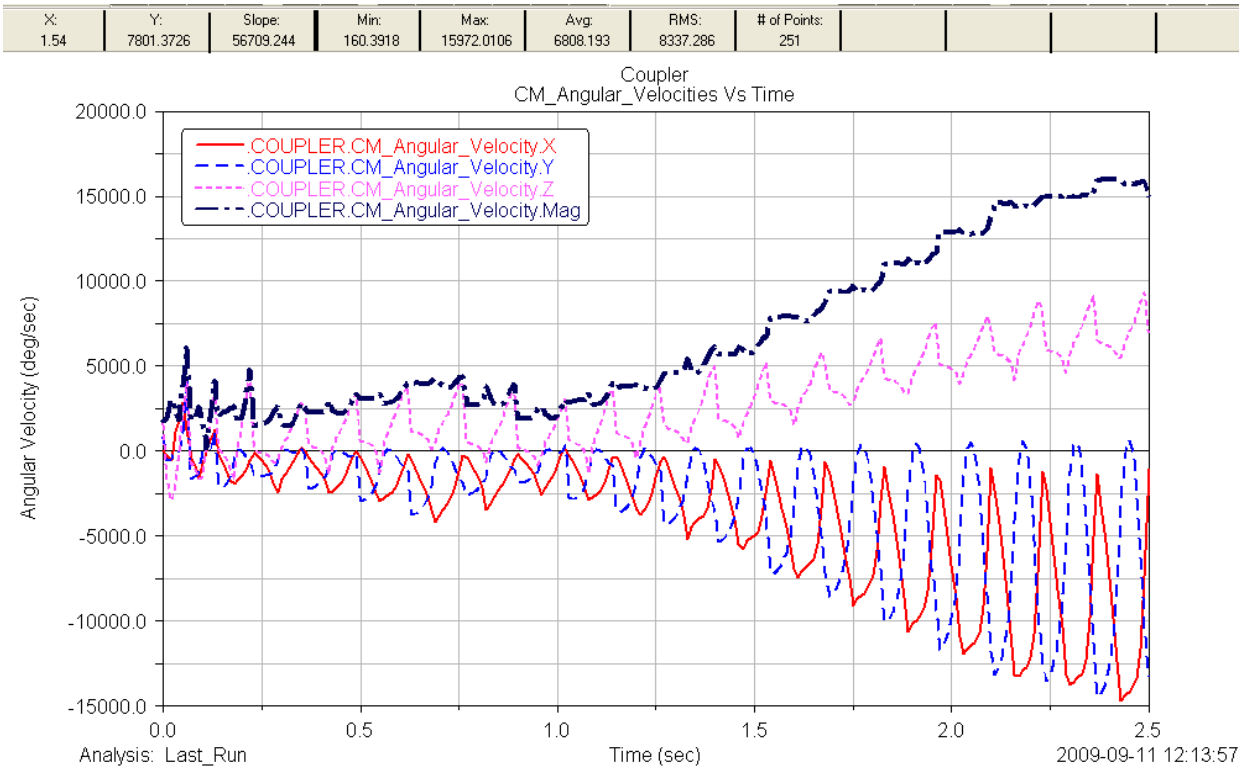

(b)

Figure 6.1.4 Output results of CM-angular-velocities for (a) crank; and (b) coupler links versus Time

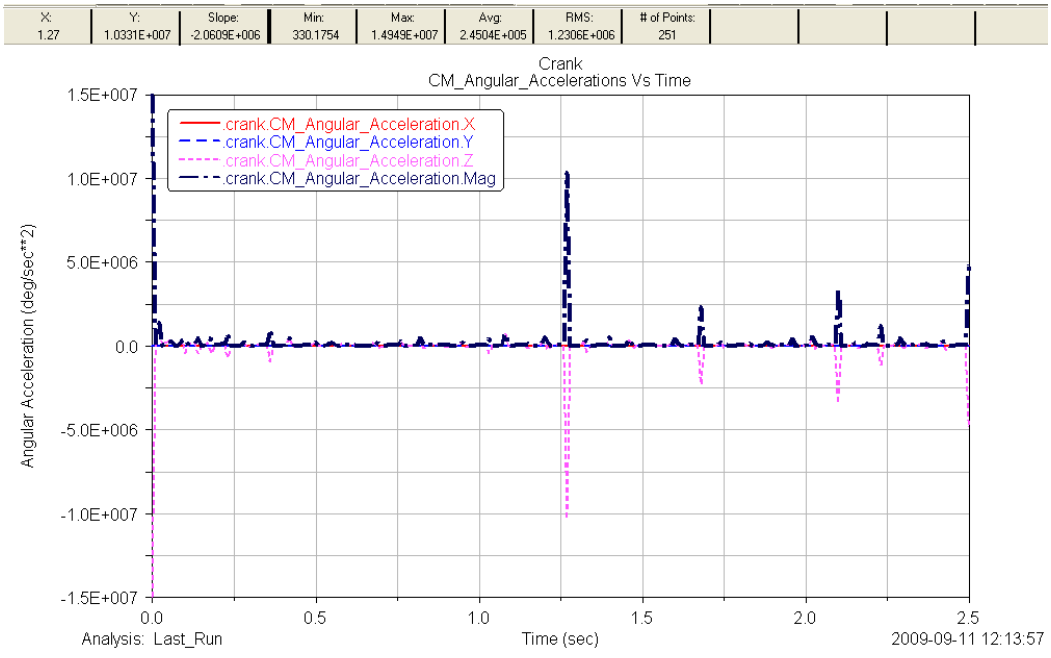

(a)

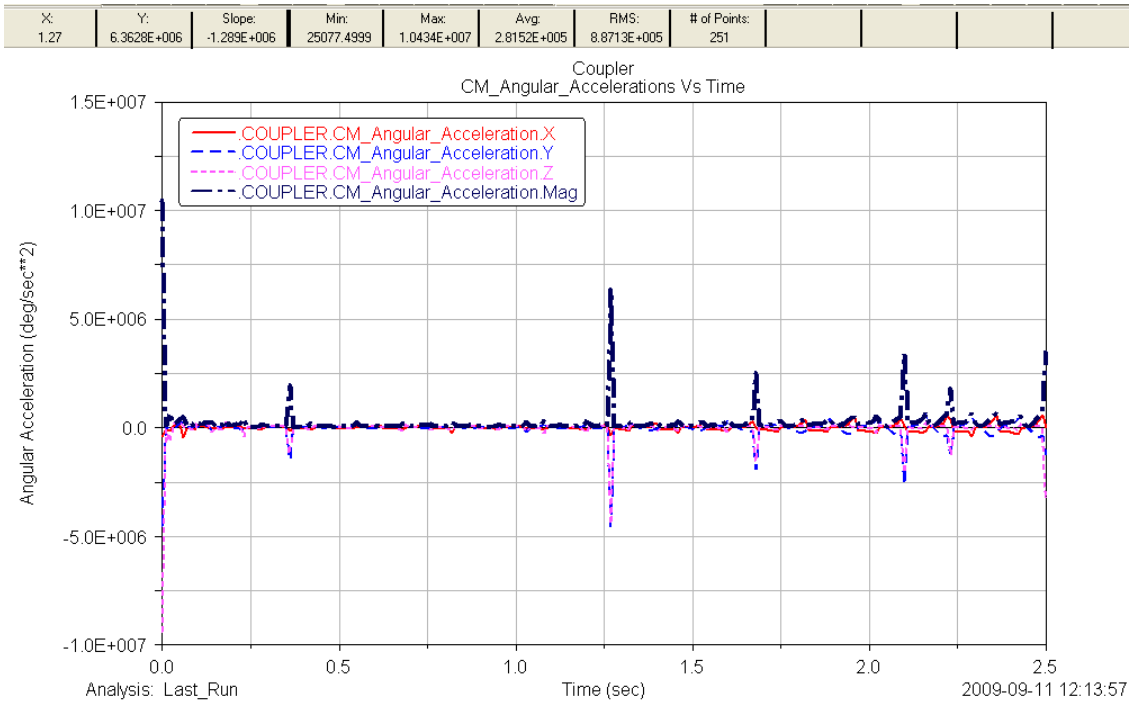

(b)

Figure 6.1.5 Output results of CM-angular-accelerations for (a) crank; and (b) coupler links versus Time

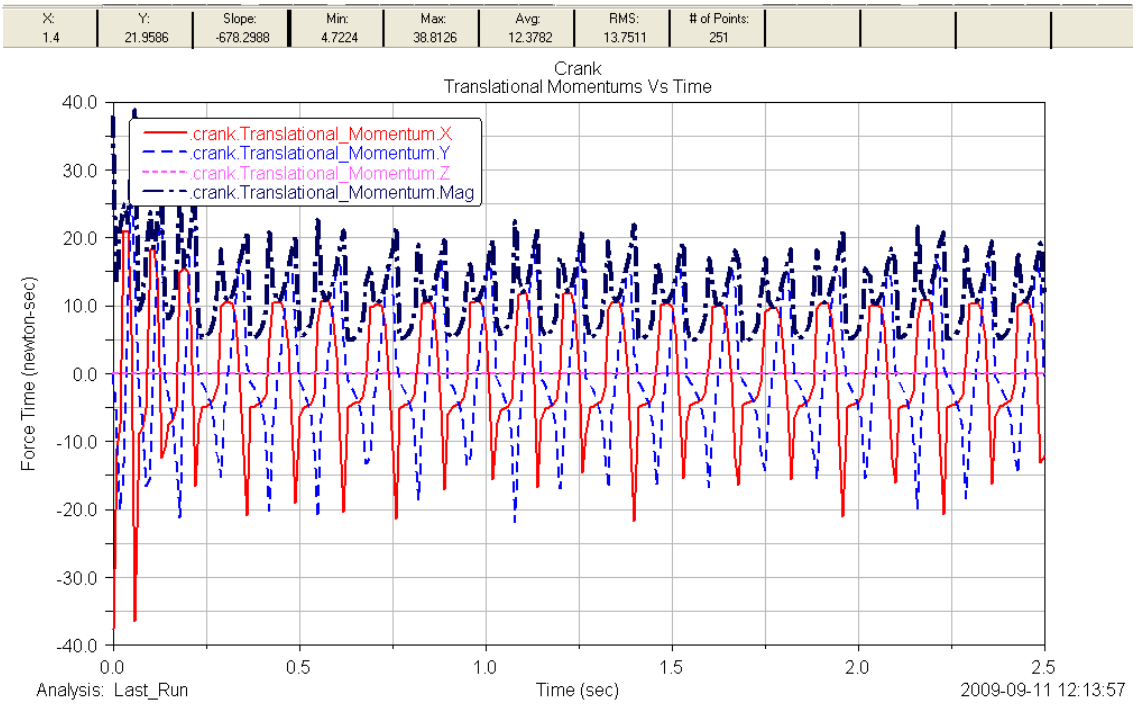

(a)

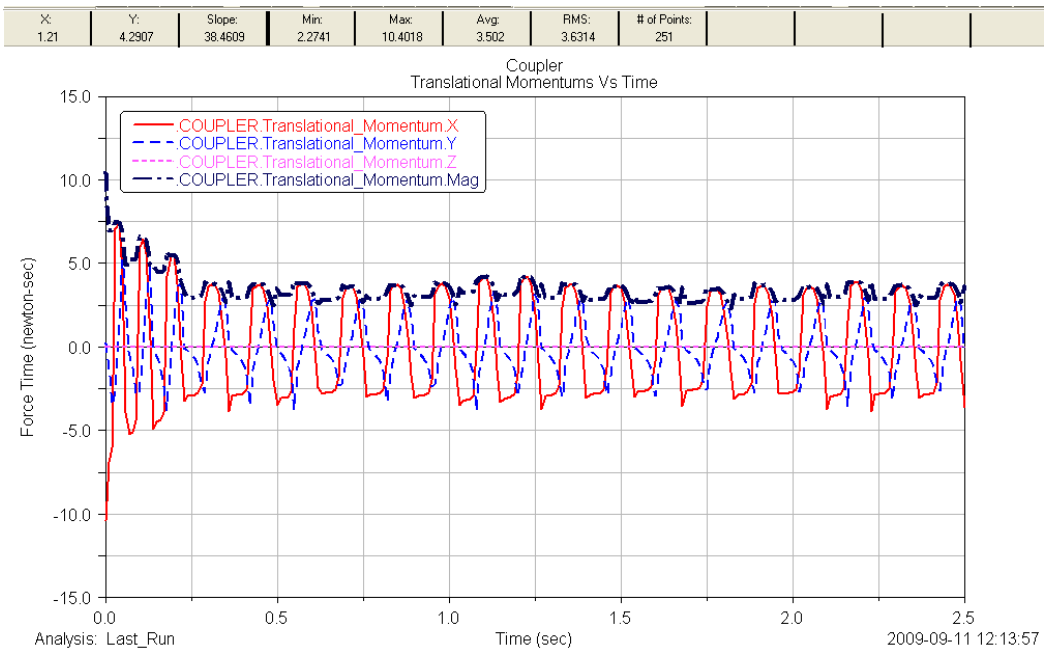

(b)

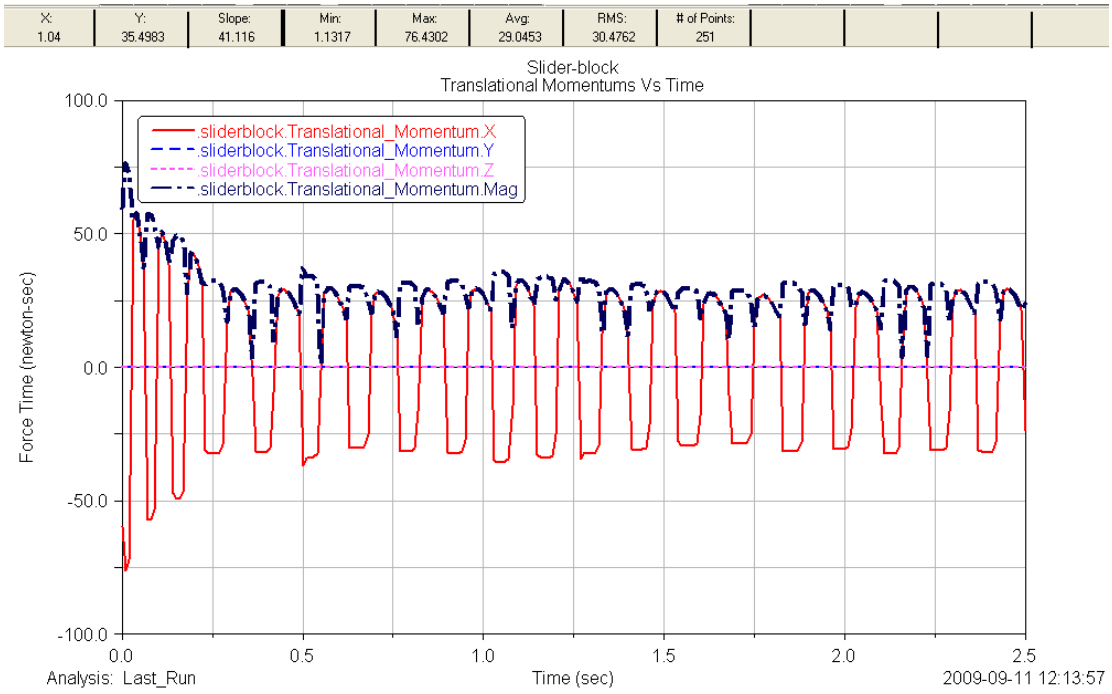

(c)

Figure 6.1.6 Output results of translational momentums of the (a) crank; (b) coupler; and (c) slider-block links about CM versus Time

The translational momentums of the three links are based on the CM_velocities of each of the links and their repective translational velocities. The crank, coupler and slider-block system have translational momentums of magnitudes12.38N-s, 3.5N-s, and 29.05N-s, respectively.

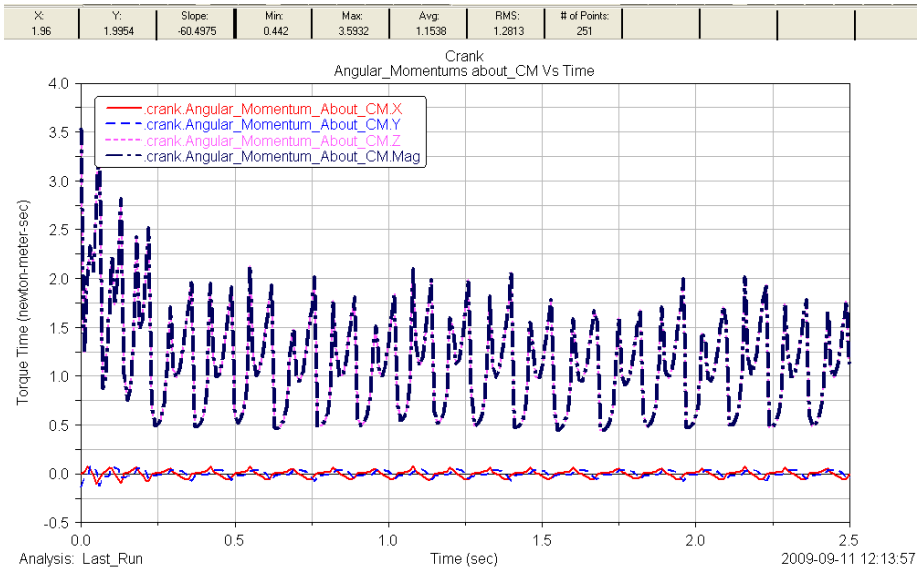

(a)

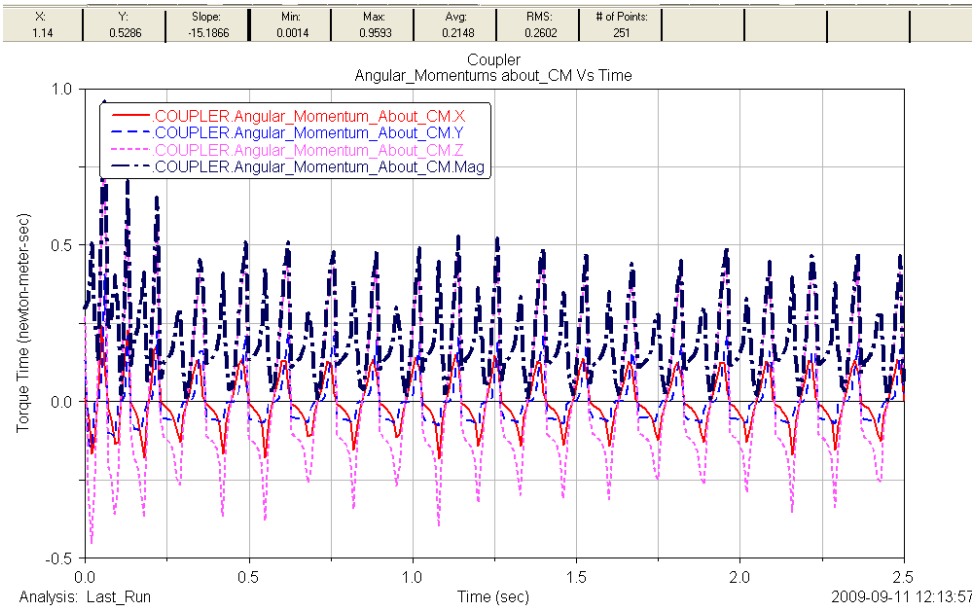

(b)

Figure 6.1.7 Output results of angular momentums of the (a) crank; and (b) coupler links about CM versus Time

Figures (6.1.4) and (6.1.5) present output results of CM-angular velocities and accelerations for the crank and coupler links. The resulted velocities and accelerations are according to the input torque applied to crank about the z-axis of rotation. The magnitude of the angular velocity for this crank is 50.4 rad/sec. Both the links take some time to initiate the fluctuating average velocities and accelerations (the average values for each output plots are given by the plot tracker at the top of each plots). This is also true for the translational and angular momentums. Figures (6.1.1b), (6.1.4b), (6.1.5b), and (6.1.7b) are output results for positions, angular velocities, accelerations, and angular momentum, respectively that confirm that the coupler is in a state of complete spatial motion. Even though the input torque is a constant value; the output results for each plots is not uniform due to the effect of the gravitational acceleration imposed to the mechanism i,e the effect of gravity is not the same as the system goes through different positions and orientations to cover the first 2.5 seconds.

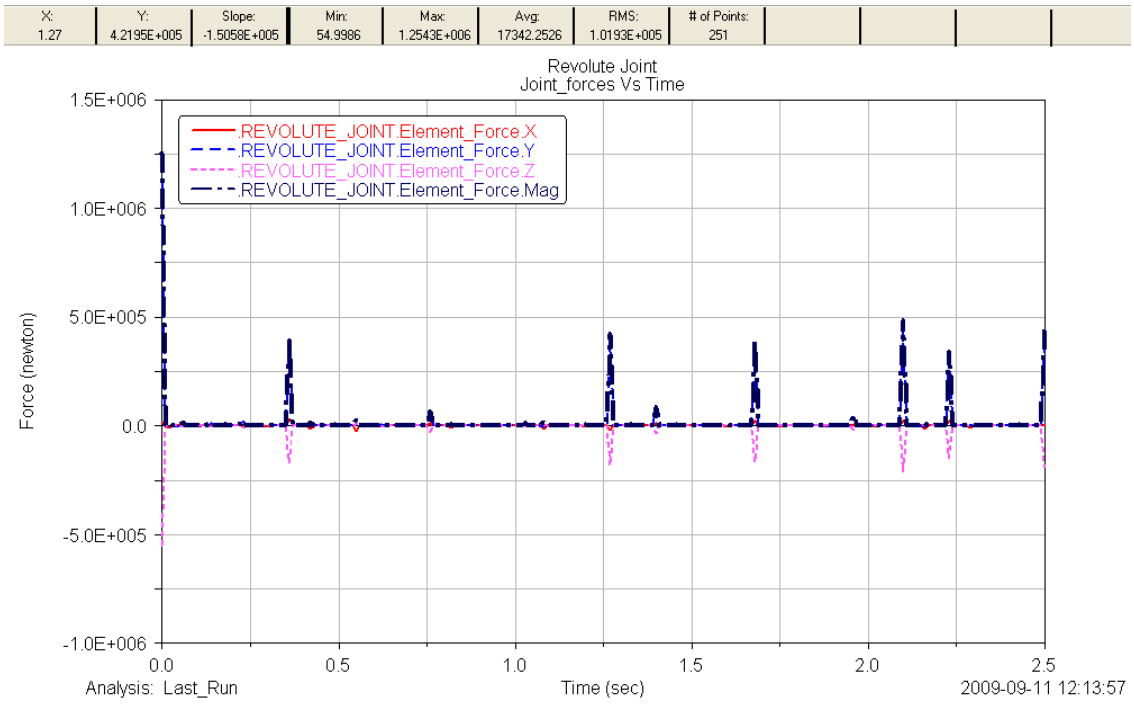

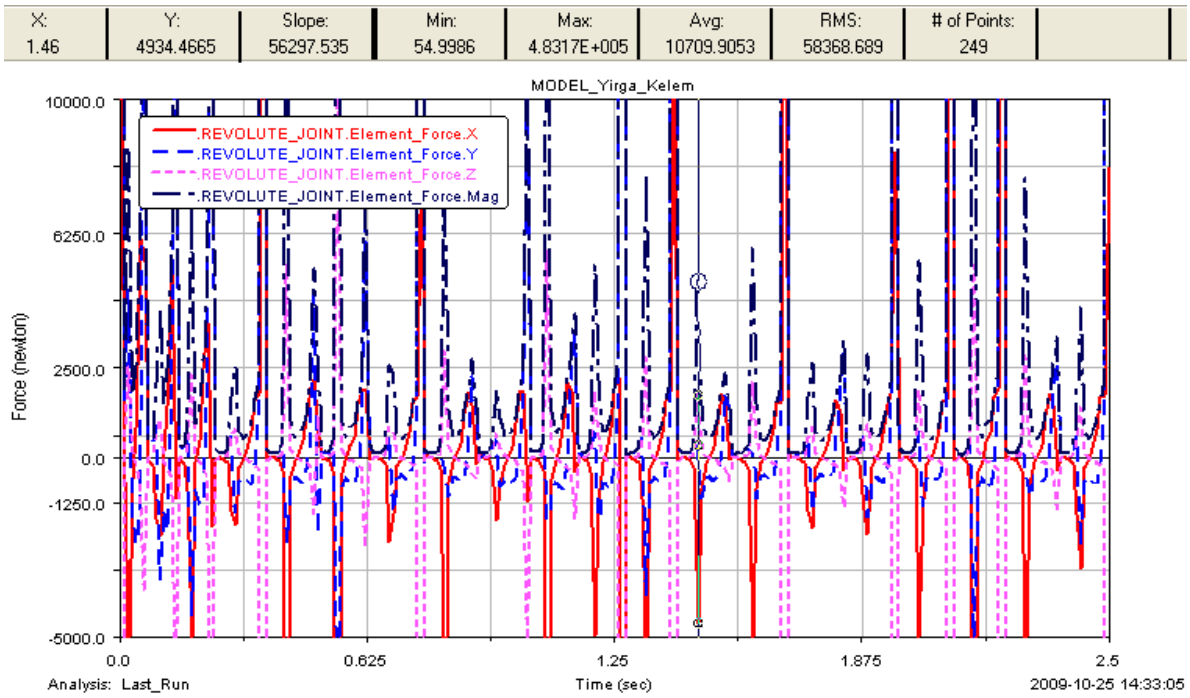
X: 1.46
Y: 4934.4665
Slope: 56297.535
Min: 54.9986
Max: 4.8317E+005
Avg: 10709.9053
RMS: 58368.689
# of Points: 249
MODEL_Yirga_Kelem
.REVOLUTE_JOINT.Element_Force.X
.REVOLUTE_JOINT.Element_Force.Y
.REVOLUTE_JOINT.Element_Force.Z
.REVOLUTE_JOINT.Element_Force.Mag
Force (newton)
10000.0
6250.0
2500.0
0.0
-1250.0
-5000.0
0.0
0.625
1.25
1.875
2.5
Time (sec)
Analysis: Last_Run
2009-10-25 14:33:05

(a)

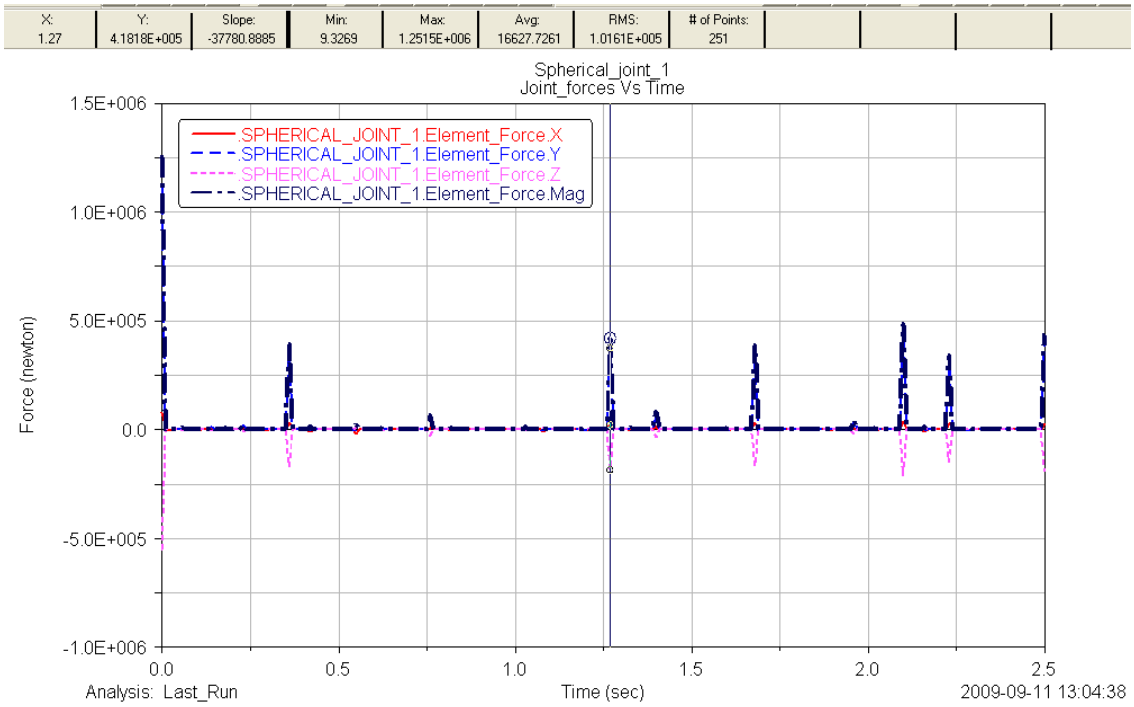
X: 1.27
Y: 4.1818E+005
Slope: -37780.8885
Min: 9.3269
Max: 1.2515E+006
Avg: 16627.7261
RMS: 1.0161E+005
# of Points: 251
Spherical_joint_1
Joint_forces Vs Time
.SPHERICAL_JOINT_1.Element_Force.X
.SPHERICAL_JOINT_1.Element_Force.Y
.SPHERICAL_JOINT_1.Element_Force.Z
.SPHERICAL_JOINT_1.Element_Force.Mag
Force (newton)
1.5E+006
1.0E+006
5.0E+005
0.0
-5.0E+005
-1.0E+006
0.0
0.5
1.0
1.5
2.0
2.5
Time (sec)
Analysis: Last_Run
2009-09-11 13:04:38

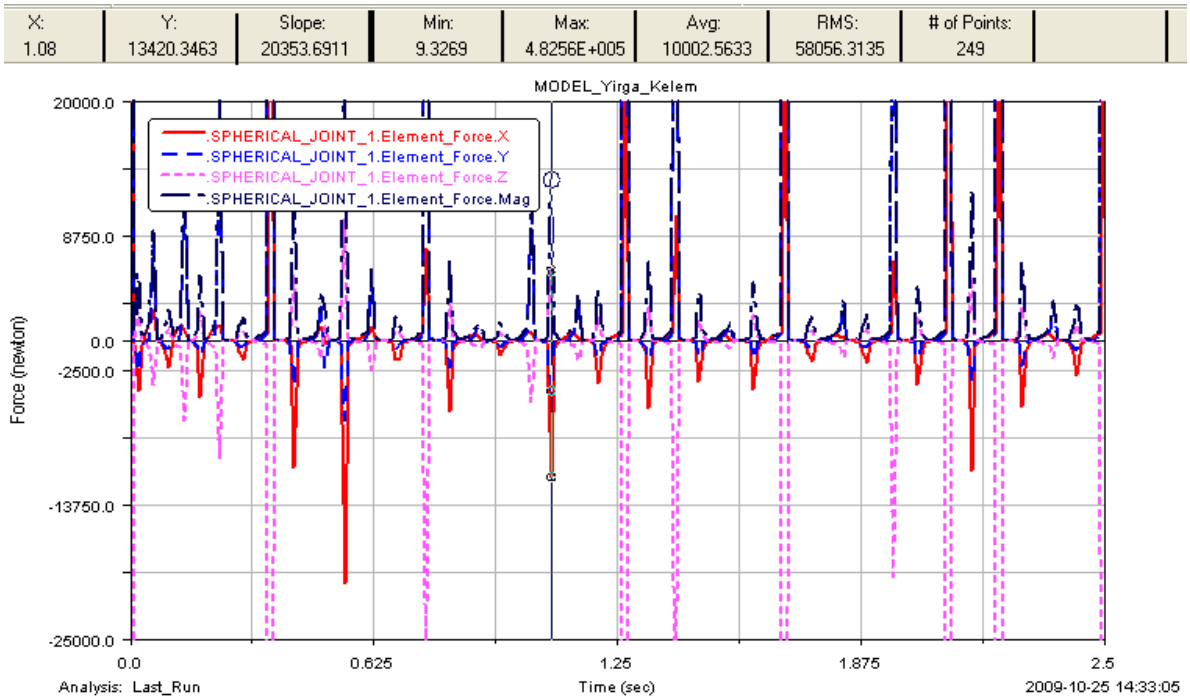
X: 1.08
Y: 13420.3463
Slope: 20353.6911
Min: 9.3269
Max: 4.8256E+005
Avg: 10002.5633
RMS: 58056.3135
# of Points: 249
MODEL_Yirga_Kelem
.SPHERICAL_JOINT_1.Element_Force.X
.SPHERICAL_JOINT_1.Element_Force.Y
.SPHERICAL_JOINT_1.Element_Force.Z
.SPHERICAL_JOINT_1.Element_Force.Mag
20000.0
8750.0
0.0
-2500.0
-13750.0
-25000.0
Force (newton)
0.0
0.625
1.25
1.875
2.5
Analysis: Last_Run
Time (sec)
2009-10-25 14:33:05

(b)

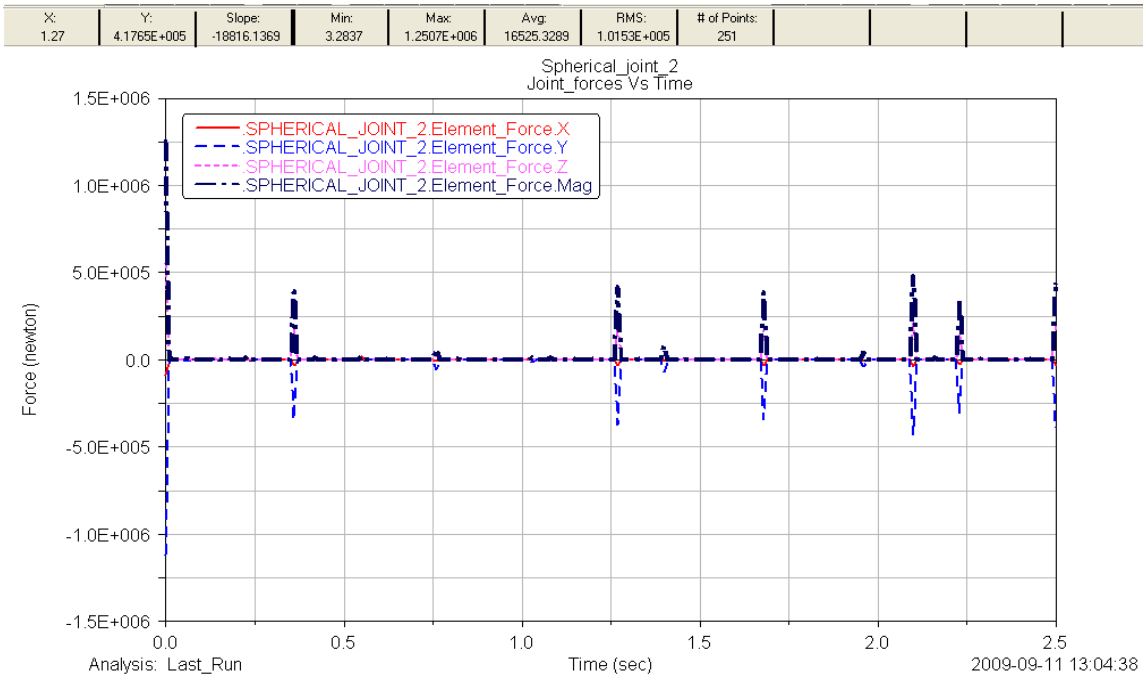
X: 1.27
Y: 4.1765E+005
Slope: -18816.1369
Min: 3.2837
Max: 1.2507E+006
Avg: 16525.3289
RMS: 1.0153E+005
# of Points: 251
Spherical_joint_2
Joint_forces Vs Time
.SPHERICAL_JOINT_2.Element_Force.X
.SPHERICAL_JOINT_2.Element_Force.Y
.SPHERICAL_JOINT_2.Element_Force.Z
.SPHERICAL_JOINT_2.Element_Force.Mag
1.5E+006
1.0E+006
5.0E+005
0.0
-5.0E+005
-1.0E+006
-1.5E+006
Force (newton)
0.0
0.5
1.0
1.5
2.0
2.5
Analysis: Last_Run
Time (sec)
2009-09-11 13:04:38

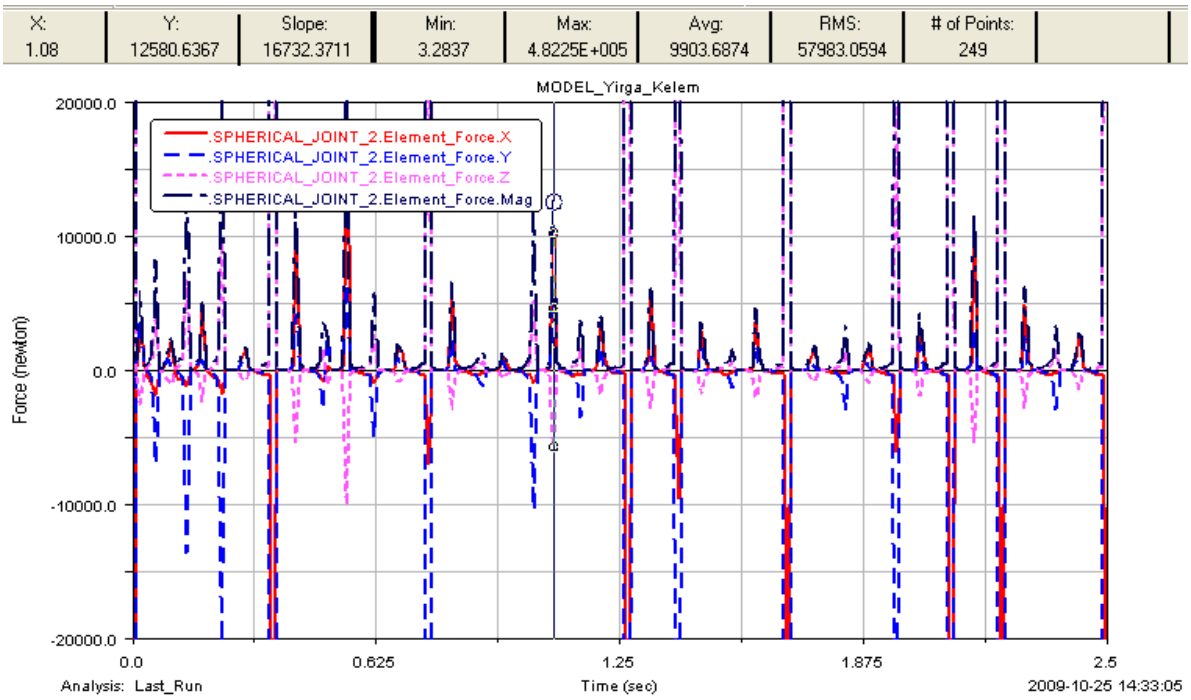
X: 1.08
Y: 12580.6367
Slope: 16732.3711
Min: 3.2837
Max: 4.8225E+005
Avg: 9903.6874
RMS: 57983.0594
# of Points: 249
MODEL_Yirga_Kelem
.SPHERICAL_JOINT_2.Element_Force.X
.SPHERICAL_JOINT_2.Element_Force.Y
.SPHERICAL_JOINT_2.Element_Force.Z
.SPHERICAL_JOINT_2.Element_Force.Mag
20000.0
10000.0
0.0
-10000.0
-20000.0
Force (newton)
0.0
0.625
1.25
1.875
2.5
Analysis: Last_Run
Time (sec)
2009-10-25 14:33:05

(c)

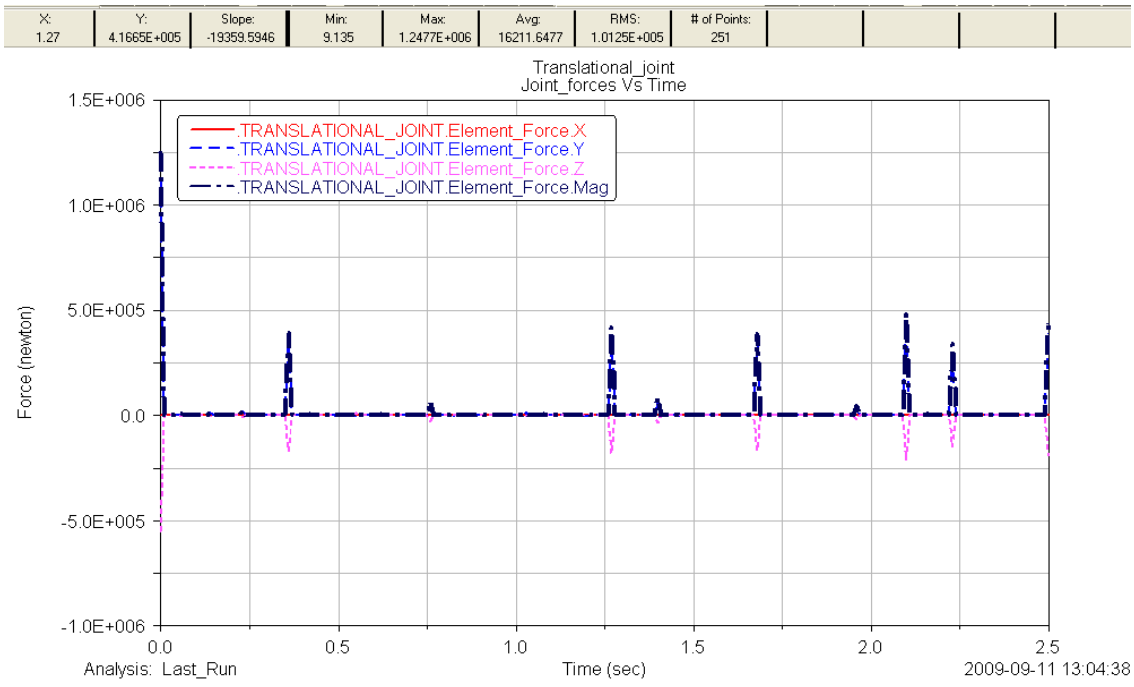
X: 1.27
Y: 4.1665E+005
Slope: -19359.5946
Min: 9.135
Max: 1.2477E+006
Avg: 16211.6477
RMS: 1.0125E+005
# of Points: 251
Translational_joint
Joint_forces Vs Time
.TRANSLATIONAL_JOINT.Element_Force.X
.TRANSLATIONAL_JOINT.Element_Force.Y
.TRANSLATIONAL_JOINT.Element_Force.Z
.TRANSLATIONAL_JOINT.Element_Force.Mag
1.5E+006
1.0E+006
5.0E+005
0.0
-5.0E+005
-1.0E+006
Force (newton)
0.0
0.5
1.0
1.5
2.0
2.5
Analysis: Last_Run
Time (sec)
2009-09-11 13:04:38

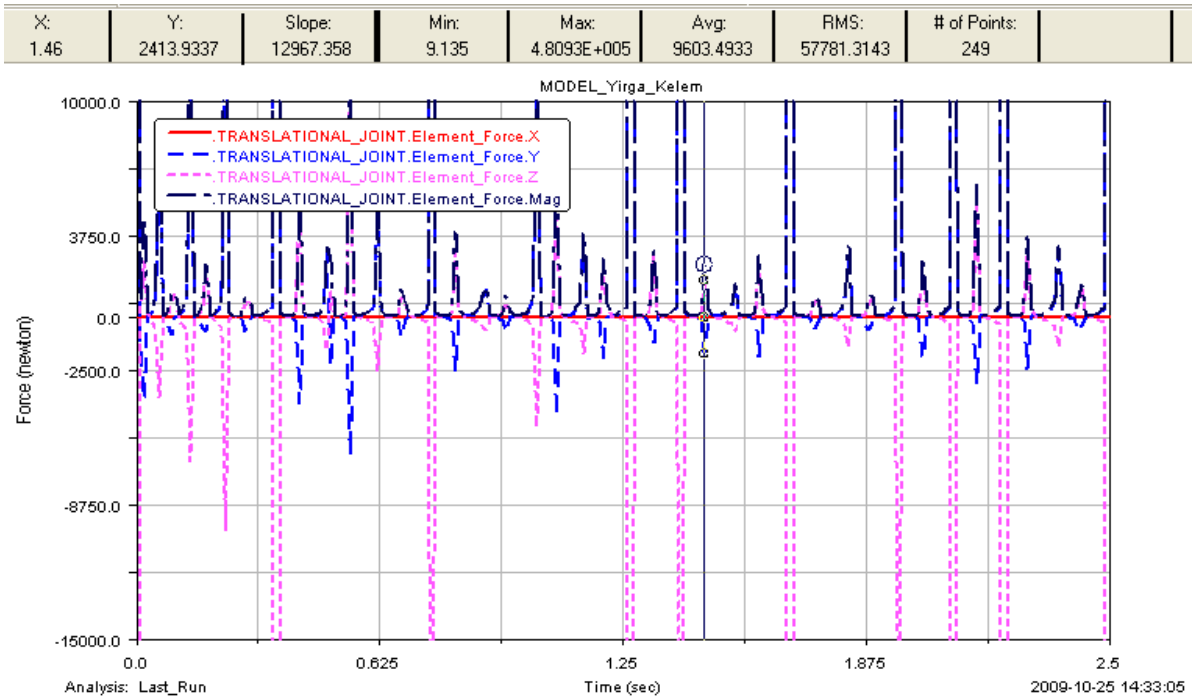

(d)

Figure 6.1.8 Output results of Lagrange multipliers for the (a) Revolute joint near the crank; (b) Spherical joint-1; (c) Spherical joint-2; and (d) Translational joint with their zoomed-in joint force elements Vs Time

Most of the joint forces time is spent in fluctuating in some average time except for some critical values at which large amount of force is acted for a while(for milliseconds). This might be occurred due to the friction developed between the mating surfaces that are parts of the kinematic joints. Moreover, whenever the links are changing their direction during motion; one part tries to penetrate on the other where an impact force is generated. One reason to implement spherical joints at the coupler end parts as compared to the other lower joints is that to decrease the wearing effect on each other of the surfaces. For each of the joint force elements, the respective zoomed-in figure is given in the above figure.

6.2 Improving the Model (Optimization)

In this section, the model will be refined by parameterizing some critical values that can influence the performance of the lens-polishing mechanism, and then study the effect of these parameters and optimize the model based on these parameters.

There are many parameters that affect the performance of a polishing mechanism. In polishing mechanism the critical parameters may be the crank angle orientation, driving crank's mass, and the input working torque that bring variations on the coupler's length or slider-block's position, velocity etc.

6.2.1 Parameterizing the Design Variables

The model that made up to this stage consists of values that are all fixed, i.e. the lengths, mass and geometrical constraints are pre-defined constants. In order to conduct a design study and improve our model, we need to set variable parameters that can be easily changed, so that we can see the effect of these parameters on the performance of the whole mechanism model by iteration.

Now let us create design variables to represent the design points in the model that illustrates the optimization processes. Then, we can use design variables to run design studies and optimization for the selected design variables.

It is obvious that creating at least one design variable will affect the whole system's configuration. Hence, taking some critical parameters will be enough to demonstrate the concept of optimization.

In the preceding sections, the effects of varying the crank's mass on the slider-block system CM_position, CM_velocity, and coupler's CM_angular velocity will be considered as illustrative examples for the existing designed mechanism. In this section, we have to understand that the optimization of the crank mass, the coupler and sliding-block positions and velocities are going to be made simultaneously according to the limited crank mass design variable between the provided minimum and maximum values.

6.2.2 Creating a Design Variable for the Driving Crank

This is done by creating a design variable for the crank mass. This should be done by re-defining the mass and geometry properties so far given as an input values. Doing this, the effect will be discussed for the change made on sliding system for the first 2.5 seconds. Optimizing the

driving crank's mass is an important aspect of this section since too much or too large mass of it will affect the slider-block system (polishing pads') center of mass position and velocity efficiencies of the mechanism in the x-direction.Of course, the coupler's angular velocity will be affected too. In ADAMS, re-defining of the design variables for the driving crank's mass is made by varying the density of the driving crank.

6.2.3 Optimizing the Position of Slider-block using GRG Algorithm

As we perform a manual study, we will see how the slider-block CM_ positions and velocities vary as we manually modify the design variable already set as DV_23 (density variations). The density variation is considered between the materials which have densities 2740kg/m^3 of almunium to7801 kg/m^3 of steel as minimum and maximum values, respectively. Cast iron's density (7080 kg/m^3) is taken here to initiate the manual study of all the following trials.

Running a design study used to look quickly at a range of design variable values, and see how they affect the design. ADAMS/postprocessor gives us the option of displaying various plots, as well as a design study reports. The design study report includes the design sensitivity of the slider-block location due to the design variable explained in the above. Iterating between these values will be made and the best optimum value will be obtained.

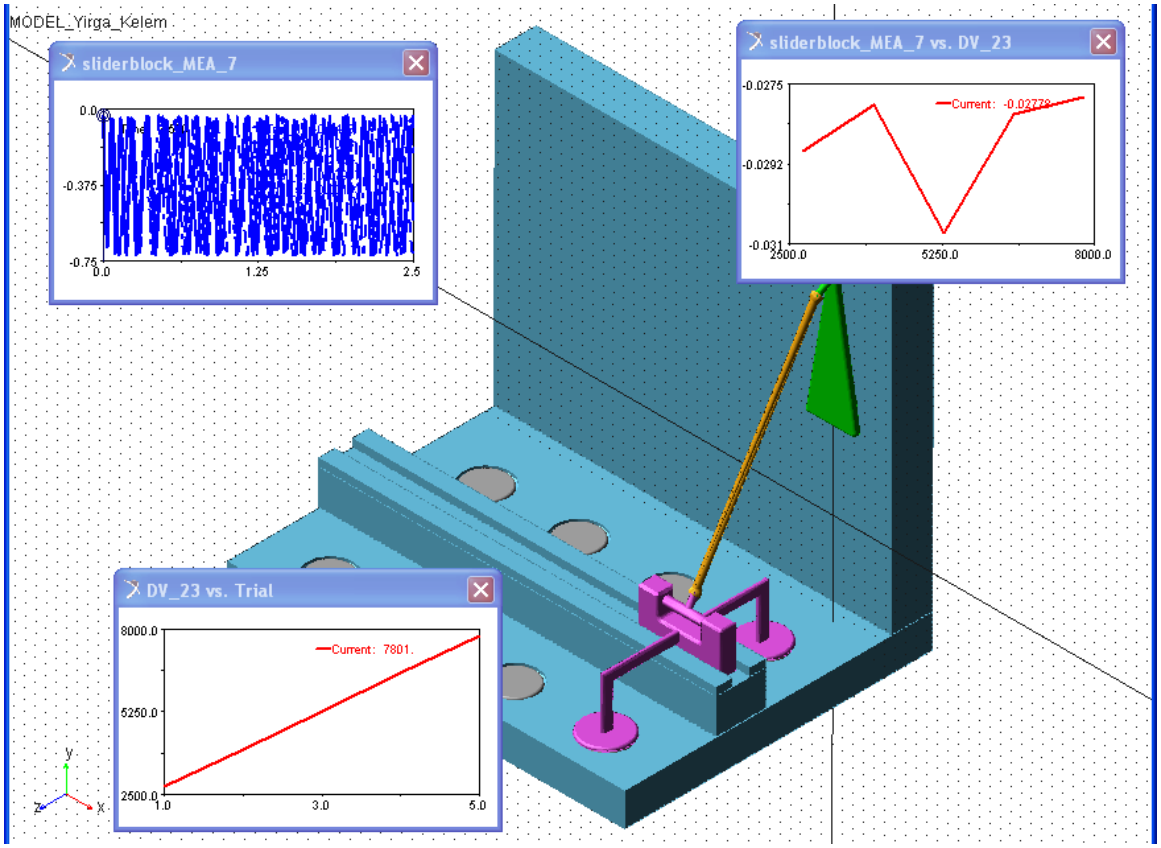
MODEL_Yirga_Kelem
sliderblock_MEA_7
0.0
-0.375
-0.75
0.0
1.25
2.5
sliderblock_MEA_7 vs. DV_23
-0.0275
-0.0292
-0.031
Current: -0.02778
2500.0
5250.0
8000.0
DV_23 vs. Trial
8000.0
5250.0
2500.0
Current: 7801.
1.0
3.0
5.0
y
z
x

(a)

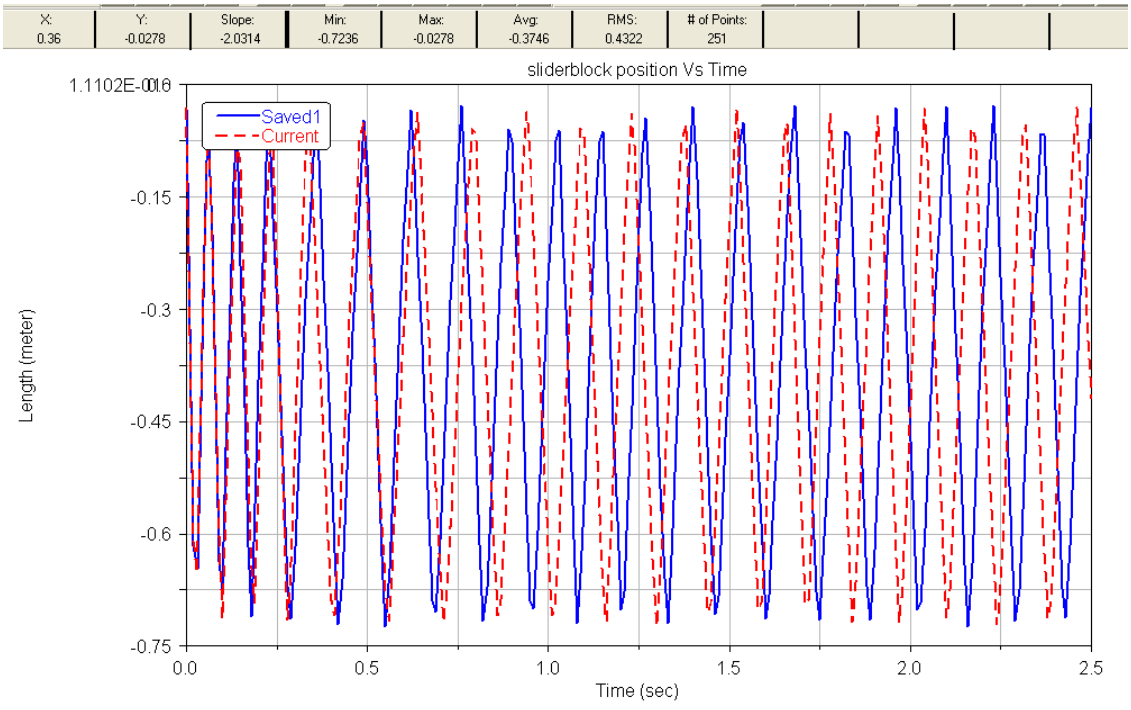
X: 0.36
Y: -0.0278
Slope: -2.0314
Min: -0.7236
Max: -0.0278
Avg: -0.3746
RMS: 0.4322
# of Points: 251
sliderblock position Vs Time
Saved1
Current
-0.15
-0.3
-0.45
-0.6
-0.75
Length (meter)
0.0
0.5
1.0
1.5
2.0
2.5
Time (sec)

(b)

```
Design Study Summary

Model Name : MODEL_Yirga_Kelem
Date Run   : 2009-09-11 14:56:41

Objectives

   O1) Maximum of sliderblock_MEA_7
       Units         : meter
       Maximum Value:   -0.0277808 (trial 5)
       Minimum Value:   -0.0307737 (trial 3)

Design Variables

   V1) DV_23
       Units         : NO UNITS

Trial          O1              DV_23         Sensitivity

   1        -0.028963          2740.0      7.8496e-007
   2        -0.027970          4005.3     -7.1554e-007
   3        -0.030774          5270.5     -7.6987e-008
   4        -0.028165          6535.8      1.1827e-006
   5        -0.027781          7801.0      3.0334e-007
```

(c)

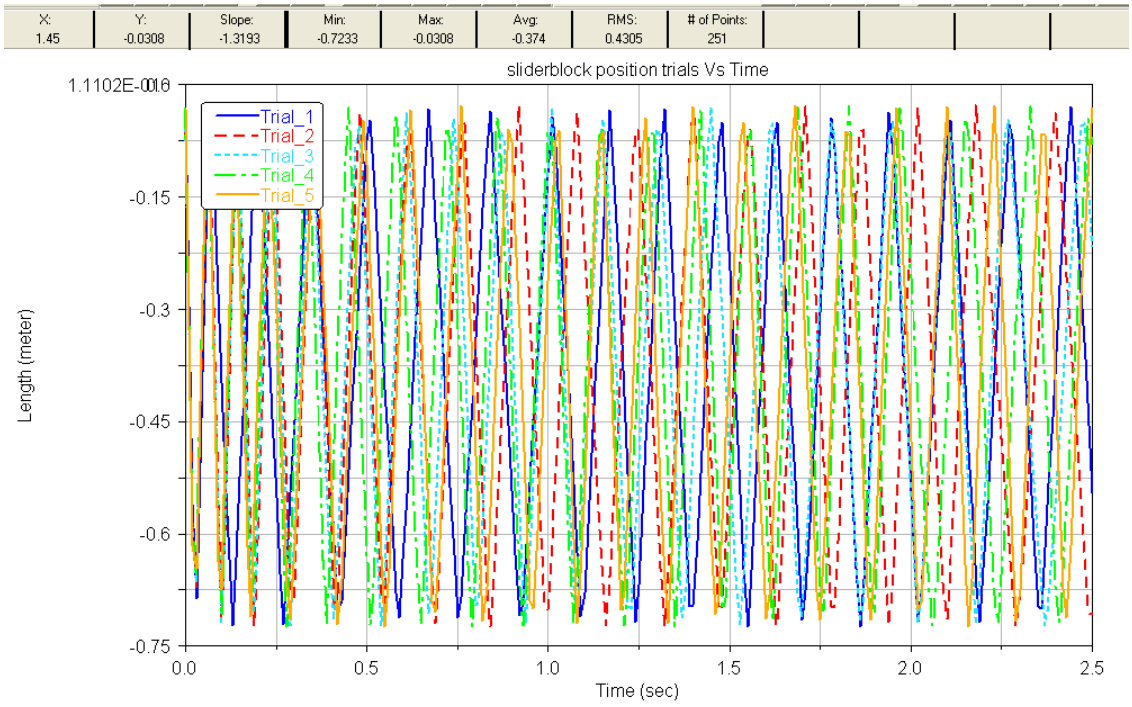

(d)

Figure 6.2.1 Design study results a) running design study; b) driving crank's mass effect on slider-block position Vs Time; c) report; d) slider-block position trials for 2.5s

Figure (6.2.1) shows the output results of the CM-position in the x-direction for the slider-block system.Thus, optimizing the slider-block's position by varying the crank mass technically called the design variable (DV_23) is the prime objective of this section.

A design study is made by trial and error by varying the crank's mass to observe its effect on the slider-block's position. Figure (6.2.1b) shows the first trial in red colour and then Fig. (6.2.1d) shows five trials for the first 2.5seconds. Eventhough; Fig.(6.2.1c) shows that the sensitivities are small values, the position could be improved to a better value. Slider-block's position Vs time, the Slider-block's position Vs design variables (DV_23), design variable (DV_23) Vs trials are obtained in Fig.(6.2.1a).

The final step in this mdeling is running an optimization.We will now work on finding an optimal design that best meets the performance parameters, while satisfying the design constraints.Optimization involves determining which objective function we want to minimize or maximize, selecting the design variables we want to change, and specifying constraint functions that must be satisfied.

The optimization algorithm considered is the GRG with tolerance of 0.001 and with an increment of 0.000001.

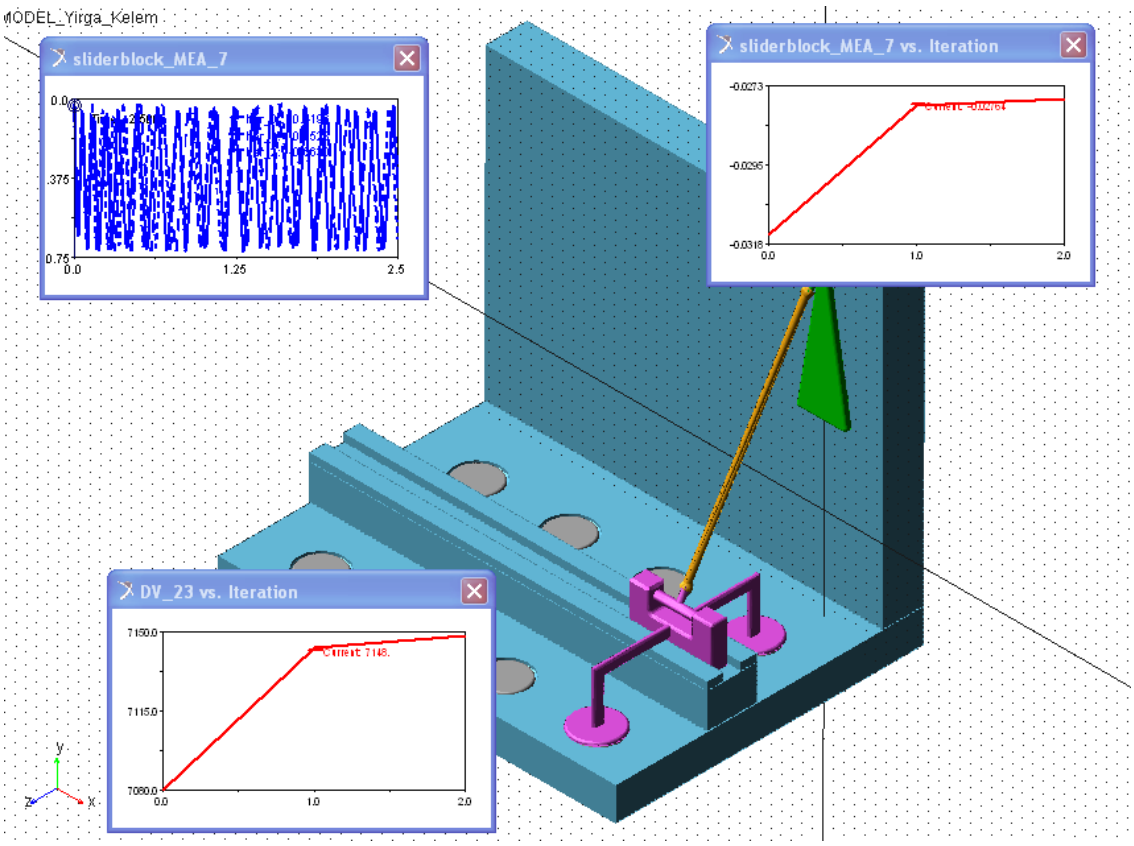

(a)

```
Optimization Summary

Model Name : MODEL_Yirga_Kelem
Date Run   : 2009-09-11 15:14:02

Objectives

   O1) Maximum of sliderblock_MEA_7
       Units         : meter
       Initial Value:    -0.0314899
       Final Value  :    -0.0276388 (-12.2%)

Design Variables

   V1) DV_23
       Units         : NO UNITS
       Initial Value:          7080
       Final Value  :       7148.16 (+0.963%)

Iter.          O1              DV_23

   0        -0.031490           7080.0
   1        -0.027825           7142.8
   2        -0.027639           7148.2
```

(b)

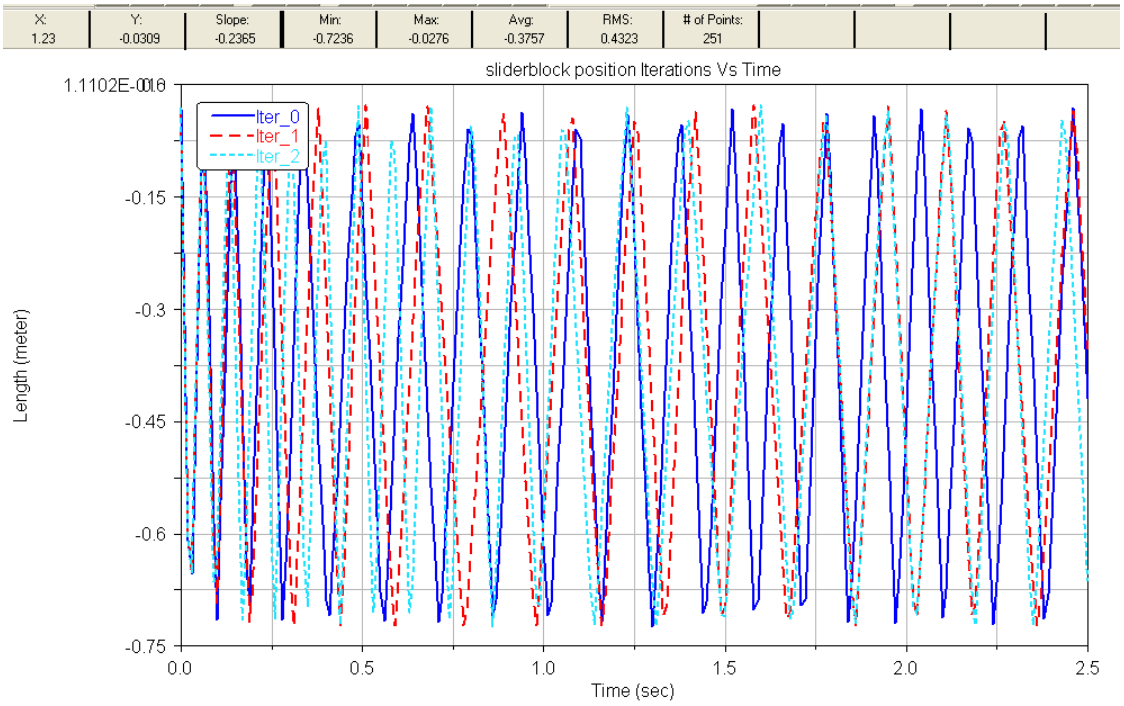

(c)

Figure 6.2.2 Optimization (a) running an optimization b) report; c) slider-block position iterations Vs Time

The best optimized final mass value is obtained to be 7148.16(+0.963%) and with a final optimized position variation of -0.0276388(-12.2%); which is obtained after three iterations using GRG. As it is shown in the optimization summary table in the above, the percentage errors

in position and mass are too small figures. From the above optimization algorithm, the design variable doesn't bring any significant effect thus no design change could be made.

6.2.4 Optimizing the CM_Velocity of Slider-block System using GRG Algorithm

Figure (6.2.3) shows the output results of the CM-velocity in the x-direction for the slider-block system.Thus, optimizing the slider-block's velocity by varying the crank mass is the proceeding section's objective.

Figure (6.2.3b) shows the first trial in red colour and then Fig.(6.2.3d) shows five trials for the first 2.5seconds. Figure (6.2.3c) shows that the sensitivity values. Just like the previous section, the translational velocity could be improved to better values. Slider-block's velocity Vs time, the Slider-block's velocity Vs design variables (DV_23), design variable (DV_23) Vs trials are shown in Fig.(6.2.3a).

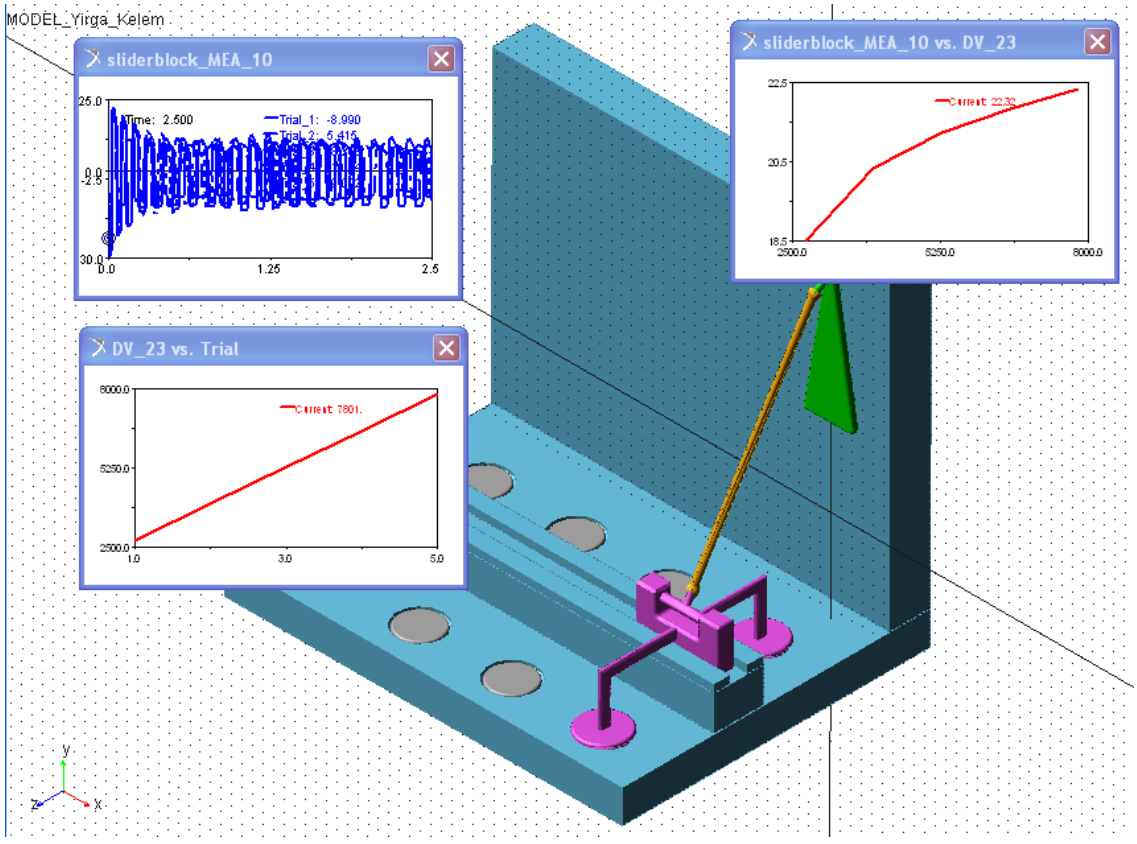

(a)

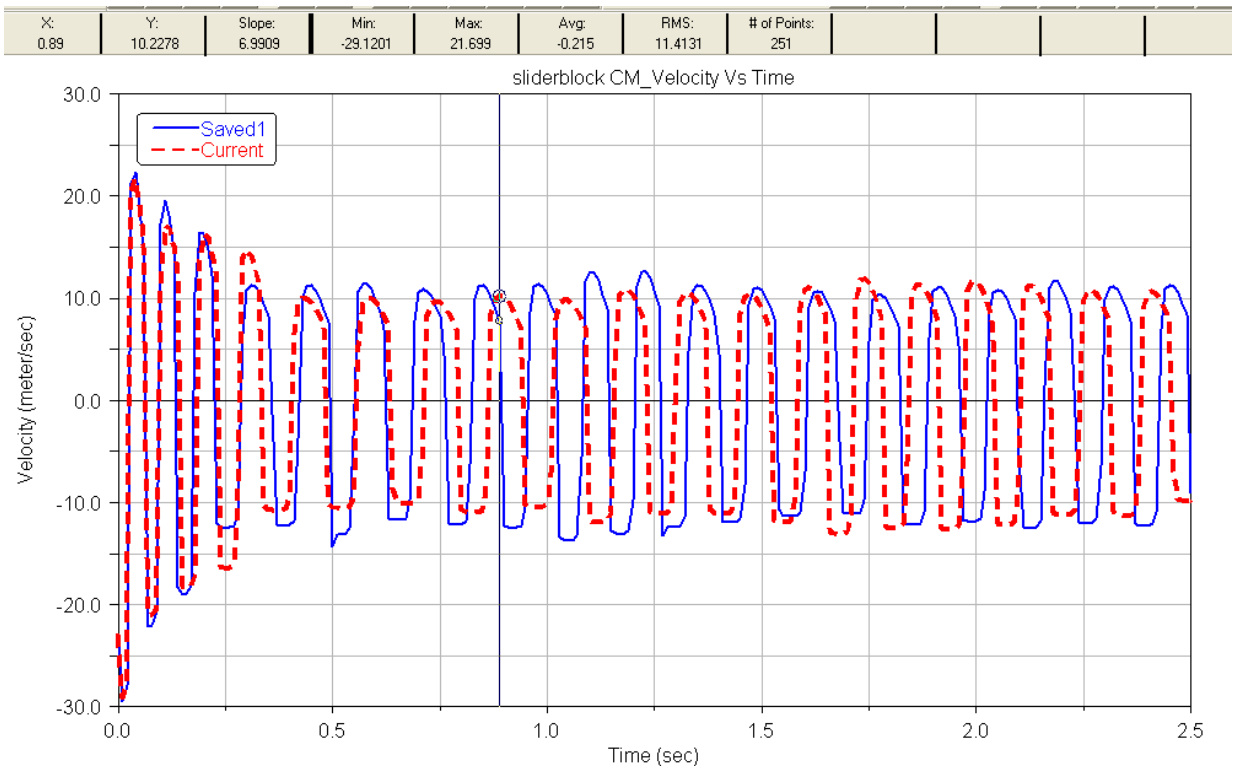

(b)

```
Design Study Summary

Model Name : MODEL_Yirga_Kelem
Date Run   : 2009-09-11 15:42:08

Objectives

   O1) Maximum of sliderblock_MEA_10
       Units        : meter/sec
       Maximum Value:      22.3236 (trial 5)
       Minimum Value:      18.5096 (trial 1)

Design Variables

   V1) DV_23
       Units        : NO UNITS

Trial          O1             DV_23        Sensitivity

   1           18.510          2740.0       0.0014307
   2           20.320          4005.3       0.0010812
   3           21.246          5270.5      0.00059244
   4           21.819          6535.8      0.00042596
   5           22.324          7801.0      0.00039885
```

(c)

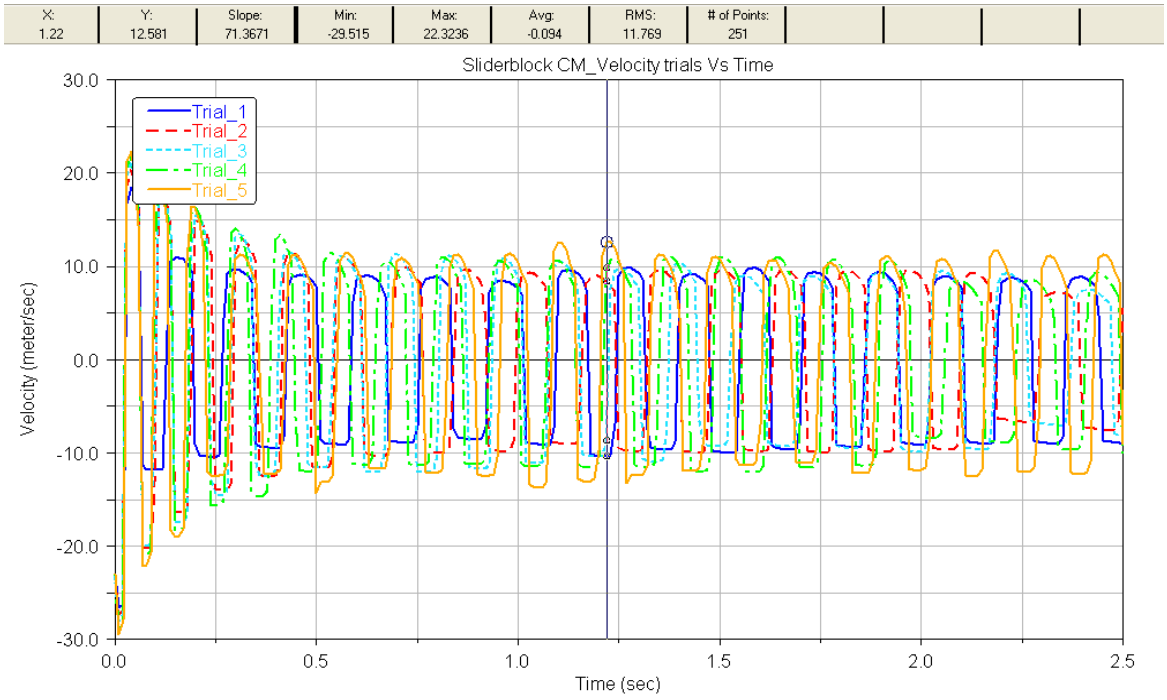

(d)

Figure 6.2.3 Design study results a) running design study; b) driving crank's mass effect on slider-block velocity Vs Time; c) report; d) slider-block velocity trials for 2.5s

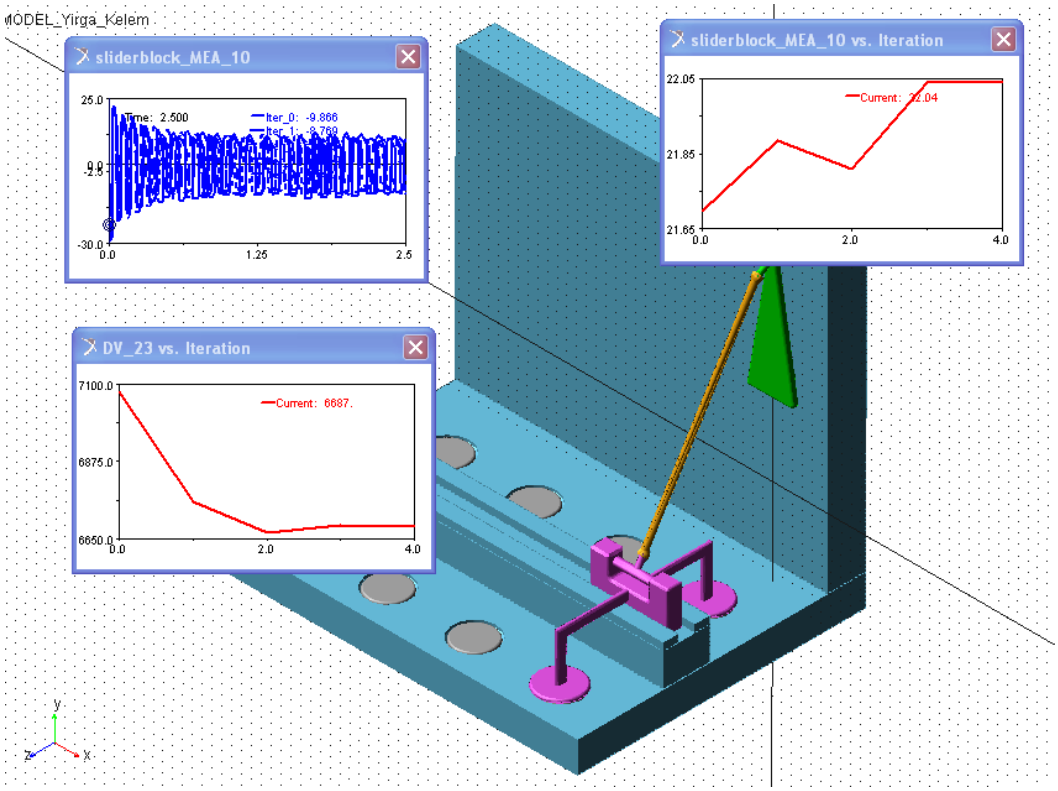

(a)

```
Optimization Summary

Model Name : MODEL_Yirga_Kelem
Date Run   : 2009-09-11 15:53:20

Objectives

   O1) Maximum of sliderblock_MEA_10
       Units         : meter/sec
       Initial Value:       21.699
       Final Value  :      22.0392 (+1.57%)

Design Variables

   V1) DV_23
       Units         : NO UNITS
       Initial Value:         7080
       Final Value  :      6686.67 (-5.56%)

Iter.         O1             DV_23

   0           21.699          7080.0
   1           21.883          6756.5
   2           21.811          6665.6
   3           22.038          6689.9
   4           22.039          6686.7
```

(b)

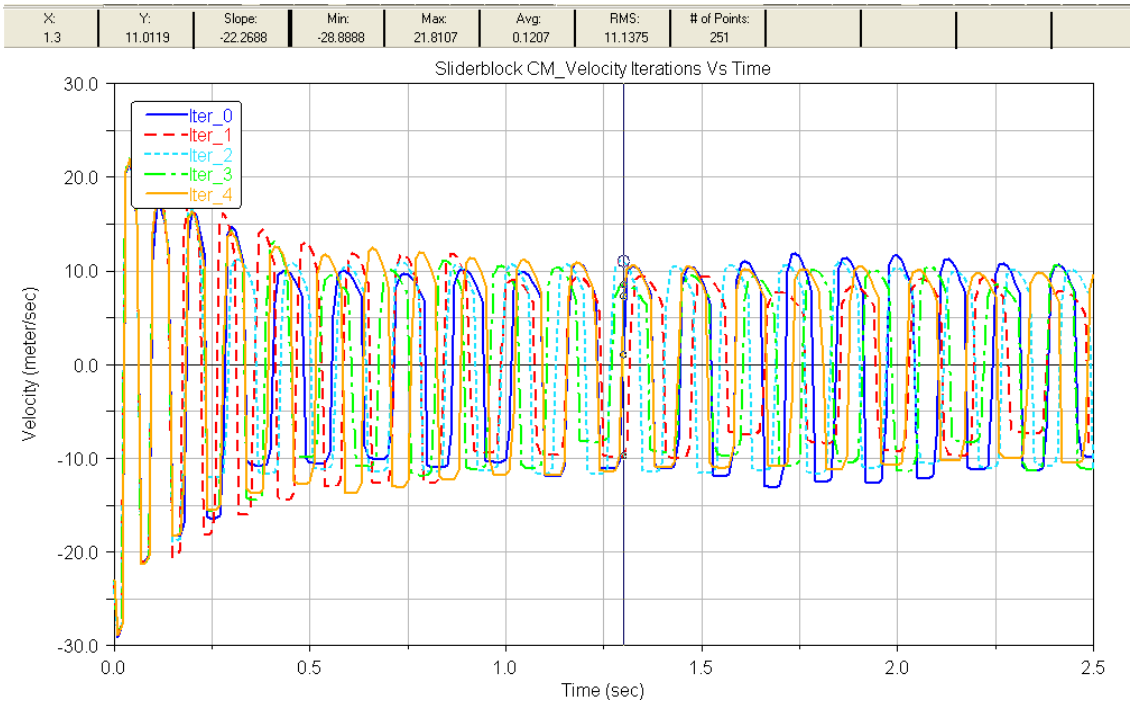

(c)

Figure 6.2.4 Optimization (a) running an optimization b) report; c) slider-block velocity iterations Vs Time

The optimization summary of Fig.(6.2.4) shows us, the best optimized final mass value is obtained to be 6686.67(-5.56%) and with a final velocity of 22.04m/s(+1.57%); which is obtained after five iterations. From the above optimization algorithm, the design variable doesn't bring any significant effect thus no design change is going to be made. The optimization algorithm considered is the GRG with tolerance of 0.001 and with an increment of 0.000001.

6.2.5 Optimizing the Angular Velocity of the Coupler using GRG Algorithm

As it has been shown in Fig.(6.1.4), the output results of the magnitude of the CM-angular velocity of the coupler shows a great divergence after 1.25 seconds. More over, as it is shown in Fig.(6.1.1b), the angular orientations of the coupler show a very high fluctuation in their respective axes. Thus, optimizing the coupler's angular velocity by varying the crank mass technically called the design variable (DV_23) is the main objective of this section. Obviously, the same process has been made to the slider-block system.

A design study is made taking trials by varying the crank's mass to observe its effect on the angular velocity magnitude. Figure (6.2.5b) shows the first trial in red colour and then Fig. (6.2.5a) shows five trials for the first 2.5seconds. Figure (6.2.5c) shows that the sensitivities are large enough figures. Therefore, the angular velocity needs to be improved. Coupler's angular velocity Vs time, the coupler's angular velocity Vs design variables (DV_23), design variable (DV_23) Vs trials are obtained in Fig. (6.2.5a). Detail analysis can be observed in Figs.(6.2.5c) and (6.2.5d) clearly.

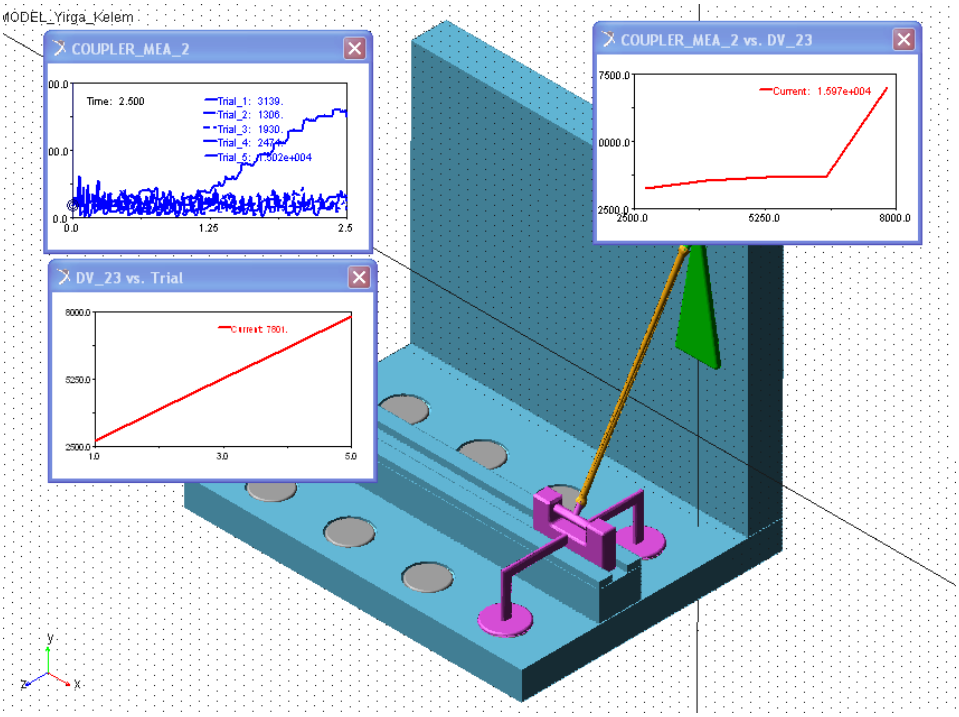
MODEL_Yirga_Kelem
COUPLER_MEA_2
Time: 2.500
Trial_1: 3139.
Trial_2: 1306.
Trial_3: 1930.
Trial_4: 2474.
Trial_5: 1.502e+004
COUPLER_MEA_2 vs. DV_23
Current: 1.597e+004
DV_23 vs. Trial
Current 7801.

(a)

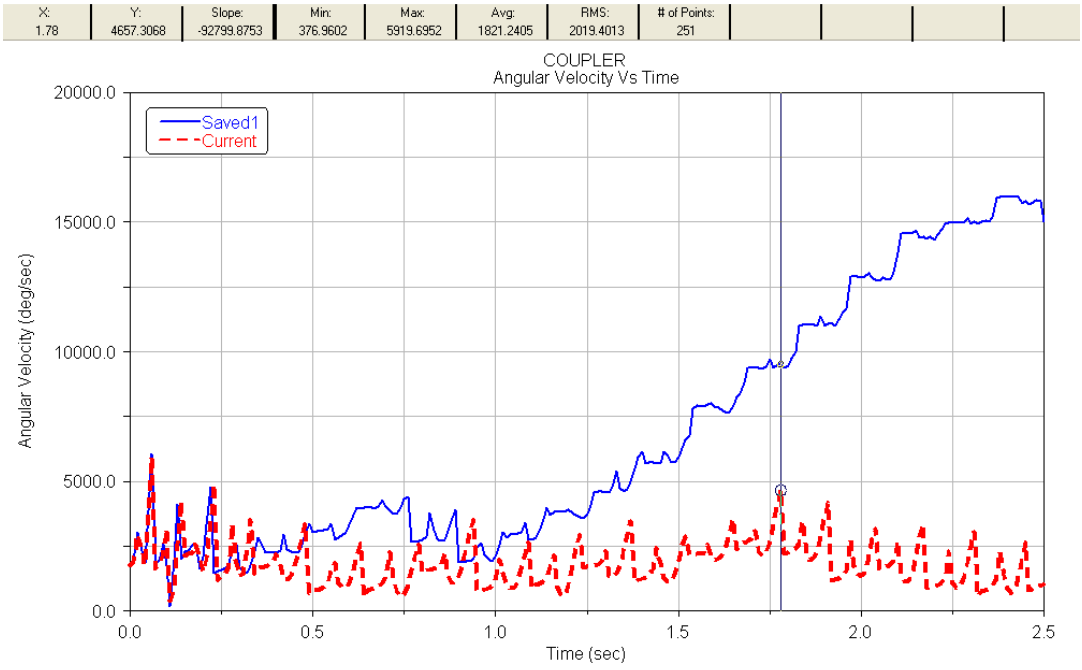
X: 1.78
Y: 4657.3068
Slope: -92799.8753
Min: 376.9602
Max: 5919.6952
Avg: 1821.2405
RMS: 2019.4013
# of Points: 251
COUPLER
Angular Velocity Vs Time
Saved1
Current
Angular Velocity (deg/sec)
Time (sec)
20000.0
15000.0
10000.0
5000.0
0.0
0.5
1.0
1.5
2.0
2.5

(b)

```
Design Study Summary

Model Name : MODEL_Yirga_Kelem
Date Run   : 2009-09-11 16:32:38

Objectives

   O1) Maximum of COUPLER_MEA_2
       Units         : deg/sec
       Maximum Value:        15972 (trial 5)
       Minimum Value:      4680.63 (trial 1)

Design Variables

   V1) DV_23
       Units         : NO UNITS

Trial          O1             DV_23        Sensitivity

   1           4680.6          2740.0         0.76787
   2           5652.2          4005.3         0.50853
   3           5967.5          5270.5         0.16360
   4           6066.2          6535.8          3.9536
   5           15972.          7801.0          7.8292
```

(c)

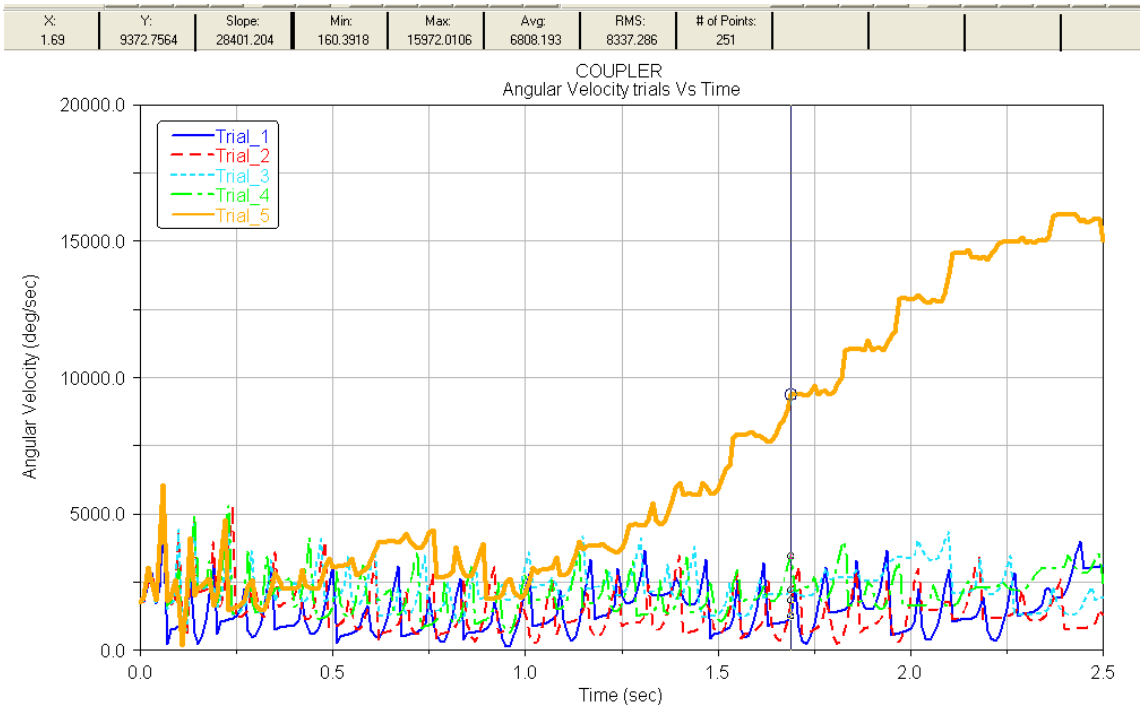

(d)

Figure 6.2.5 Design study results a) running design study; b) driving crank's mass effect on coupler angular velocity (magnitude) Vs Time; c) report; d) coupler angular velocity trials for 2.5s

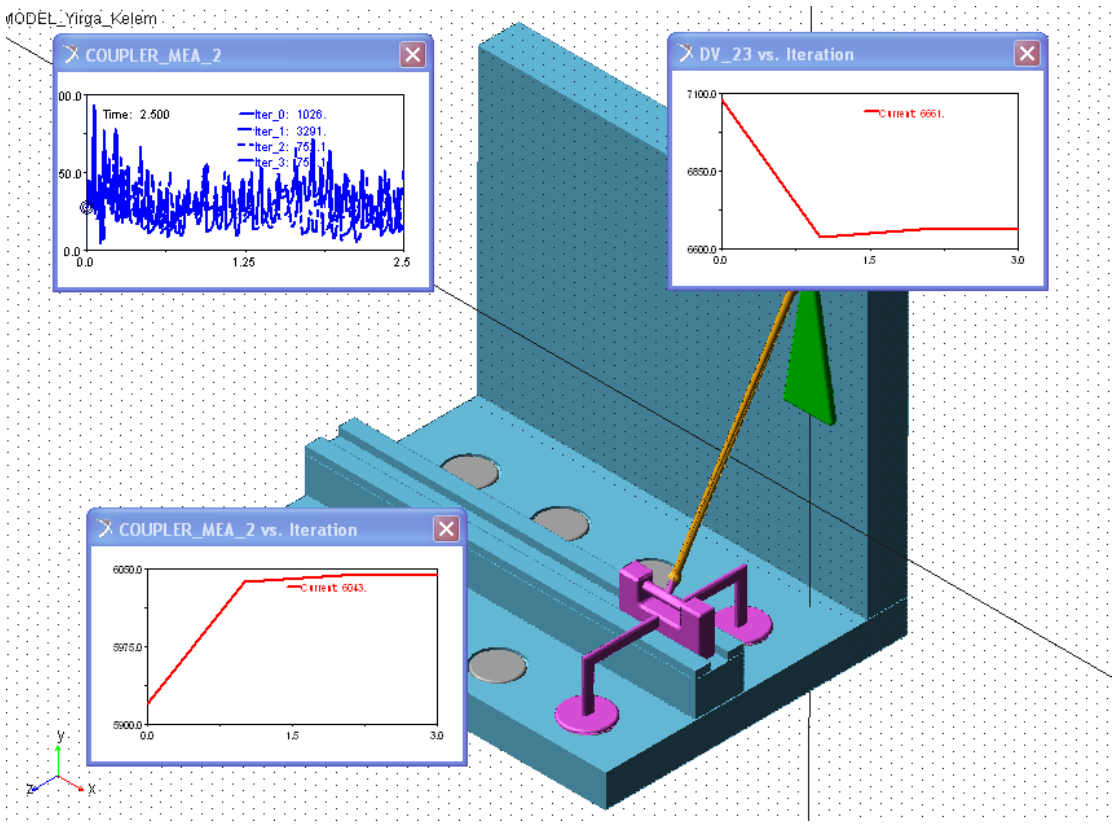

(a)

```
Optimization Summary

Model Name : MODEL_Yirga_Kelem
Date Run   : 2009-09-11 16:38:47

Objectives

   O1) Maximum of COUPLER_MEA_2
       Units        : deg/sec
       Initial Value:       5919.7
       Final Value  :      6043.14 (+2.09%)

Design Variables

   V1) DV_23
       Units        : NO UNITS
       Initial Value:         7080
       Final Value  :      6660.57 (-5.92%)

Iter.         O1             DV_23

   0           5919.7          7080.0
   1           6037.1          6638.4
   2           6043.1          6660.6
   3           6043.1          6660.6
```

(b)

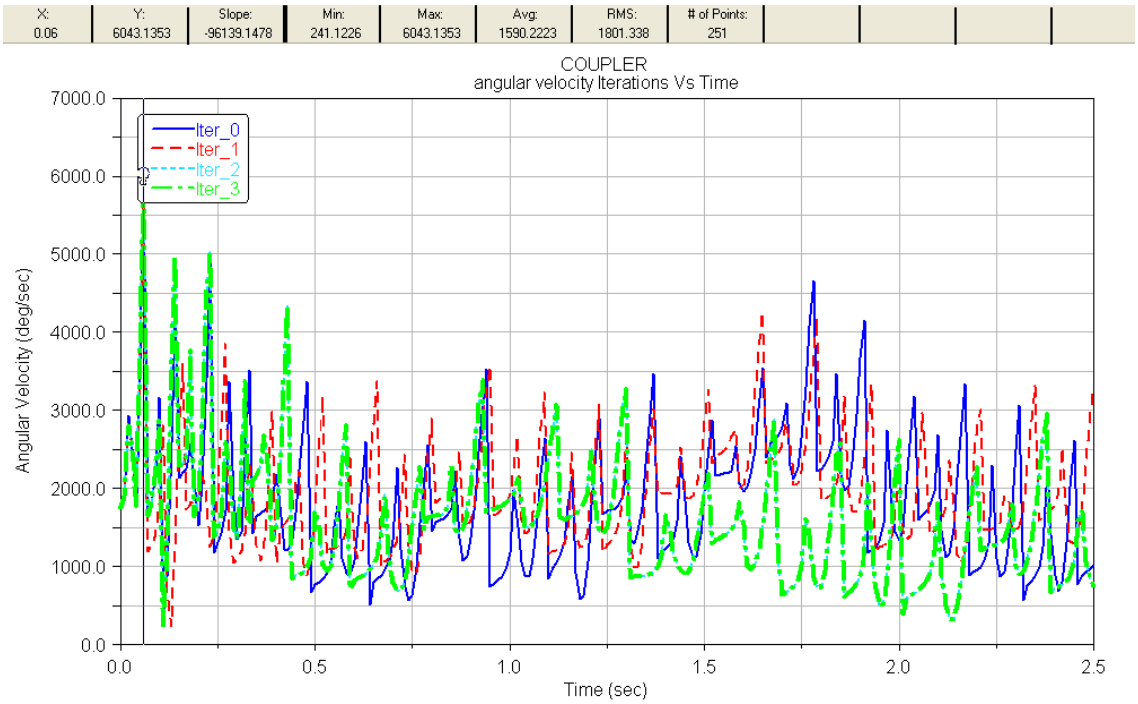

(c)

Figure 6.2.6 Optimization (a) running an optimization b) report; c) coupler angular velocity iterations Vs Time

Figure 6.2.6 shows coupler's angular velocity Vs time, design variables (DV_23) Vs iteration, coupler's angular velocity Vs iteration. A mass of 7080kg/m^3 is given to trigger the optimization process with in the provided minimum and maximum mass values as shown in the design study summary in Fig (6.2.5c).

As it is shown in the Optimization summary in Fig.(6.2.6b), the effect of the mass 6660.57kg/m^3(-5.92%) that are the second and third iterations brought about 6043.14deg/sec (+2.09%) coupler's angular velocity variation. Here, the percentages are small figures thus the iteration is made well. Of course, these percentage values can be reduced to some lesser figures by increasing the iteration time which takes several minutes to compute.

CHAPTER 7-CONCLUSION AND RECOMMENDATION FOR FUTURE WORK

7.1 Conclusion of the Thesis Work

The main objective of this thesis work has been to model an optimized spatial four-bar mechanism and simulating its dynamic force analysis using a software package.

The computer program that has been used for solving the equations developed in the analysis problem and that integrates the differential equations is MSC.ADAMS 2005.

In this thesis a formulation for spatial dynamic analysis of multibody mechanical systems, employing the Cartesian coordinates and the Newton-Euler's approach, was presented. Euler parameters were used to define the angular orientation of bodies, which leads to a mathematical formulation without singularities. Additionally, a simple and brief description of the standard mechanical joints of spatial multibody mechanical systems was presented. The analysis of the motion and joint force characteristics is done by solving a set of DAEs derived from the formulation.

The stiff numerical integration method has been applied in solving a mixed system of algebraic and differential equations of motion by integrating the acceleration in the forward integration process. This algorithm has served as a forerunner in the development of the numerical methods in the area of mechanical systems. The algorithm has been formulated into a computer program for three-dimensional motion known as MSC.ADAMS.

As it has been discussed previously, the constraint violation problem is more reflective in the position and velocity when the numerical integration progresses with the given time step size. Thus, optimization process of the drifts occurred in these two quantities is presented using Generalized Reduced Gradient(GRG) algorithm. In general, any type of spatial-four bar mechanism with required degree of freedom can be designed using the methodologies so far explained.

A representative applicable numerical example has been designed and modeled in chapter five using MSC.ADAMS software package. The system was driven by an input torque and gravity as external loads. The objective here is to design a practically sound mechanism for polishing lenses which are used as fire control instruments in the Ethiopian Defence Industries and colleges where military maintenance areas are found.This mechanism will mainly reduce the breakage of lenses during manual polishing operations.

The mechanism so far designed is a mixed combinations of planar and spatial linkage motions but the overall system has one degree of freedom, single loop with different constraint joint combinations. In order to keep the analysis simple, the friction and the lubrication effects were not included in the existing model.

In the optimization section, the effect of the driving crank's mass on the slider-block system position and velocity has been studied. Of course, the effect of the crank mass on the angular velocity of the coupler is also considered. The sensitivities evaluated for the slider-block system are very small figures to bring design changes on the mechanism.

It is observed that, optimization is a very time consuming process and running a good design study will help us choose better design variables and come to an optimized solution faster. The optimization process highly depends on the tolerance, increment, optimization algorithm, and range of design variable. In order to come to the best optimization process, we need to try different scenarios and refine our parameters each time.

To conclude, for the lens polishing mechanism, best optimized design can be obtained by studying other parameters (see section 6.2) and design layouts by including experimental works.The lens-polisher links and joints can be easily produced, assembled in a machine shop because all results are compared with the existing litratures, and found to be well-matched.

7.2 Recommendation for Future Works

Up to now, the primary goal of this thesis work is fulfilled and the work can be as bench mark for further research for those who are interested in designing spatial mechanisms with any combination of links and kinematic pairs. In chapter one, the assumptions and limitations of this thesis are given. Firstly, the linkages are assumed as being made up of a continuum of particles that are constrained not to move relative to one another. While actual bodies are never perfectly rigid, i.e deformation effects are often negligible when considering the motion of a machine that is made up of multiple bodies, hence modeling as elastic bodies could be done. Secondly, compliant mechanism like springs, dampers, and actuators can be included as per the design request. Thirdly, the two links are assumed to be joined at a point in this work. The introduction of radial clearance at the joints in spatial multibody systems significantly influences the prediction of components' position, velocity and drastically increases the acceleration and reaction moment peaks at the joints. Moreover, the system's response clearly tends to be non-linear when a clearance joint was included due to the eccentricity formed. This is a fundamental

feature mainly in high speed and precision mechanisms where the accurate predictions are essential for the design of the mechanical systems.

Fourthly, with regard to the lens-polishing spatial mechanism, the thesis work is on four-bar spatial mechanisms, but this work can be extended to multi-linkage spatial mechanisms of more than four links. Lastly, all friction effects are neglected in the dynamic analysis of the designed lens-polisher mechanism but could be considered in the dynamic analysis.

REFERENCES

1. Anirvan DasGupta, “Mobility Analysis of a class of RPSPR Kinematic Chains”, *Journal of Mechanical Design*, 2004, Vol.126, ASME, New York, NY, pp. 71-77.
2. Glen Mullineux, ”Modeling Spatial Displacements Using Clifford Algebra” *Journal of Mechanical Design*, 2004, Vol.126, ASME, New York, NY, pp. 420-424.
3. Uicker J.J., Jr., “Dynamic Force Analysis of Spatial Linkages”, *Journal of Applied Mechanics*, Trans. ASME, Vol. 89, No. 2, pp. 418-424, 1967.
4. John J. Uicker, Jr, Gordon R. Pennock and Joseph E.Shigley,”Theory of Machines and Mechanisms” 3rd ed., Oxford University Press, Inc., 2003.
5. C.Y.HO, “Tensor Analysis of Spatial Mechanisms” IBM Journal, May 1966.
6. Robel Mitiku,” Computer-Aided Dynamic force analysis and simulation of a four-bar planar linkages” thesis of Master of Science on Mechanical Engineering Dept., AAU, 2004.
7. Nikravesh, Parviz E., “Computer-Aided Analysis of Mechanical Systems,” Prentice-Hall, Inc., New Jersey, 1988.
8. Javier Garcia de Jalon and Eduardo Bayo,”Kinematic and Dynamic Simulation of Multibody Systems. The Real-Time Challenge”, ISBN 0-387-94096-0, 440 pp., Springer-Verlag, New-York, 1994.
9. Brian.T. Rundgren, “Optimized Synthesis of a dynamically based force generating planar Four Bar Mechanism”, thesis of Master of Science, Blacksburg, Virginia Polytechnic Institute and State University, 2001.
10. Mabie, H. H., and Reinholtz, C. F., “Mechanisms and Dynamics of Machinery”, 4th Edition, John Wiley and Sons, New York, NY, 1987.
11. Rigelman, G. A., and Kramer, S. N., “A Computer-Aided Design Technique for the Synthesis of Planar Four Bar Mechanisms Satisfying Specific Kinematic and Dynamic Conditions”, *Journal of Mechanisms, Transmissions, and Automation in Design,* 1988, Vol. 110, September, pp. 263-268.
12. Denavit, J., and Hartenberg, R. S., 1960, “Approximate Synthesis of Spatial Linkages,” *Journal of Applied Mechanics, Transactions ASME*, Series E, Vol. 27, No. 1, pp. 201-206.

13. Premkumar, P., and Kramer, S. N., 1986, “A Computer-Aided design Technique for the Optimum Synthesis of RRSS Path Generation Spatial Mechanisms with Prescribed Input Timing,” *ASME Journal of Mechanisms, Transmissions, and Automation in Design*, Vol. 108, No. 4, pp. 538-542.
14. Premkumar, P., and Kramer, S. N., 1989, “Position, Velocity, and Acceleration Synthesis of the RRSS Spatial Path-Generating Mechanism Using the Selective Precision Synthesis Method,” *ASME Journal of Mechanisms, Transmissions, and Automation in Design*, Vol. 111, pp. 54-58.
15. Uicker, J. J., Jr., Denavit, J, and Hartenberg, R. S., 1964, "An Iterative Method for the Displacement Analysis of Spatial Mechanisms," *Journal of Applied Mechanics, Transactions of the ASME*, Series E, Vol. 86, No. 2, June, pp. 309-314.
16. Robert L. Norton,”Design of Machinery: An introduction to the synthesis and analysis of mechanisms and machines” 2nd ed., McGraw-Hill. Inc., 1999.
17. Amitabha Ghosh, Asok Kumar Mallik, “Theory of mechanisms and machines”3rd ed., Affiliated East-West Press Private Limited, Newdelhi,2003.
18. J. Baumgarte, “A New Method of Stabilization for Holonomic Constraints”, Journal of Applied Mechanics, Vol. 50, pp. 869-870, 1983.
19. Matthew E. Doyle,” Foundation of CADSPAM: Computer Aided Design of SPAtial Mechanisms”, Thesis of Master of Science, Blacksburg, Virginia Polytechnic Institute and State University, 1997.
20. Hazem A. Attia, “Dynamic Simulation of Constrained Mechanical Systems Using Recursive Projection Algorithm”, journal of the Brazil society of mechanical society and engineering, vol.28, pp.37-44, 2006.
21. João Paulo Flores Fernandes,” Dynamic Analysis of Mechanical Systems with Imperfect Kinematic Joints” Ph.D. Dissertation, University of Minho, Guimarães, Portugal, 2004.
22. Edward J.Haug,” Kinematics and dynamics of mechanical systems” volume one: basic methods.The university of Iowa, copyright 1989 by Allyn and Bacon series in engineering, a division of Simon & Schuster,160 Gould Street,Needham Heights,Massachusetts 02194, USA.

23. Troy C. Schank," Optimal Aeroelastic Trim for Rotorcraft With Constrained, Non-Unique Trim Solutions", Ph.D. Dissertation, Georgia Institute of Technology, 2008
24. Hamid Jahed and Arash Tajik,"Mechanical Engineering Design Workshop, ME380 Final Project Manual on Trebuchet Design", University of Waterloo, 200 University Ave West, Waterloo, 2006.
25. ADAMS/View online help, MSC.Software Corporation, 2005.

APPENDICES

Appendix–A

Snapshot animations and joint torques

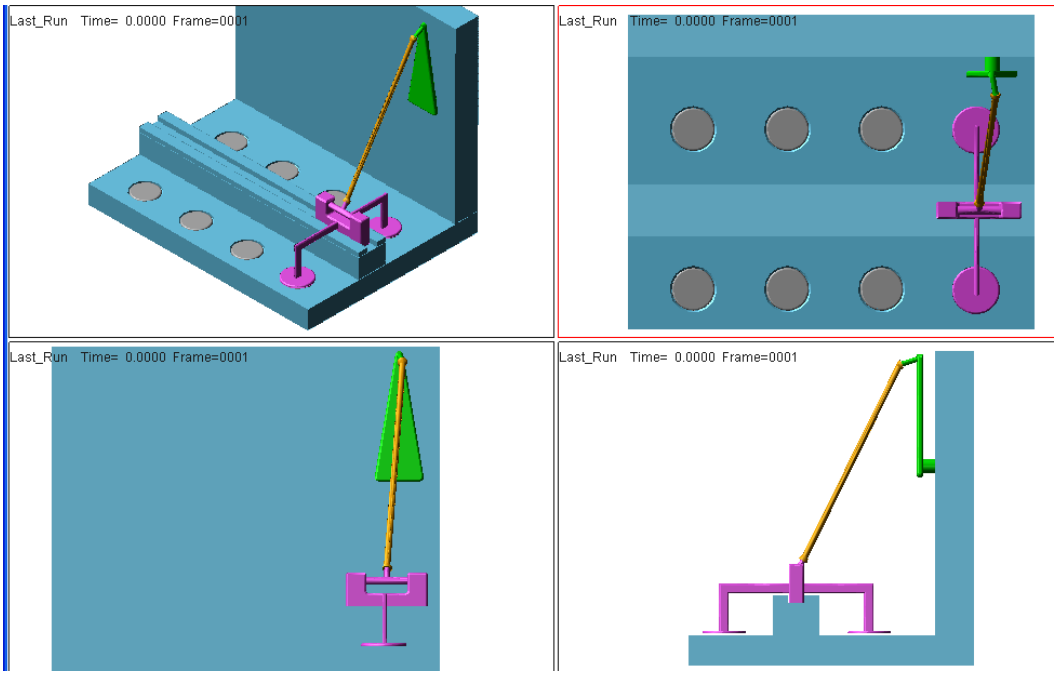

(a)

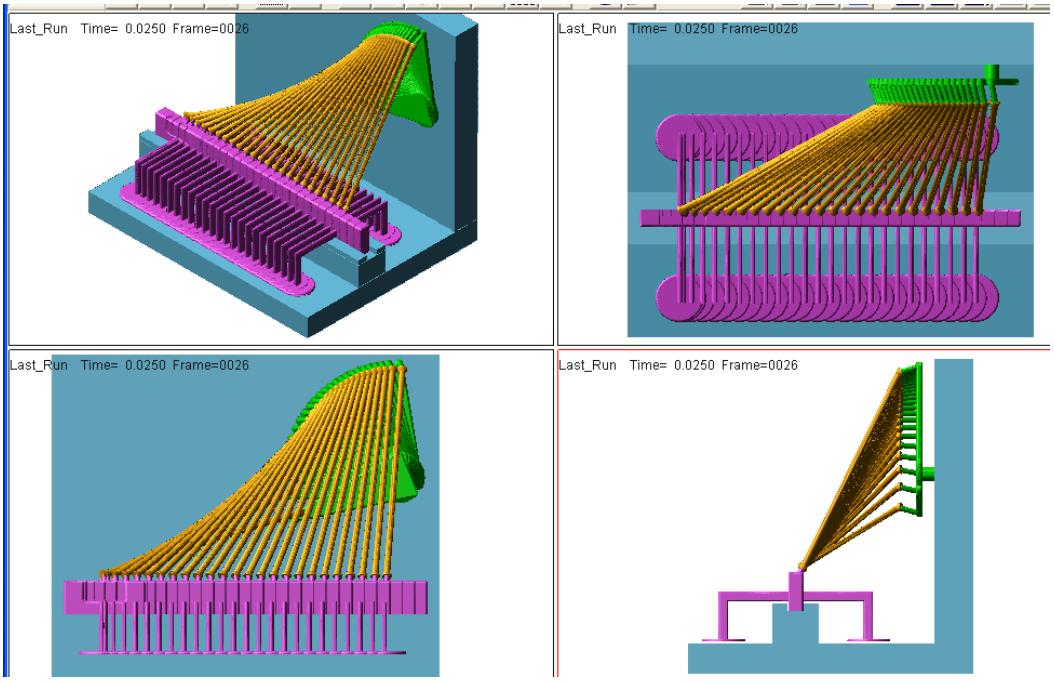

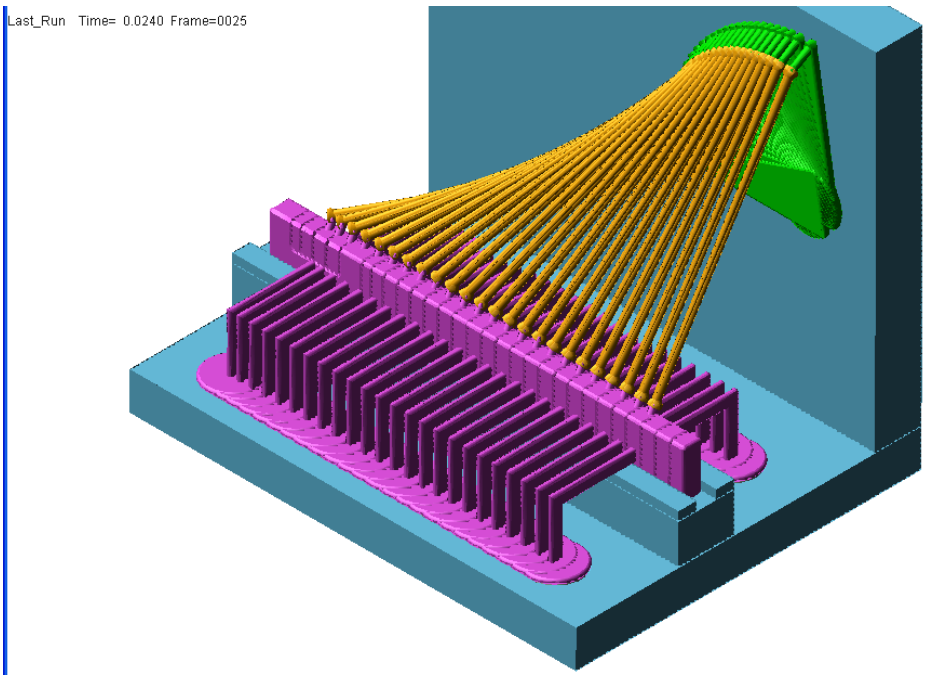
Last_Run Time= 0.0240 Frame=0025

(b)

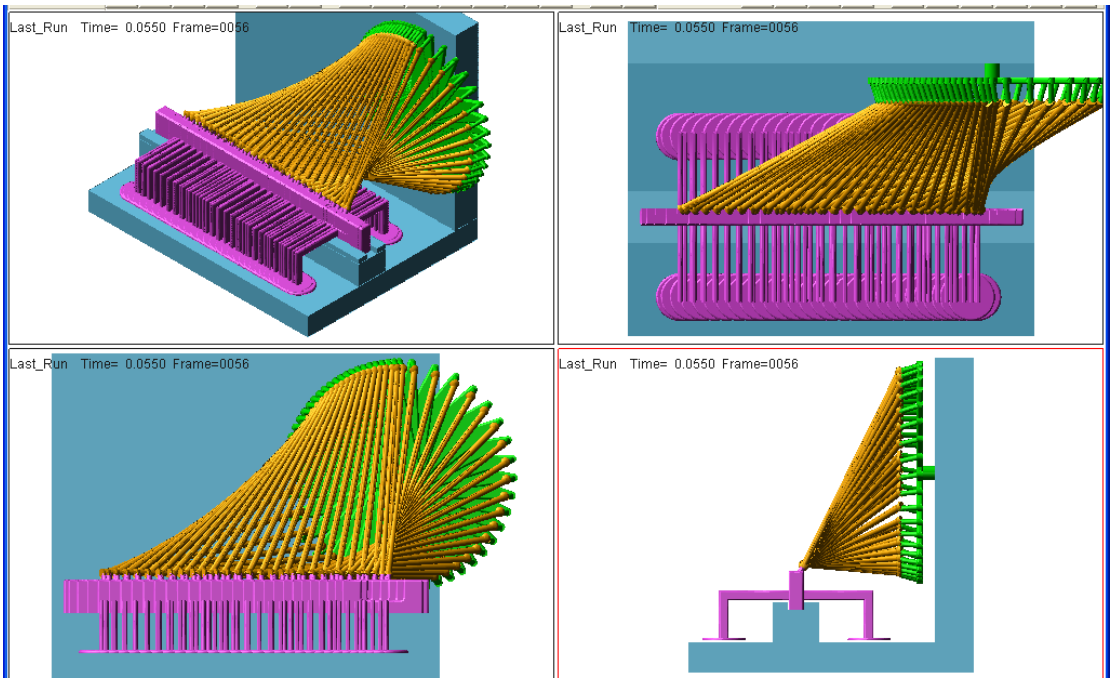
Last_Run Time= 0.0550 Frame=0056
Last_Run Time= 0.0550 Frame=0056
Last_Run Time= 0.0550 Frame=0056
Last_Run Time= 0.0550 Frame=0056

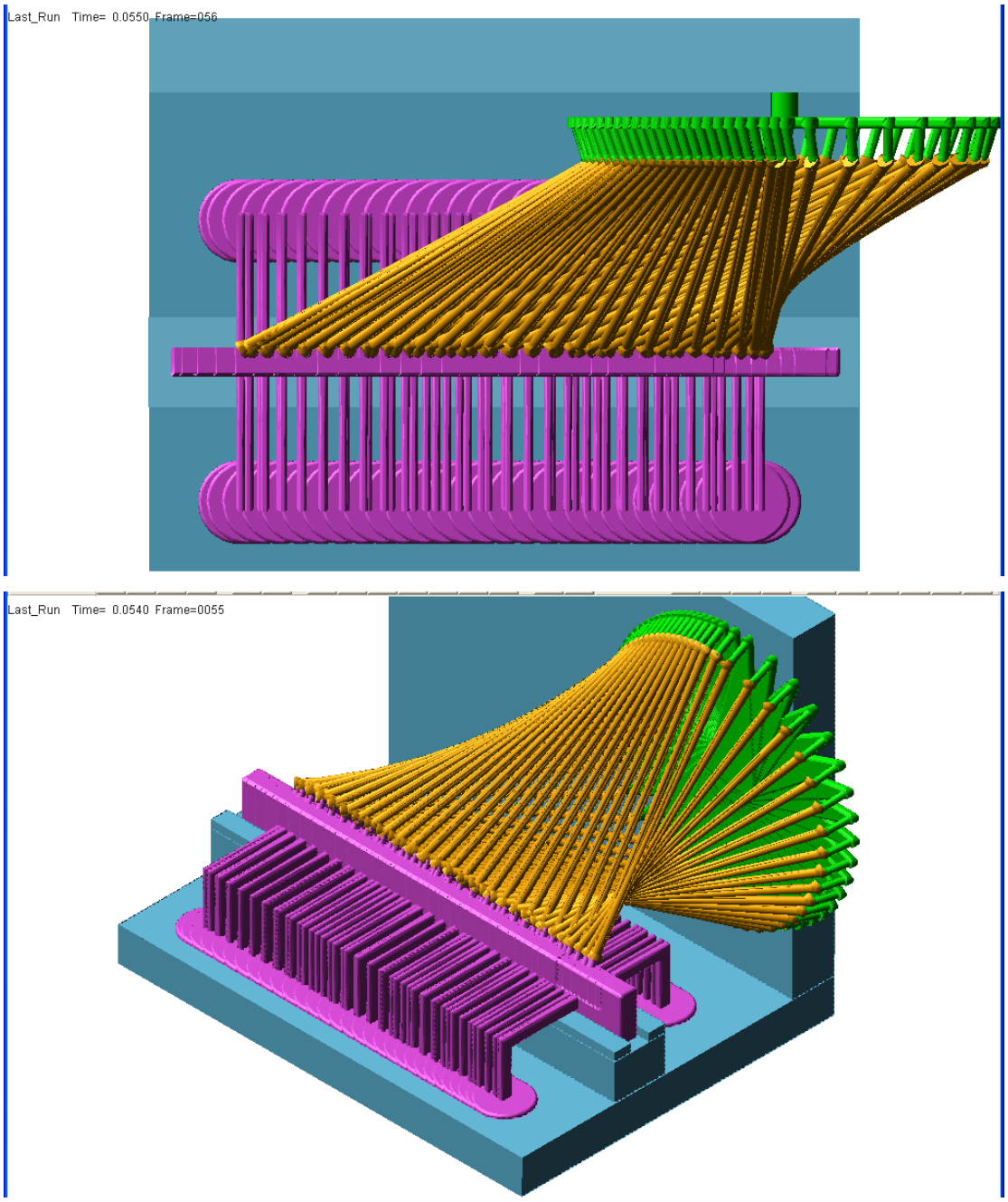

(c)

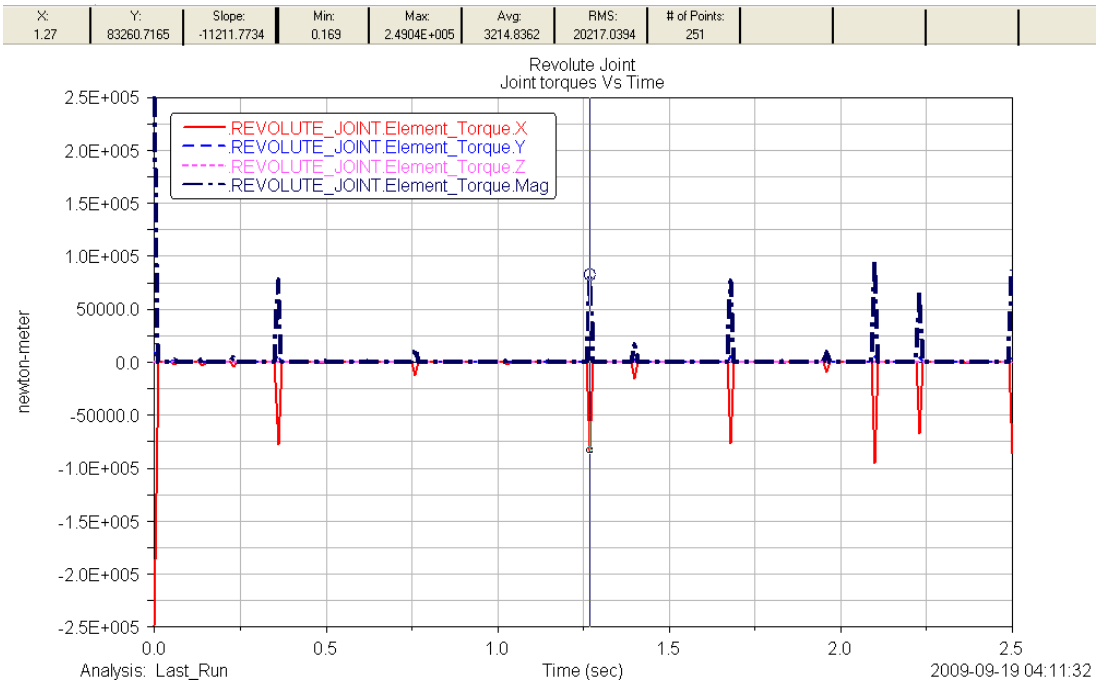
X: 1.27
Y: 83260.7165
Slope: -11211.7734
Min: 0.169
Max: 2.4904E+005
Avg: 3214.8362
RMS: 20217.0394
# of Points: 251
Revolute Joint
Joint torques Vs Time
REVOLUTE_JOINT.Element_Torque.X
REVOLUTE_JOINT.Element_Torque.Y
REVOLUTE_JOINT.Element_Torque.Z
REVOLUTE_JOINT.Element_Torque.Mag
newton-meter
2.5E+005
2.0E+005
1.5E+005
1.0E+005
50000.0
0.0
-50000.0
-1.0E+005
-1.5E+005
-2.0E+005
-2.5E+005
0.0
0.5
1.0
1.5
2.0
2.5
Analysis: Last_Run
Time (sec)
2009-09-19 04:11:32

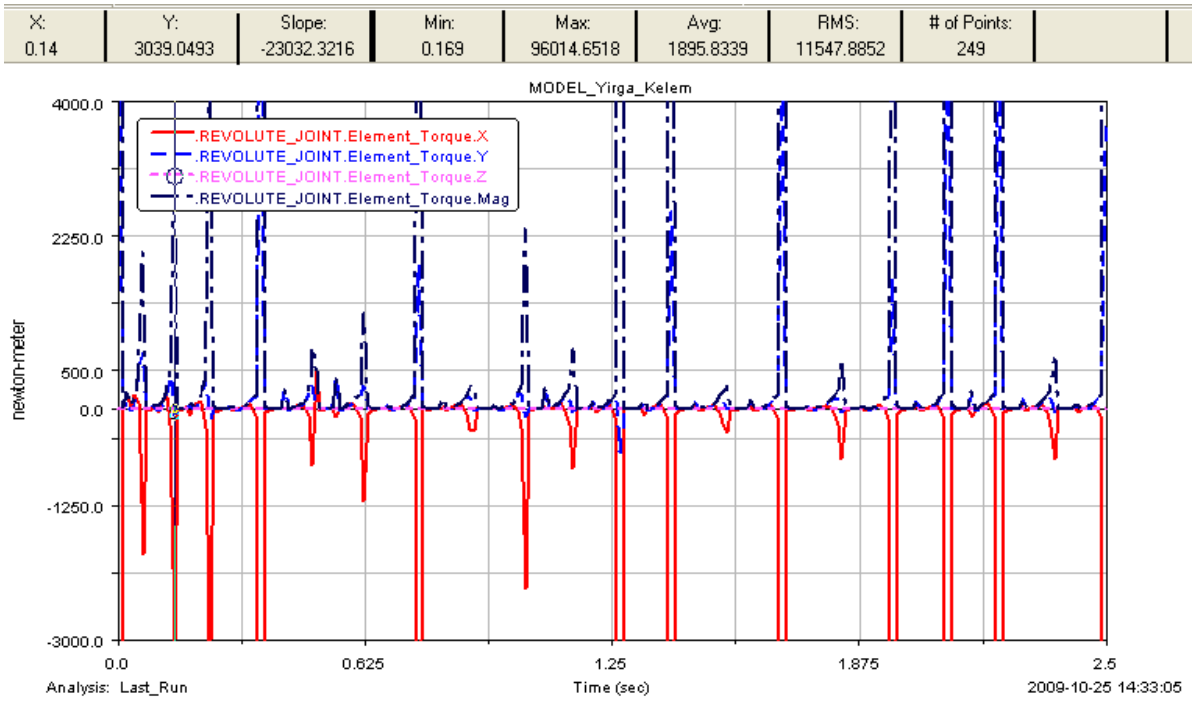
X: 0.14
Y: 3039.0493
Slope: -23032.3216
Min: 0.169
Max: 96014.6518
Avg: 1895.8339
RMS: 11547.8852
# of Points: 249
MODEL_Yirga_Kelem
.REVOLUTE_JOINT.Element_Torque.X
.REVOLUTE_JOINT.Element_Torque.Y
.REVOLUTE_JOINT.Element_Torque.Z
.REVOLUTE_JOINT.Element_Torque.Mag
newton-meter
4000.0
2250.0
500.0
0.0
-1250.0
-3000.0
0.0
0.625
1.25
1.875
2.5
Analysis: Last_Run
Time (sec)
2009-10-25 14:33:05

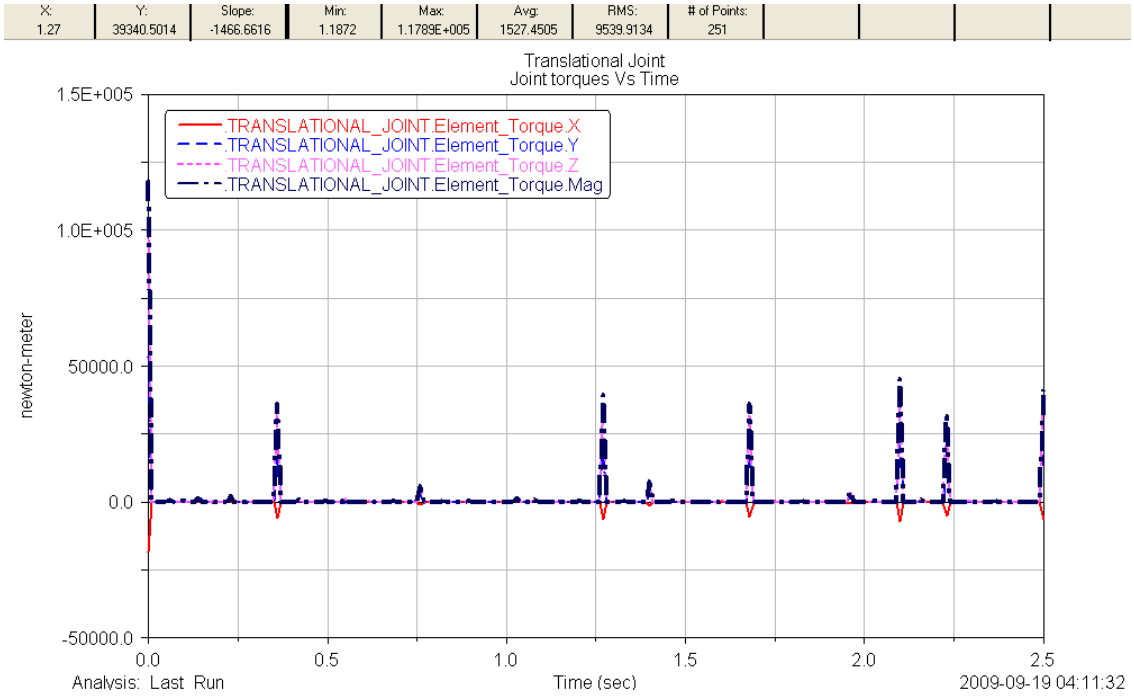

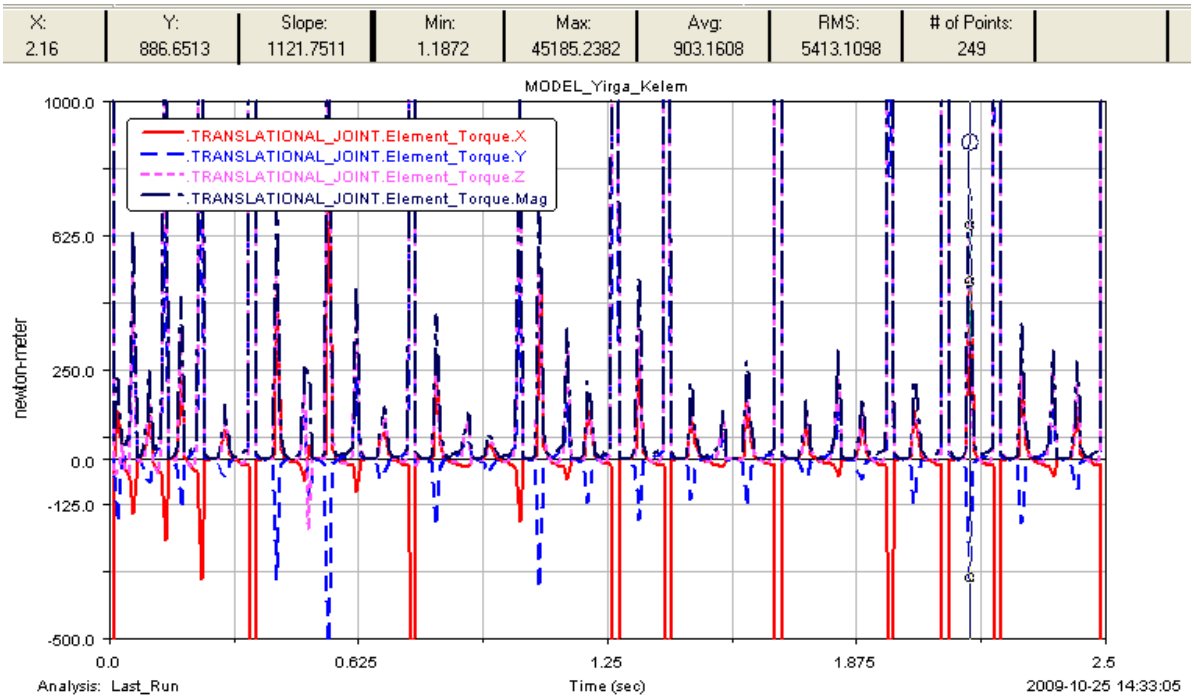

(d)

Figure (A.1) This appendix shows the different views of the lens-polishing slider-crank four bar spatial mechanism at (a) equilibrium (0.00seconds); (b) about half rotation of the crank to complete half path of the slider-block system; (c) about one complete rotation of the crank to a complete full rotation of the slider-block system; (d) torque experienced by the revolute and translational joints, respectively.

Appendix–B

Technical drawing of the lens-polishing spatial mechanism (1st angle projection)

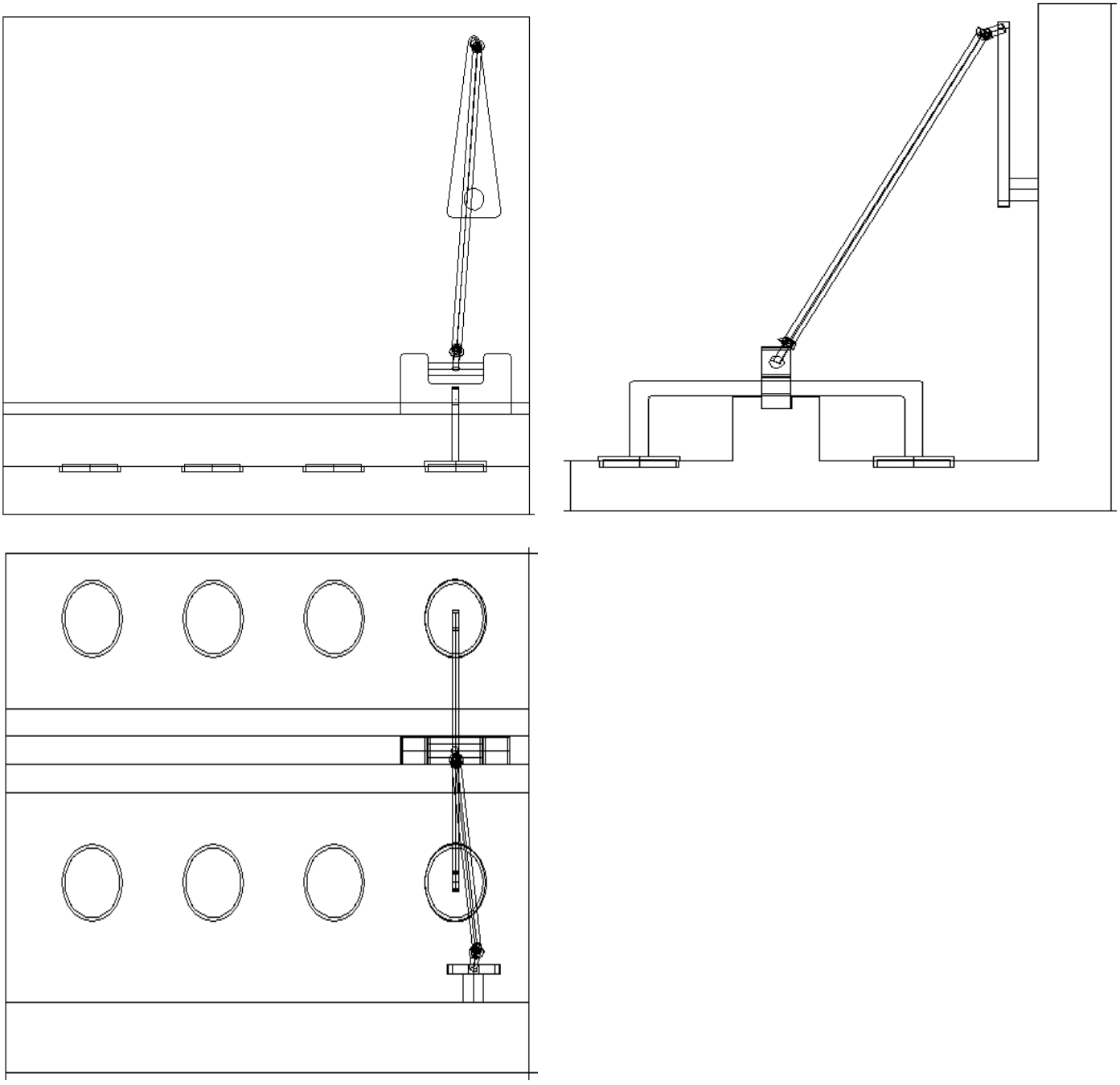

(a)

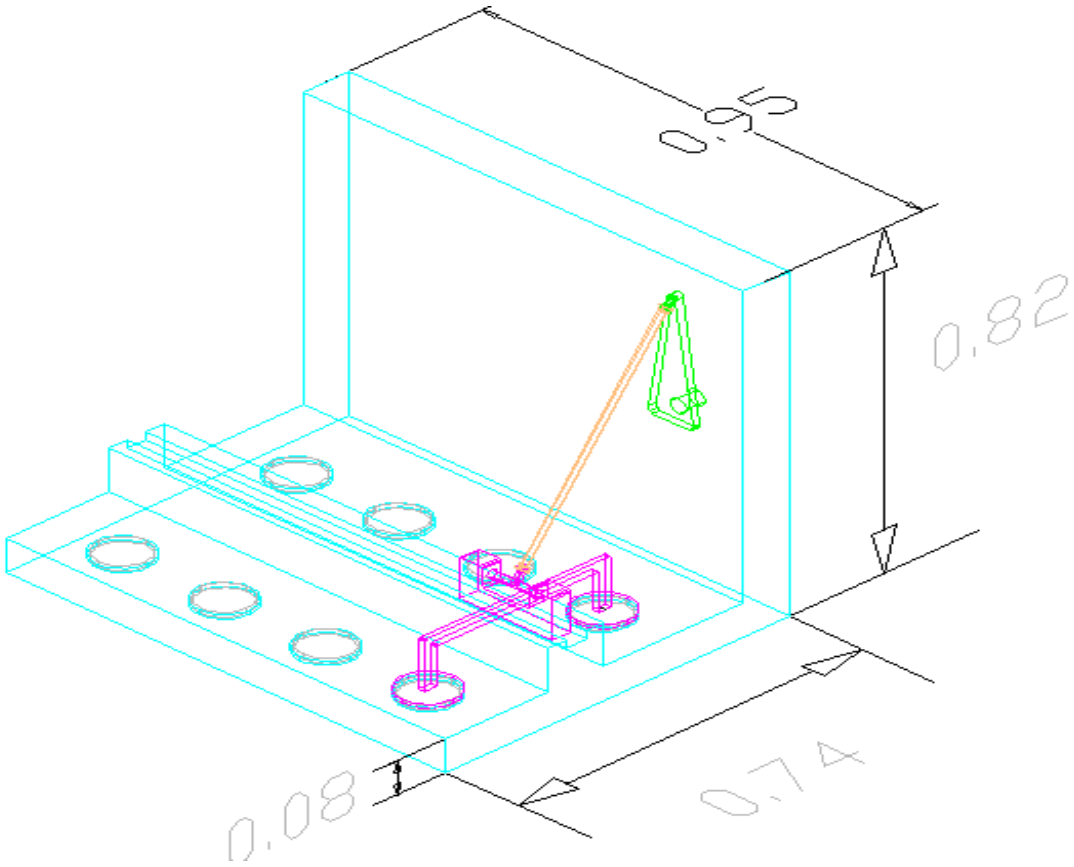

(b)

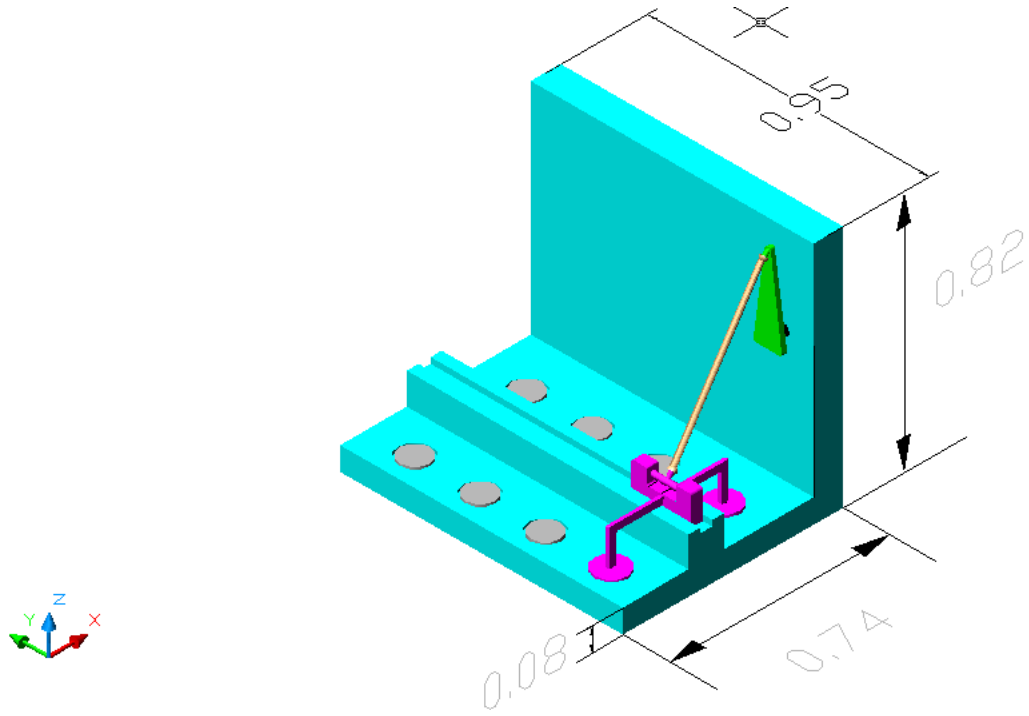

(c)

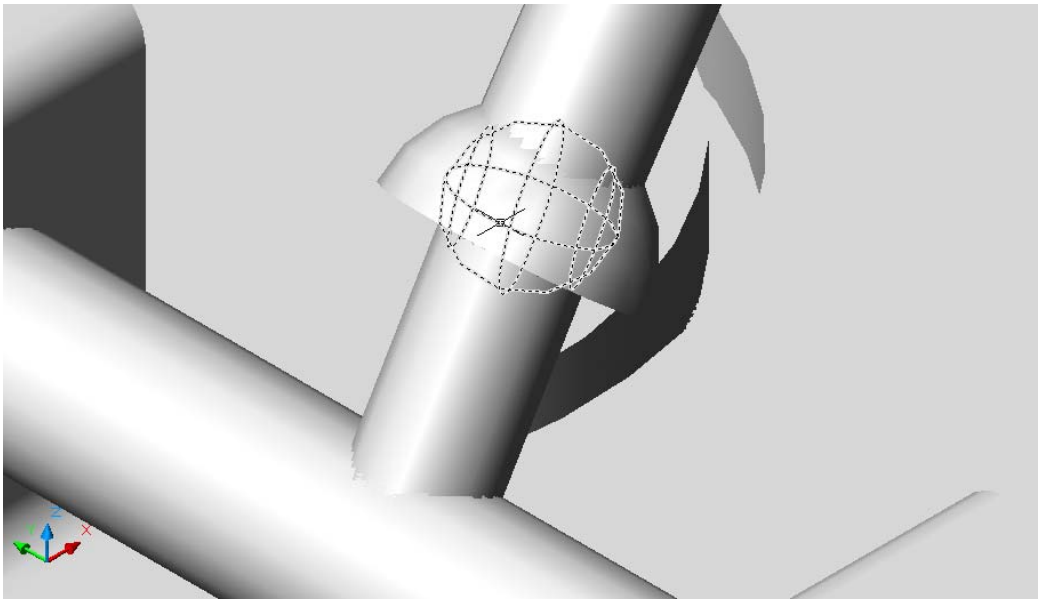

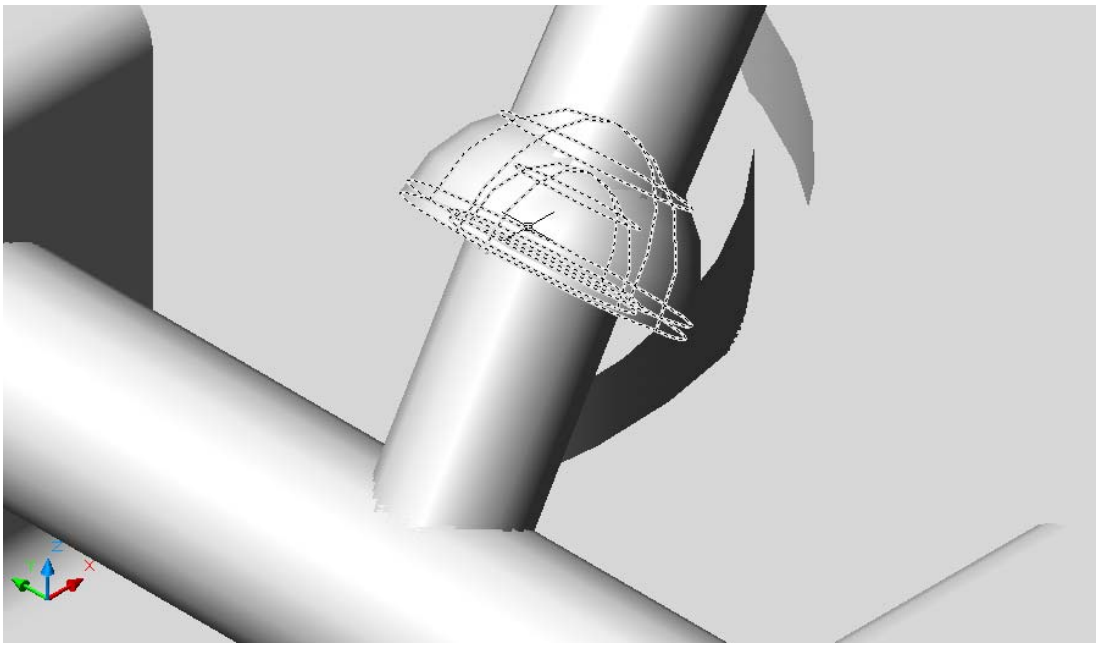

(d)

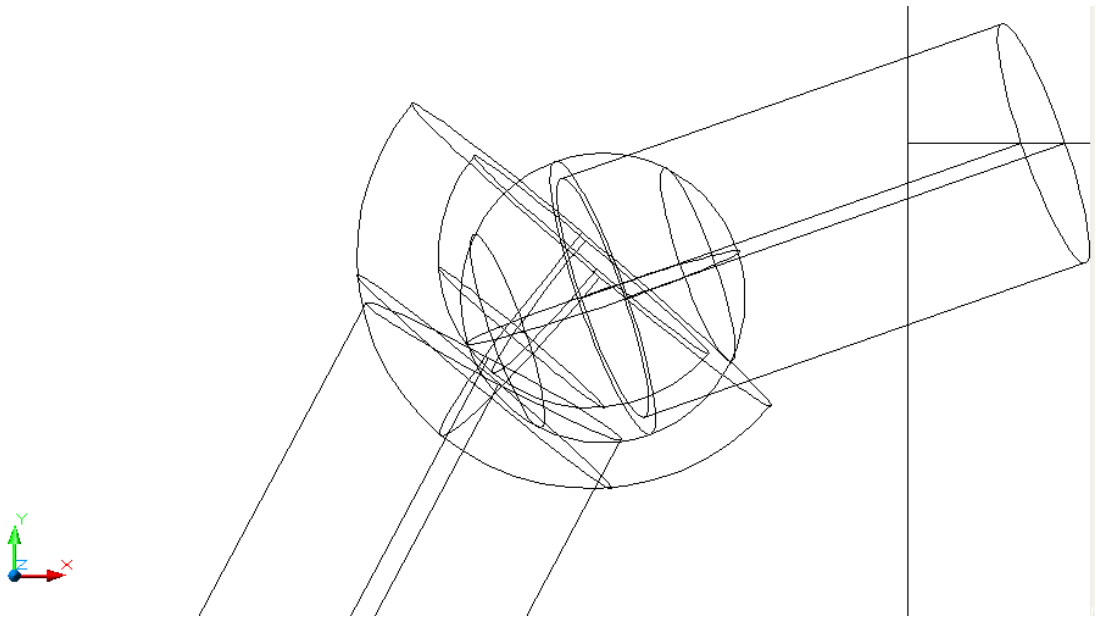

(e)

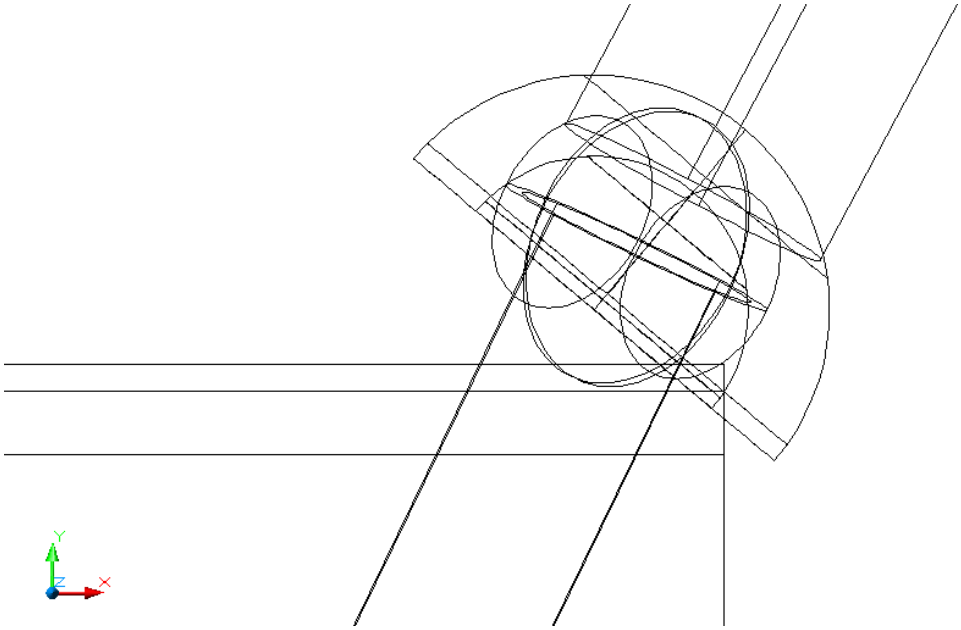

(f)

Figure (B.1) Technical drawings; a)Three views of the mechanism; b) three-dimensional view and wireframed ;c) three-dimensional view and smooth shaded; d) 3-D view of lower second spherical joint zoomed-in and smooth shaded; e) side view of upper spherical first joint zoomed-in and wireframed; f) side view of lower second spherical joint zoomed-in and wireframed.

Appendix–C

Part drawing of the lens-polishing spatial mechanism with sectional views